Acknowledgments

The work presented in this thesis has been developed at the Department of Civil Engineering of University of Minho, Portugal, and at the Division of Non Destructive Testing and Environmental Measurement Methods of Federal Institute for Materials Research and Testing (BAM) in Berlin, Germany.

The author would like to greatly acknowledge the financial support of “Sustainable Bridges” European Project for funding that work by the grant number FP6-PLT-01653 and the constant support from our partner institution (BAM) from Berlin, Germany for priceless help during experiments and data processing. Especially acknowledged is constant support from Dr. Christiane Trela from BAM and Dr. Francisco Fernandes from UMinho.

I would like to acknowledge the help of my supervisor, Paulo Cruz, friends, co-workers and family who, through their wisdom, patience and love made my stay in Portugal, Germany and in other countries possible. That period of my life was a time of changes, personal and professional improvement, which will have significant influence for my entire life.

It is difficult for me to mention all the people who through their mental or physical support made that work possible for me to accomplish. However, I would like to give many special thanks to: Kasia Niwinska, Kasia Dadas-Gacek, Ewa, Ana Cecilia, Konrad with family, Francisco, Luis with family, Fernando, Rolando with family, Kesio, Gihad with family, Abraham, Christiane with family, Jens, Christoph and Astrid. Their professional and personal help gave me a lot of hope in difficult moments of my life. Thank you all.

I would like also to give my sincere thanks to my mother, my father and my two brothers, Sebastian and Tomek, and, of course to my little sister Agatka. I want also to say thank you to my grandmother Janina, grandfather Antoni and to Piotr.

I dedicate that thesis to my grandmother Jolanta.

In general we look for a new law by the following process: First we guess it. Then we compute the consequences of the guess to see what would be implied if this law that we guessed is right. Then we compare the result of the computation to the nature, with experiment or experience; compare it directly with observation, to see how it works. If it disagrees with experiment it is wrong. In that simple statement is the key to the science.

- Richard P. Feynman, The Character of Physical Law

Abstract

In the last decades the number of bridges increased considerably due to the significant expansion of the roadway and railway networks. Nowadays some of those structures evidence a varied range of defects. To ensure the continuous safety and functionality of those bridges, condition and safety assessments, followed by adequate maintenance and rehabilitation actions, which requires gathering an extensive amount of data related with the bridge characteristics and condition, must be carried out frequently. In this context, Non-Destructive Testing (NDT) techniques are becoming increasingly popular and indispensable to collect reliable and valuable information without damaging the structure.

In the particular case of concrete bridges, which is addressed in this thesis, the location of the tendon ducts and ordinary reinforcement is fundamental in rehabilitation design. In addition, the verification of the quality of work during the execution of the works and initial life is fundamental in order to prevent the occurrence of early deterioration, such as reinforcement corrosion. Ground penetrating radar (GPR) is one of the leading techniques that are specially prepared for these purposes.

The thesis aims to give answers to the real problems raised by design offices and bridge owners concerning verification of the structural geometry of reinforced and prestressed concrete elements and verification of the structural integrity of concrete bridges. The innovations in non-destructive testing technology include application and combination of 2D and 3D radar investigations with new and cost-effective methods for regular and accurate acquisitions with software for 3D reconstruction for the verification of structural geometry and integrity of concrete bridges In addition, improvement, validation and application of radar tomography technique for the verification of structural geometry and integrity of concrete bridges is presented.

The intention of the author is to focus the attention of civil engineering society that non-destructive testing is not only used as a tool itself, but can be an integral part of structural assessment process.

Resumo

Nas últimas décadas o número de pontes aumentou consideravelmente devido à significativa expansão das redes rodoviárias e ferroviárias. Actualmente algumas dessas estruturas evidenciam diversas anomalias. Para assegurar a segurança e funcionalidade dessas pontes, é imprescindível avaliar periodicamente o estado de conservação e aplicar acções de conservação e reabilitação, o que requer a aquisição de um vasto conjunto de dados relacionados com as características e com o estado de conservação da ponte. Neste contexto, as técnicas de ensaio não destrutivas (NDT), têm-se tornado, gradualmente, mais populares e indispensáveis para conseguir dados fiáveis, sem ter de danificar a estrutura.

No caso particular de pontes de betão, que são objecto desta tese, a localização das bainhas de pré-esforço e da armadura passiva é fundamental para o projecto de reabilitação. Adicionalmente, a aferição da qualidade do betão é fundamental para prevenir a deterioração precoce, como por exemplo a devida à corrosão das armaduras. O radar de prospecção geotécnica (GPR) é uma das técnicas especialmente vocacionadas para estes propósitos.

Esta tese tem por objectivo dar uma resposta a alguns dos problemas reais sentidos pela administração, construtores e projectistas, relacionados com a verificação da geometria de alguns elementos estruturais de pontes de betão armado e pré-esforçado, bem como com a aferição da integridade dessas estruturas. O contributo desta investigação, inclui a aplicação desta técnica de ensaio não destrutiva e a combinação de análises 2D e 3D com novos, económicos e precisos métodos de reconstrução de imagem, para além de se centrar na melhoria, validação e aplicação da técnica de tomografia à resolução dos problemas em epígrafe.

A principal intenção do autor com este trabalho foi tornar evidente que esta técnica de ensaio não destrutiva é mais do que uma mera ferramenta, mas que pode e deve ser uma parte integrante do processo de diagnóstico.

Contents

List of Figures

Chapter 1 - Introduction

Exhaustive preliminary inspections using non-destructive inspection techniques (NDT) are becoming common in restoration and retrofitting projects as well as within maintenance programmes of civil engineering structures. A widely known NDT technique is the ground penetrating radar (GPR), which is a very attractive option as it can reliably acquire non-visible information without causing damage to the structure, which is often critical due to conservation and economic factors. Despite the fact that practitioners are becoming more conscious of the potential of this non-destructive technique, its use is still not frequent outside the academic community, at least for structural (non-geotechnical) applications. In Portugal, only a small number of investigative institutes possess the necessary equipment and use it frequently.

The most usual way of performing GPR surveys is by collecting the echoes of hidden features. In that way, a GPR system sends electromagnetic radiation pulses into the investigation area through a transmitting antenna. The generated electromagnetic wave is partially reflected by changes in bulk electrical properties of the features or objects encountered by the radiowave and the reflection is picked up by the receiving antenna. This information results in 2D radargrams which is the most frequent technique of analyzing radar data. However, in other cases individual radargrams might provide insufficient information, being difficult to interpret or failing to detect small objects or defective/damaged areas. This calls for more advanced techniques that can be applied in order to obtain higher quality or additional information.

The first advanced technique is to obtain a 3D volume of the radar data by acquiring a dense subset of parallel 2D radar profiles. This technique has been successfully applied in numerous applications of NDT investigation of civil structures by providing a visualization of the radar data within the investigated area by showing the results as depth slices (Lualdi *et al.* 2003) or by providing more realistic images of linear objects, such as pipes, cables, rebars and large voids through isosurfaces (Binda *et al.* 2003). Additionally, the technique allows non-specialized radar users to better understand results by providing realistic shapes of embedded features.

The second advanced technique described in the thesis is denoted by tomography. Originally developed in medicine and in several other fields (geophysics) with the aim of reproducing the internal structure of an object from measurements collected externally. In geotechnical applications, cross-hole tomography is commonly used to determine the position of cracks in rocky ground and to assess the condition of deep foundation piles. Some of the works in geophysical applications can be seen in Becht *et al.* (2004), Tronicke *et al.* (2001), Tronicke *et al.* (2002). In the case of structural civil engineering, radar tomography is quite a recent technique. It is generally used to map the interior of objects like columns, walls and other elements that can be accessed from two or more sides. Tomography is a rather distinct processing mode, which makes use of direct transmission acquisitions. In this acquisition mode, the transmitter and the receiver antennas are separated and located successively in various positions, in order to cover entirely the area under investigation with electromagnetic rays, being the direct pulse recorded. In general terms, the radar velocity tomography technique was already successfully applied for the inspection of masonry structures (Binda *et al.* 2003, Topczewski *et al.* 2006). In case of concrete, tomographic research was primarily based on acoustic waves (Olson 2004), while the use of radar tomography technique was not reported before according to the authors' knowledge.

Nowadays, due to maturity of GPR systems, they are increasingly being used as a diagnostic and quality assurance tool for concrete structures (Maierhofer & Kind 2002). The use of this tool has been validated by numerous authors for the assessment of the metallic reinforcement bars (Maierhofer *et al.* 2003, Dérobert *et al.* 2002), in the inspection of grouting quality inside plastic tendon ducts (Giannopolous *et al.* 2002, Forde 2004), and in the diagnosis of defects in concrete structures (Taffe *et al.* 2003). The inspection of bridge decks, particularly in the case of prestressed concrete bridges, is a critical task, but has been successfully carried out by many researchers (Scott *et al.* 2003, Hugenschmidt 2002). GPR is progressively replacing other techniques, such as radiographies, being GPR usually considered faster and safer to apply. Generally, radioactive methods require special certified operators and the closure of an extended perimeter around the test location for security and health purposes (Mitchell 2004).

1.1 Scope and objectives of the research

The main motivation of that thesis is to improve and apply radar technique for the different maintenance problems which are present in the bridge population and propose, basing on the involvement in the “Sustainable Bridges” Project effective solutions for bridge owners, construction companies or design offices dealing with rehabilitation or maintenance of newly built or existing bridges. The intention of the author is to focus the attention of civil engineering society that non-destructive testing is not only used as a tool itself, but can be an integral part of structural assessment process. The thesis aims to give answers to the real problems raised by design offices and bridge owners concerning:

a) verification of the structural geometry of reinforced and prestressed concrete elements like rebars or plastic and metallic tendon ducts;

b) verification of the structural integrity of concrete bridges, especially for the detection of the areas with different concrete compaction.

The innovations in non-destructive testing technology will include:

a) application and combination of 2D and 3D radar investigations with new and cost-effective methods for regular and accurate acquisitions with software for 3D reconstruction for the detection of structural elements and verification of the concrete compaction,

b) improvement, validation and application of radar tomography technique for the verication of structural geometry and integrity of prestressed concrete bridges,

c) creation of methodologies for bridge owners, design offices and radar operators concerning use of radar technique in the reflection and transmission mode for the inspection of concrete bridges. The purpose of those methodologies is to show advantages and disadvantages of radar technique from the most general level to the most detailed one and, to indicate, that the testing using radar technique is an expensive process. Thus, the deep understanding of radar technique is crucial to obtain good results in cost-effective way.

The purpose of development of the radar tomography technique for the civil engineering applications is not to exclude of any of existing NDT methods, but to supplement them. That method is fully complementary to for instance acoustic methods. Radar sends electromagnetic waves and use of this technique is limited by presence of steel or other materials which are causing high attenuation to electromagnetic waves, but these waves are easily penetrating for instance air voids. In case of acoustic methods impactor sends mechanical waves inside tested structure. Waves will not penetrate through air voids but will penetrate through steel. Additionally, radar transmission measurements are much faster than transmission measurements using any acoustic transducers, what can significantly reduce the costs of the on-site work.

In comparison to the radar reflection measurements, tomography can provide higher penetration depths with the same resolution and provide additional information about structural integrity (like to define type of material used and its condition). Tomography can be used to map: voids, moisture content, ferro-magnetic materials. Information obtained by radar reflection and transmission measurements can be applied in the various fields of civil engineering. Detailed description of the possible applications of radar for the civil engineering industry is one of the objectives of the thesis and will be described in the conclusions.

1.2 Outline of the thesis

This thesis is composed by 8 chapters and one appendix. In general, it can be divided in three parts. The first part, described in Chapters 2 and 3, aims to show the current state of the art of Non Destructive Techniques, in general, and of Ground Penetrating Radar in particular. Second part, described in chapters 4 and 5, consists of experiments using radar technique in reflection and transmission mode on laboratory specimens and on real bridges. The last part, described in chapters 6 and 7, includes the methodologies for radar in reflection and transmission mode, including the newest achievements in the technology, advanced testing and data processing procedures, and possible areas of application for the concrete bridge inspection.

In chapter 2 a description and background of the main NDT techniques applied for the bridge inspection is given and in chapter 3 a detailed description of GPR technique is presented.

Chapter 4 consists of calibration measurements using radar in reflection and transmission mode in the laboratory conditions.

Reflection measurements were performed on the large concrete specimen aiming to show the combination between 2D and 3D image visualisation techniques for the geometrical evaluation of structural elements as well as in the mapping of typical defects and inclusions frequently found in structures.

Transmission measurements were performed in the BAM laboratories on two large concrete specimens and in the UMinho laboratories on two masonry walls (Topczewski *et al.* 2006). After those measurements, significant conclusions were drawn. Although the voids and metallic tendon ducts were detected, significant number of artefacts was present in the final results. Detailed quality checks of input data indicated, that significant time variations are present in the signal and the source of them is unknown. It led to the conclusion that additional tests are needed for checking of the time axis stability. Thus, additional calibration measurements were proposed and performed in the BAM and UMinho laboratories. The tests indicated that in the every Radar equipment, time drift problem is present. To control it, calibration procedures were proposed and applied in the BAM laboratories.

To validate the radar technology, number of tests in reflection and transmission modes for the verification of structural geometry and integrity was performed in 3 big concrete bridges in the north of Portugal. In chapter 5, the results and the conclusions from those tests are presented. In the first two case studies bridge inspection using GPR system with high frequency antennas aimed to accurately detect the position of the metallic tendon ducts. In the last case study, GPR was used for the early detection of material and construction defects. Additionally, the application of advanced GPR tomography aimed to characterize the quality of the concrete, indicating the presence of execution defects. Also combination between radar reflection profiling and radar tomography was one of the objectives of the research.

In chapter 6 guidelines for end-users of radar systems and bridge owners concerning use of GPR in the reflection mode for inspection of concrete bridges are presented. They include detailed procedures for the planning of the investigation, possible areas of applicability and data acquisition including data interpretation. Those procedures aim to give also general idea to the people responsible for the maintenance programmes how to apply in the cost-effective way the GPR technique.

In chapter 7 guidelines for the end users of radar systems and bridge owners concerning use of GPR in the transmission mode for inspection of concrete bridges are presented. Those guidelines are the main output from the conclusions drawn during participation in the “Sustainable Bridges” European Project. They include detailed procedures for the planning of the investigation, possible areas of application and data acquisition including data interpretation. Those guidelines are supplemental to the guidelines presented in chapter 6 and are aiming to indicate the necessity of combining 2D, 3D, and tomography measurements for the acquiring the most complete and adequate data sets for further evaluation of internal geometry and integrity of tested structure.

In chapter 8, general conclusions are drawn from all the research carried out and some suggestions for future work that could be done in the assessment of bridges are presented.

Chapter 2 - State of the art of NDT applied for the bridge inspection

2.1 Introduction to waves

Before describing advanced Non Destructive Techniques (NDT) used for the bridge inspection, one must be aware of general theoretical background behind each of those techniques. Each of them is using certain kind of waves, which are propagating through tested structure and are registered in an electronic way for further interpretation.

The term “wave” is used to describe a disturbance that varies in time and space and transports energy. The basic wave physics that are applied in the different NDT will be described at the end of the thesis as an Appendix. There are two ways to categorize waves. The first is based on the direction of movement of the individual particles of the medium relative to the direction in which the wave travels. In this way, we can distinguish three wave types in solids:

- Longitudinal (with particle vibrations parallel to wave direction);
- Transverse or shear (with particle vibrations perpendicular to wave direction);
- Surface or Rayleigh (with particle vibrations on the elliptical orbit in symmetrical mode).

The second way to categorize waves relies on the ability to propagate through a vacuum. In this case, we can specify two categories of waves: mechanical and electromagnetic.

A mechanical wave is a wave which is not capable of transmitting its energy through vacuum. Mechanical waves require a medium in order to transport their energy from one location to another. The examples of the mechanical waves are: ocean waves, seismic waves or acoustic waves. Because mechanical waves cause displacements in the medium in which they propagate, the propagation velocity is affected by the properties of the medium. Specifically, the stiffness of the medium, or dynamic modulus of elasticity, has a significant effect on the propagation velocity, as does the density of the medium. In solids, mechanical waves comprise: longitudinal or compression waves (Primary or P-waves), transverse or shear waves (Secondary or S-waves) and surface waves (Rayleigh waves). An example can be seen on the Figure 2.1. More detailed description of basics of the acoustic wave methods is provided in the Appendix A.

An electromagnetic wave is a wave which is capable of transmitting its energy through a vacuum (i.e., empty space). These waves are propagated by changes in the electrical and magnetic state and do not require a medium to propagate. In solids, electromagnetic waves consist of a transverse wave with an electric and magnetic component. The electromagnetic spectrum is shown in Figure 2.2. The electromagnetic waves, depending on the wavelength, can be distinguished as: radio waves, microwaves, infrared, visible light, ultraviolet, x-rays, gamma rays. The electromagnetic spectrum, shown in the chart, extends from just below the frequencies used for modern radio (at the long-wavelength end) to gamma radiation (at the short-wavelength end), covering wavelengths from thousands of kilometres down to fractions of the size of an atom. It must be noted that electromagnetic waves, which have a short wavelength have high energy; waves which have long wavelength have low energy.

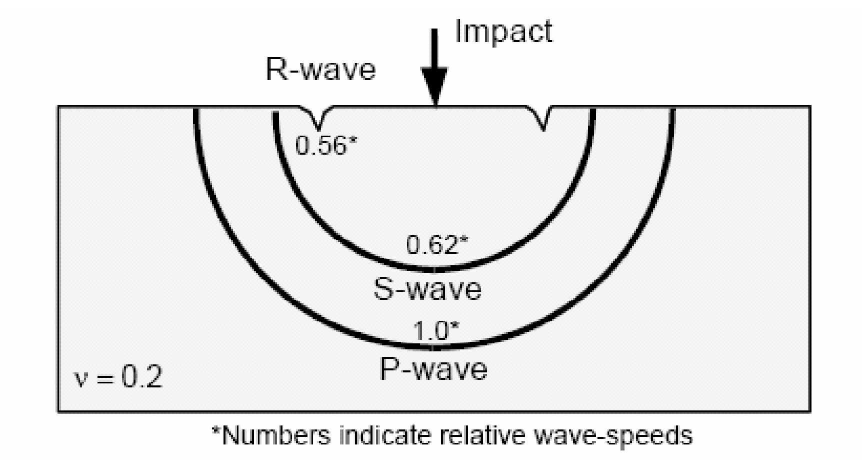

Figure 2.1 – Basic mechanical wave types in solids (Malhorta & Carino 1991)

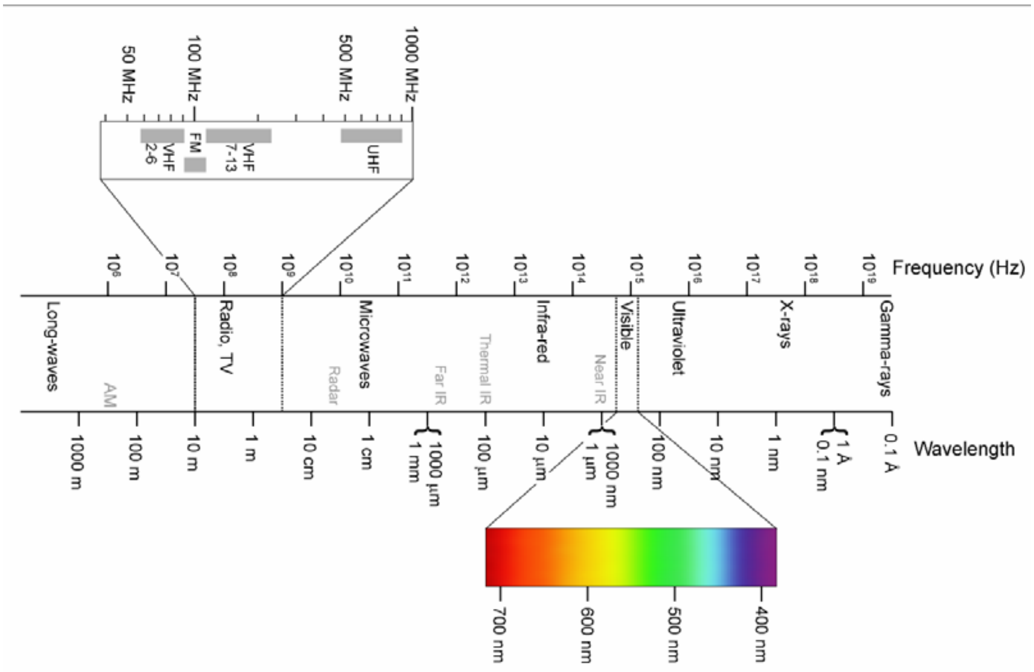

Figure 2.2 - Electromagnetic wave spectrum showing wavelenghts and common terms for various portions of the spectrum (www.wikipedia.com)

2.2 Basic maintenance strategies applied for the bridge inspection

Depending on the wave type and the frequency used, NDT applied for the inspection of concrete and masonry structures can be classified in various ways. An example of such classification is shown in Table 1. The methods presented in that classification present current state of the art in the Non Destructive Methods applied for the inspection of bridges. Depending on the type of structure tested (concrete or masonry), required resolution and penetration depth different combinations of techniques can be used. Generally, combination of techniques using different kind of waves is used to solve problems given to NDT experts. Those methods are considered as special (in-depth) inspection techniques and are used when the common maintenance methods (like visual inspection) fail.

That method is one of the most frequently applied techniques for the bridge inspection. Visual inspection is based on the propagation of the electromagnetic waves within the visible light. However, the results from that kind of inspection are only superficial and can give just an estimation of what can be happening inside the structure.

Table 1 Frequency of various Non-Destructive Techniques

Method	Wave Form	Frequency
Radiography	Gamma	1,00E+21 Hz
	X-Rays	1,00E+17 Hz
Thermography	Far Infra-red	1,00E+12 Hz
Radar	Radio and micro waves	50MHz - 2.5 GHz
Ultrasonic	Mechanical	50kHz -10 MHz
Sonic	Mechanical	50Hz - 20 kHz

Because any of those methods do not give full information about the structure tested, different approaches and guidelines for bridge inspection are being created worldwide (AASHTO 2000, Ryall 2001, Crawford 1997, DMJM Harris 2003, Bergmeister 2003). In case of AASHTO Manual, its principal interest is the definition of five distinct types of bridge inspections. These definitions of different inspection types allow bridge owners and bridge inspectors to coordinate inspection resources to maximize efficiency. The five types of inspection are initial, routine, damage, in-depth and special, as briefly described below.

• **Initial inspection** – These inspections are the first inspections of any new bridge and are completed with two primary goals. First, to obtain all structure inventory and appraisal data, and second, to determine the baseline structural conditions and identify current or potential problem areas.

• **Routine inspection** – Routine Inspections are completed on a regular frequency (usually every 2 years) to determine the physical and functional condition of a bridge and to identify changes from previous inspections.

• **Damage inspection** – These inspections are completed to assess known damage resulting from environmental or human actions. Each damage inspection is unique with the general goal of identifying the need for further action.

• **In-depth inspection** – The goal of in-depth inspections is to identify deficiencies not normally detected during routine inspections. They are generally completed from close-up with a more hands-on approach and are commonly referred to as “arms length” inspections. These inspections are not normally “complete” bridge inspections (i.e., only limited areas or certain details are inspected).

• **Special inspections** – Special Inspections are usually completed to monitor a single known defect or condition.

In Germany, the German Society for Non-Destructive Testing is developing guidelines for NDT methods in civil engineering. The guideline for radar method for non-destructive testing in civil engineering can be found in Taffe & Maierhofer (2003) and is divided by 5 chapters:

1. Dissemination of guidelines concerning NDT-CE
2. Fundamentals of radar method
3. Measuring procedures
4. Data processing and evaluation
5. Case studies: brickwork, concrete, asphalt, subsoil
6. Documentation and qualification

They are also other guidelines for the NDT testing which are currently translated into English. Providing theses guidelines in English language will make them accessible to a larger number of researchers, developers and users. So experts in other European countries will benefit from the information given in these guidelines. Together with expert knowledge in these countries they can contribute to the harmonization of European standards.

For higher levels of inspection, the assessment of internal condition of bridges concerning their internal geometry or integrity must be preceded by NDT methods. For that purpose, different techniques using mechanical, electromagnetic or radiographic waves must be used. Below, in chapters 2.3, 2.4 and 2.5 short explanation of those methods is given.

2.3 Sonic/ultrasonic methods (Mechanical methods)

The acoustic method refers to the transmission and reflection of mechanical stress waves through a medium at sonic and ultrasonic frequencies (Figure 2.1). The mechanical impulse is generated by transducer by hitting one of the surfaces of the tested structure. Then another transducer registers the vibration caused by transmitter and the travel time of the generated pulse is measured. By knowing transmitter- receiver distance and corresponding travel time, speed of the stress wave can be determined. The value of the speed indicates the quality of the material. In general terms, more compacted materials with higher density will have high propagation velocities of the stress waves. Air interfaces will be registered as places with very low propagation velocity.

The choice of appropriate frequency depends on the type of the evaluated structure. The transducers for concrete and modern masonry have ultrasonic frequencies between 25 kHz – 150 kHz which are sensitive to minor flaws and are able to locate small anomalies. Low frequency sonic waves between 500 Hz - 20 kHz are more effective for investigation of older masonry because of its greater energy content and resistance to attenuation in the presence of multiple cracks and flaws. Among commonly used sonic and ultrasonic methods, we can distinguish (Table 2). Due to the fact, that any of the acoustic method is not within the scope of that research, no further detailed description of the mentioned methods is provided.

Those methods can be applied for the geometry or integrity determination of concrete and masonry structures (Abraham 2002, Berra 1992, Binda 2003, Bungey & Millard 1996, Colla 1997, Colla 2001, IAEA 2002, Krause *et al.* 1997, Krause *et al.* 2000, Malhorta & Carino 1991, Olson 2004, Shevaldykin 2003). In particular, those methods can be applied successfully for the location of grouting faults inside the metallic tendon ducts, determination of the uniformity of the concrete, measuring the changes in the properties of concrete, correlation of pulse velocity and strength as a measure of concrete quality and detection of voids and cracks.

Table 2 Classification of the basic types of acoustic non-destructive methods

Ultrasonic methods (concrete and masonry structures)	**Sonic methods** (masonry structures)
Ultrasonic pulse velocity	Sonic pulse velocity
Ultrasonic tomography	Sonic tomography
Impact-echo	Impact-echo
Spectral analysis of surface waves	Sonic resonance method

2.4 Electromagnetic methods

Electromagnetic methods are one of the most frequently applied techniques for the bridge inspection. That's due to their speed, quite high accuracy and diversity of potential applications. While in case of acoustic methods measurement is very local and quite time consuming, the techniques using electromagnetic waves like radar, thermography or covermeter are quite rapid. Below short description of the mentioned techniques is given:

2.4.1 Radar

That technique is commonly applied for geophysical and civil engineering problems. It case of manmade materials, it can rapidly scan concrete and masonry surfaces finding layers between different materials, voids, rebars, tendon ducts or timber beams. The Ground Penetrating Radar (GPR) system sends electromagnetic radiation pulses into the ground via a transmitting antenna, the resulting wavefront is partially reflected by changes in bulk electrical properties of the ground, and the reflection is picked up by a receiving antenna (Figure 2.3). The signals are processed and amplified to provide a time travel record which is subjected for further analysis and interpretation (McCann & Forde 2001, Daniels 2004). More detailed description of this technique with particular applications of 2D, 3D and tomography imaging is the topic of this thesis and will be described further.

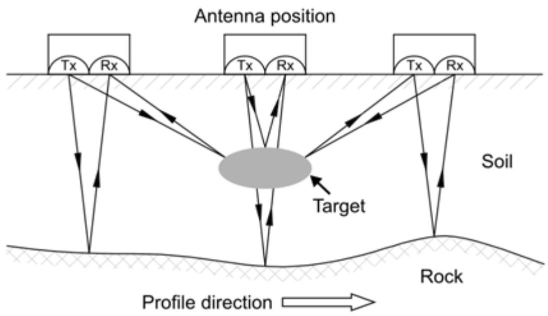

Figure 2.3 - Schematic illustration of the GPR technique used in reflection mode (Fernandes 2006)

2.4.2 Infra-Red thermography

Thermal imaging is a technique for converting a thermal radiation pattern, which is invisible to the human eye, into a visual image. To achieve this, an infrared camera is used to measure and image the emitted infrared radiation from an object. All objects at temperatures above absolute zero (as measured by the Kelvin, or Rankin temperature scales) emit heat energy. The amount of emitted energy increases with temperature. It has been observed that structures with defects such as debonding render and mosaic or delaminating concrete emit differing amounts of infra-red radiation. If a concrete surface with an even colour and texture is viewed with an infra-red camera it will appear quite uniform when the concrete is free of defects. However, if there are any cracks or delaminations within the concrete, the surface will heat up faster under solar irradiation in these areas and hot spots will be observed in the thermal record (McCann & Forde 2001, Maierhofer *et al.* 2002, Maierhofer *et al.* 2003). These areas can then be examined more closely and marked on the structure for identification and future investigation. Figure 2.4 shows example of column and corresponding thermogram indicating rebar corrosion induced delamination. Thermography was successfully applied indoors. However, due to problems with heating up the external surfaces and uncontrolled heat flow due to outside temperature differences, that technique is still very complicated to apply in the outdoor conditions. Great care should be given while performing such experiment and then interpreting the results.

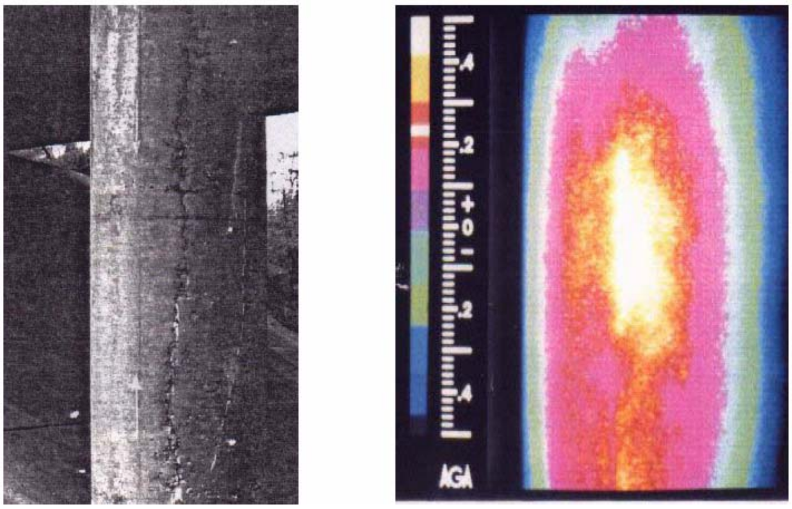

Figure 2.4 – Thermogram (left image) showing rebar corrosion induced delamination (Duke 2004)

2.4.3 Covermeter

Covermeter is a commonly used instrument, which allows locating rebars embedded in the concrete and determining the thickness of concrete overlaying the reinforcement rods. The method is based on the principle that the presence of steel rod within the concrete affects the filed of an electromagnet (McCann & Forde 2001, Bungey & Millard 1996). The covermeter consists of two coils positioned on an iron-cored inductor. When an alternating current is passed through one of the cores a current is induced in the other, which is then amplified and measured. The influence of steel on the induced current has a non-linear relationship with the thickness of the concrete and is also influenced by the diameter of the rod. However, modern covermeters are designed and calibrated to accommodate these effects and with careful application, excellent results can be achieved. More recent and specialized applications involve the sizing of rebars using covermeter. That method can be fully supplemental to for instance radar method, because it can give in fast and cheap way information about surface reinforcement without need of specialized staff to operate it. Figure 2.5 shows typical image of surface steel mesh.

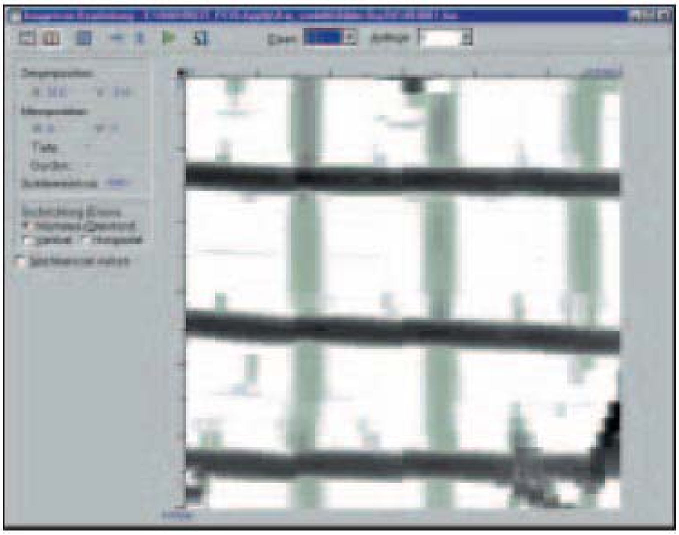

Figure 2.5 Typical image obtained from covermeter measurements (HILTI Corporation)

2.5 Radiography

However x-rays and gamma rays are part of the electromagnetic spectrum (Table 1), the high energy of this group calls for special treatment (McCann & Forde 2001, Bungey & Millard 1996). Employing highly penetrating x-rays, gamma rays, and other forms of radiation that do not damage the part itself, radiography provides a permanent visible film record of internal conditions. X-rays or gamma-rays will penetrate through solid media but will be partially absorbed by the medium. The amount of absorption, that will occur, is dependent upon the density and thickness of the material which the radiation is passing through, and also the characteristics of the radiation. A radiograph is a photographic record produced by the passage of x-rays or gamma rays through an object onto a film (Figure 2.6). When film is exposed to x-rays, gamma rays, or light, an invisible change called a latent image is produced in the film emulsion. The areas so exposed become dark when the film is immersed in a developing solution, the degree of darkening depending on the amount of exposure. After development, the film is rinsed, preferably in a special bath, to stop development. The film is next put into a fixing bath, which dissolves the undarkened portions of the sensitive salt. It is then washed to remove the fixer and dried so that it may be handled and interpreted. The developing, fixing, and washing of the exposed film may be done either manually or in automated processing equipment.

Radiography is capable of detecting any feature in a component or structure provided that there are sufficient differences in thickness or density within the test piece. Large differences are more readily detected than small differences. The main types of defect, which can be distinguished, are porosity, voids and inclusions where the density of the inclusion differs from that of the basic material. Generally speaking, the best results would be obtained when the defect is an appreciable thickness in a direction parallel to the radiation beam. Plain defects such as cracks are not always detectable and the ability to locate a crack will depend upon its orientation to the beam. The sensitivity in radiography depends on many factors but generally if a feature causes a change in absorption of 2% or more compared to the surrounding material, then it will be detectable (Brown *et al.* 2003, Cartz 1995, Derobert 2002, IAEA 2002, McGuire *et al.* 1995, Mitchell 2004).

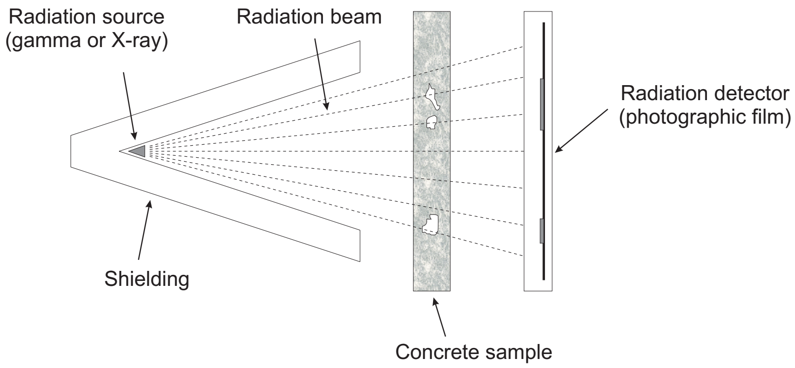

Figure 2.6 - Schematic illustration of the Radiography technique

The first group of radiographic methods is designated as x-rays. In case of x-rays, they are produced when electrons, traveling at high speed, collide with matter or change direction. In the usual type of x-ray tube, an incandescent filament supplies the electrons and thus forms the cathode, or negative electrode, of the tube. A high voltage applied to the tube drives the electrons to the anode, or target. The sudden stopping of these rapidly moving electrons in the surface of the target results in the generation of x-radiation. X-rays require an instrumentation system employing an electrically powered linear accelerator to generate x-rays. As will be appreciated from the medical use of x-rays, significant precautions need to be taken with regard to the use of personnel in the vicinity of an x-ray. However, in electrically lossy materials such as concrete much higher doses of x-ray are required to be effective and thus safety becomes a paramount issue. Higher dosages of x-ray can be used where the component can be put into a sealed container as occurs when one is x-raying baggage at an airport, but when working on a construction site this is a totally different application. A specialist and potentially cost effective application of radiography includes checking for voiding in posttensioned bridge structures. Figure 2.7 shows developed x-ray image of a tendon duct.

Gamma-rays involve a nuclear source and require the nuclear probe to be brought into contact or into a hole drilled in the structure. This technique is less potentially dangerous than x-rays provided that the nuclear source is carefully controlled. However, the gamma-ray procedure emits far less power than the x-ray system, the images tend to be weaker and require longer “stacking” time. Thus a survey which might take 30 min using a high powered x-ray, would take several hours using a gamma-ray procedure.

The last group of radiographic techniques is called neutron radiography. It is an established non-destructive testing technique for identifying internal details, materials and assembly. A neutron flux, which passes through an object, is differentially attenuated by the various materials present. This differential can be recorded on film as the flux emanates from the specimen, revealing details of the composition of the object. This is similar in many respects to x-ray radiography, in which x-rays constitute the radiation flux. Neutron radiography has recently been used to study internal cracking patterns in concrete by causing the cracks to absorb a contrast agent which readily attenuates neutrons (McCann & Forde 2001).

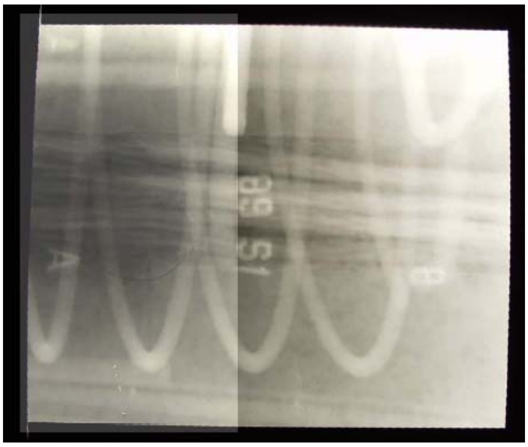

Figure 2.7 - Radiograph of a tendon duct (DMJM HARRIS 2003).Strands and reinforcement of anchorage zone are clearly seen

Chapter 3 - State of the art of Ground Penetrating Radar (GPR)

3.1 Historical notes

The history of GPR starts during first five decades of 20th century. During that time, a great deal of research on audio wave propagation above and along the surface of the Earth occurred. During the period 1950-1960 El Said (1956) reported the use of interference between direct air transmitted signals and signals reflected from the water table to the image of water table depth. In 1961 repeatable indicators of penetration into the subsurface through an ice sheet were reported by Waite & Schmidt (1961).

During the next decade the ice radio sounding activity continued. In addition, applications in other favorable geologic materials started to be explored. In that period Apollo Mission to Mars also started. Key discoveries were the understanding of wave fields about antennas on the ground surface and modified antenna directivity.

In the 1974 Geophysical Survey Systems (GSSI) has been founded. Works presented in Olhoeft (1975), Olhoeft (1987) gave a much better understanding of electrical character of natural occurring geological materials and the relationship between electrical conductivity and dielectric polarization of these materials.

During the period 1975-1990 applications started to grow because of the availability of technology and better understanding of geology. GPR was used to survey potential pipeline routes in the Canadian Arctic (1975). The impact of scattering and the need for lower frequency radars was reported was reported by Watts & England (1976). Archaeological tests were conducted by Dolphin *et al.*, 1978. Geological applications were reported by Annan *et al.* (1988). In addition, the potential use of borehole radar to investigate rock quality in potential hard rock nuclear waste diposal sites become a topic of interest (Davis & Annan 1986).

During the next years new possible applications, for example road investigations and utility mapping has grown (Ulriksen 1982). In the end of 1980's GPR finally started to come into its own during this period. Many of the previous applications were continually explored and movement to higher frequency GPR's with full digital recording appeared in commercial products. Other applications such as soil classification for agricultural needs appeared (Doolittle & Asmussen 1992). Adoption of one dimensional seismic modeling occurred in this period (Annan & Chua 1992).

The real explosion in the advancement of GPR occurred in the mid 1990's. Many groups became interested in that technology. Commercial companies started to grow and increasing their production. On the research side, much attention started to be paid by both the geophysical and electrical engineering community (e.g. digital data processing or 2D numerical simulation occurred). Advances in applications in archaeology, environmental and many other areas expanded. Environmental borehole GPR development was reported by Redman *et al.* (1996).

3.2 Present Research

Amongst other areas of interest, GPR beginning from the end of 20th century, started to become more and more as a civil engineering non destructive technique. In all cases, the structures are made up of materials such as concrete, brick, stone, asphalt, soil and wood, which are transparent to electromagnetic radiowave signals. Electrical properties of these materials are being evaluated more with increased GPR usage (Millard *et al.* 2002, Davis *et al.* 2003)

Nowadays, GPR, due to great improvement of the image processing algorithms in the software and development of higher-frequency antennas, is becoming more and more promising and powerful tool for concrete non-destructive evaluation. Many researchers and commercial institutions throughout all world are very interested in developing GPR technique, which has strong advantages comparing to other famous NDT techniques, for example radiographic NDT techniques, especially in the field of tomography data acquisition, which is one of the objectives of this work. In the chapter 3.5 comparison and examples of supplemental use of radar and other non-destructive techniques is provided.

In case of the non-destructive inspection of civil structures the applications of GPR are numerous and they are widely investigated. They consist mainly of:

- Quality Assurance Control of new structures
- Inspection of the inside of new construction
- Inspection of the inside conditions of existing constructions for rehabilitation purposes

- Inspection of walls, floors, decks
- Inspection of support columns & beams
- Inspection of tunnel walls, roofs, inverts
- Inspection of parking lots, garage
- Location of re-bars, conduits, tension cables
- Location of voids behind walls, under the concrete
- Location of tendon ducts and grouting faults inside them
- Mapping the thickness of concrete layers
- Mapping the thickness of bridge decks

In that research area many authors is dealing with use of GPR for the non-destructive assessment. Below some of the main examples of the reported use are given:

3.2.1 Location of reinforcing bars and tendon ducts

In most applications of radar in civil engineering, this method is used for the location of reinforcing bars and tendon ducts inside the concrete structures (Maierhofer & Kind 2002, Derobert *et al.* 2002, Annan 2003). Localisation of reinforcing bars inside the concrete in the present times is not a very big problem. With a good GPR equipment and imaging software it is quite easy to asses the grid of rebars, but GPR pulses operate over too low of frequency domain to obtain precisely rebar diameters. In the case of tendon ducts, it is quite clear, that plastic ducts with big diameters and no reinforcement inside are quite visible even for 900 MHz antenna. But the problem appears, when ducts are quite small, without rebars and the 900 MHz Antenna it is used. In that case the reflection between concrete cover and a duct can be almost not visible.

Successful application for detecting plastic and metallic tendon ducts with different diameters and shapes is one of the objectives of this thesis and will be described in the chapter 4 and in chapter 5. In case of detection of tendon ducts placed behind dense reinforcement grid, sometimes is not possible to detect the duct using radar technique due to total reflection of electromagnetic waves. Some examples of that application are reported in chapter 6.

3.2.2 Detection of thickness of the elements and assessment of the different elements inside the structure

BAM in Germany has tested many specimens with voids situated at different depths and with various dimensions (Taffe *et al.* 2003, Maierhofer *et al.* 2003, Maierhofer & Kind 2002). Results have demonstrated, that with the radar the depth as well as the angular position of the voids (titled or parallel to the surface) can be determined taking into account the well known propagation velocity of electromagnetic waves in dry concrete. Using a 1.5 GHz antenna voids at depths between 1 and 20 cm can be localized. The same is with detecting a thickness for example of bridge decks, but the frequency of the antenna must be chosen very carefully due to a penetration limitations.

However, simulated voids used in the referred works are easily detected only because the contrast in the dielectric properties between air/concrete interfaces is quite easily seen by modern radar systems. In case of applications for detecting areas with very poorly compacted concrete almost no research is done. This thesis aims to show such possible applications of radar technology.

3.2.3 Cover concrete evaluation

Works presented in Derobert *et al.* (2002), Derobert *et al.* (2003), Buyle Bodin *et al.* (2003) show, that estimation of the concrete cover in bridge deck or in any other parts of the construction is possible and the results can be very quantitive. In case of the referred works, the Empalot Bridge was tested. The coupling of many NDT methods, such as radar, half-potential, resistive measurements, was performed. One of the first steps in radar investigation has concerned the location of the reinforcement. Tests have shown that there is 2cm concrete cover above the reinforcement. As the final conclusion it is said, that a global approach could begin with radar investigation, as high-speed NDT, and then highlight measurements on doubtful areas by punctual measurements (like capacitor, resistive or half-cell potential ones) should be carried out. In case of any doubt, a coring can be done.

3.2.4 Detection of delaminations in bridge decks

Historically, this is the first approach used for the detection of damage in concrete bridge decks. Results of the research carried out on the Van Burren Bridge (Scott *et al*. 2003) and on the specimens in the Department of Civil Engineering, University of Sherbrooke in Canada shows that despite the progress made in recent years in the field of the radar antennas, it is still impossible to detect delamination clearly and without ambiguity with the actual GPR systems. This is certainly due to the dimension of delamination, which is small with regard to the radar wavelength in concrete, to the proximity of delamination to rebars and to the presence of the reflections coming from the reinforcement. Other works in that topic were reported by Buyle.Bodin *et al.* (2003) and Rhazi *et al.* (2003)

3.2.5 Location of grouting faults inside the tendon ducts

Nowadays is a big need for precise estimation of the position and dimensions of grouting faults inside tendon ducts. Poor filling of the post-tensioned tendon ducts and tendon corrosion due to water and potential infiltration of corrosive agents can cause many maintenance problems and can led to a closure of the bridge. Radar is one of the techniques that can be useful in detection of such voids. Works described in (Taffe *et al.* 2003, Derobert *et al.* 2002, Giannopolous *et al.* 2002) show that although it can be estimated with a GPR where probably voids can appear, but it is still difficult to assess a rebar diameter, prestressed tendon corrosion level and wire or strand fracture estimations. Also, GPR is useful rather in random assessment of potential voided areas. Precise measurements must be done with supplementary use of Impact-Echo and other NDT techniques. However, the best results in locating voids in tendon ducts can be achieved with a perpendicular orientation of the GPR antennas.

Second main difficulty in assessing voided areas inside the tendon ducts is a fact that some of the tendon ducts used in bridge structures are made of steel and it is obviously impossible for electromagnetic waves to penetrate through steel. Some results from author´s own research in the application of detecting the voids (grouting faults) inside plastic tendon ducts are shown in chapter 4 of this thesis.

3.2.6 Designated GPR inspection systems for bridges

All mentioned above GPR applications for assessment of the internal structure of the concrete are still under research. In the USA since the 1990's is a boom for NDT inspection techniques, which are very commonly used for regular bridge inspections. It is obvious, that every NDT survey should be followed by the visual inspection and extensive desk study, but these methods cannot provide full information about bridge conditions.

To become NDT survey more efficient, the Hermes system (Scott *et al.* 2003) has been developed. This is a unique and prototype GPR system that was designed as a specialized bridge deck inspection tool. System consist of an array of 64 antennas, which are capable of surveying a deck surface one lane at a time at a scan width of about 1.9 m at normal traffic speed. The data from 64 antennas in the array can be reconstructed using a procedure called wavefield - backpropagation that mathematically estimates the location of the reflection sources imaged in the original raw data. Other works for the development of complex inspection GPR systems for highway infrastructure were reported by Huggenschmidt & De Witte (1998), Huggenschmidt (2002), Warhaus *et al.* (1998).

3.2.7 Determination of dielectric properties of insitu concrete at radar frequencies

During a GPR acquisition it is sometimes necessary to have a prior knowledge of the concrete relative permittivity to know the speed of a radar signal in the concrete. The relative permittivity is very sensitive to the moisture content of the concrete & hence may not be uniform within the concrete depth. To determine the dielectric properties of concrete in the University of Liverpool, a wide band TEM horn antenna has been developed (Millard *et al.* 2002). This kind of antenna operates in the stepped frequency domain, transmitting a steady-state sinusoidal signal over a range of frequencies from 300 MHz-3 GHz. An inversion routine has been developed to determine the dielectric properties of the concrete that caused the reflection (Davis *et al.* 2003). A series of measurements have been undertaken under laboratory conditions to establish the validity of an inversion algorithm applied to the reflection coefficient data received from a TEM horn. The results exhibited a close correlation (<10%) between the reconstructed profile and the known dielectric properties. Further studies in that field were reported by Davis *et al.* (2003), Laurens *et al.* (2003), Olhoeft (1975), Olhoeft (1987).

3.2.8 Use of automated pattern recognition algorithms for the targets identification in GPR data

In every GPR data, significant number of patterns representing material layers or reflections from the embedded elements like rebars, tendon ducts or voids are present. During intensive scanning quite vast amounts of data are acquired and need to be processed and interpreted. The interpretation of those data must be done always by an experienced operator. However in case of large amounts of profiles, time needed for careful interpretation can significantly extend the time needed for acquisition itself. Additionally, sometimes even an experienced operator dealing with large amounts of data can miss some important information present in the radar images. To overcome that problem, some research is done in the field of automatic pattern recognition in the radar data (Shihab *et al.* 2002, Shihab *et al.* 2003, Shaw *et al.* 2005). Presented results are quite promising, but an improvement in the algorithms itself must be done for recognising complex shapes present in the radar data.

3.2.9 Use of Radar Tomography for the inspection of structures

In case of the non-destructive inspection of civil structures the applications of radar tomography are very rare and they are still under research. Especially in case of applications for concrete, tomography is still under research and will be one of the topics of this thesis.

In case of masonry structures this technique can be used generally to map: voids, moisture content and embedded timber elements (Binda *et al.* 2003, Topczewski *et al*. 2006). However due to the high time, hardware and software requirements necessary for acquisition, this technique is still only used to solve localized problems.

3.3 Description and principles of operation of GPR

The ground penetrating radar is a non-destructive technique based on the propagation of electromagnetic radiation, through the ground or other dielectric media. The media of propagation of radiowaves can be of quite variable nature since GPR surveys can be performed virtually in every material which permits the transmission of electromagnetic energy such as dry soil, rocks, ice and water (only in certain conditions), and construction materials, like brick and stone masonry, concrete, asphalt, etc.

3.3.1 GPR equipment

For most of the non destructive applications typical GPR equipment consist of the following elements:

- Antenna or array of antennas with a transmitter and a receiver
- Central unit
- Computer to collect data with software

Those elements can be seen in the Figure 3.1. The control unit of a radar system is an electronic device that is composed by a micro-processor, memory, mass storage medium to store setup and measurement settings, and, possibly, field data. Modern GPR systems are digitally controlled. Data is usually recorded digitally for post-survey processing and display.

The control unit is a frequency independent component, whose primary purpose is to generate electromagnetic pulses with short period and high voltage, and transmit them to the transmitter antenna, which, in turn, is responsible for radiating the investigation surface.

Radar antennas are complex electronic devices, which are specifically designed to optimize ground interaction (as they are used in contact with the surface). They are in charge of radiating the investigation medium with electromagnetic energy and of receiving the reflected energy caused by interfaces between materials of different dielectric properties during its propagation through the material under investigation.

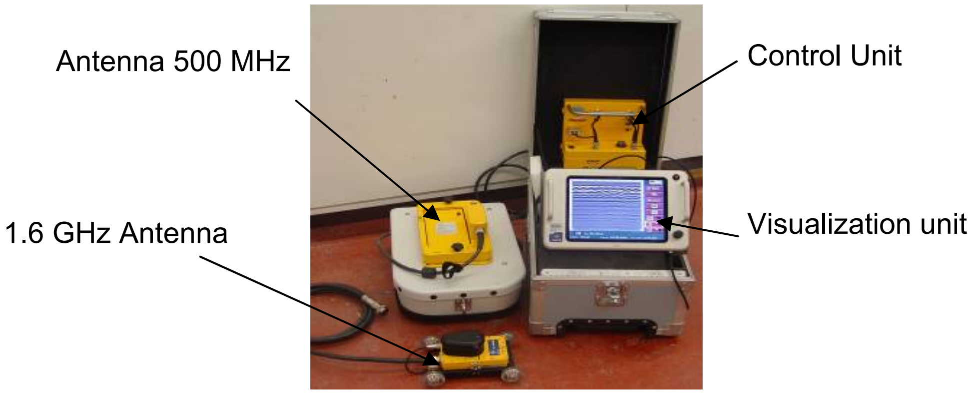

Figure 3.1 - Typical GPR System with 1.6 GHz and 500 MHz antennas from Mala Geoscience

Typical antennas are constituted by transducers, or bow-tie elements, that convert electrical current on the metallic antenna elements into electromagnetic energy that is radiated towards the ground in the form of electromagnetic pulses (transmitter). Inversely, these antennas also convert electromagnetic energy pulses into electrical current, acting as output of the electromagnetic radiation reflected back from the ground (receiver). Radar antennas are characterised by their central frequency, f. Currently, a broad range of frequencies are available, ranging from as low as 10 MHz to very high frequencies such as 2000 MHz and more. In the Table 3 the most common types of antennas are presented with their possible applications. It must be noted that higher the frequency, the lower will be the penetration depth, so it is impossible to have high resolution images at very big depth. Some compromise must be made between required resolution and depth of investigation.

Most known producers of the GPR equipment are Mala Geoscience from Sweden, Geophysical Survey Systems from the United States, IDS from Italy and a Sensors and Software from Canada. More in depth information about the GPR equipment can be found in Malhorta *et al.* (1991), Daniels (2004), and Fernandes (2006).

Table 3 Types of antennas (Geophysical Survey Systems webpage)

	Center Frequency	Depth of penetration	Typical applications
		Ground-coupled antennas	
1	1500-1600 Mhz	0.5 m	Concrete Evaluation
2	900-1000 Mhz	1 m	Concrete Evaluation, Void detection
3	400-500 Mhz	4 m	Engineering, Environmental, Void detection
4	200-300 Mhz	7 m	Geotechnical, Engineering, Environmental
5	100 Mhz	20 m	Geotechnical, Mining, Environmental
6	16-80 Mhz	25-35 m	Geotechnical
		Air launched antennas	
1	2.2 Ghz	<0.75 m	Pavement thickness and road assessment
2	1000 Mhz	1 m	Highway and bridge deck evaluation
		Borehole antennas	
1	100 Mhz	20 m	Waterproof, borehole tomography
2	1000 Mhz	1 m	

3.3.2 Acquisition methods and resultant image types

There exist two main acquisition methods with GPR. The first of them is called **reflection method.** In this method one or more radar antennae are moved over the object surface, to collect near-vertical reflections. This is the most used method in GPR acquisition. In that way, a GPR system sends electromagnetic radiation pulses into the investigation area through a transmitting antenna. The generated electromagnetic wave is partially reflected by changes in bulk electrical properties of the features or objects encountered by the radiowave and the reflection is picked up by the receiving antenna. In Figure 3.2 the general description of this methodology is presented.

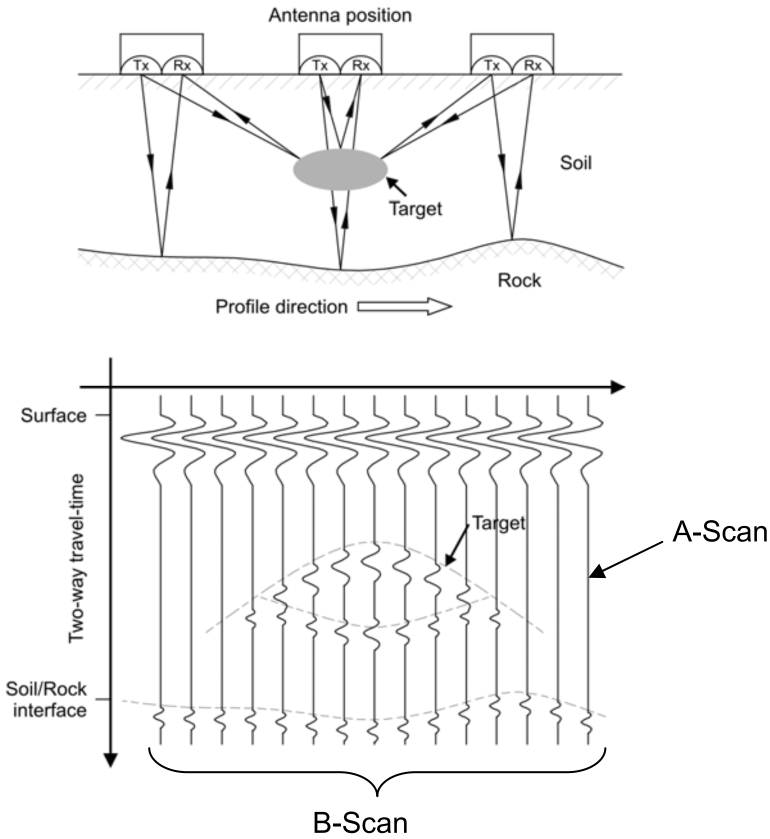

Figure 3.2 - General methodology for GPR field acquisition in reflection mode (upper image) and 2D radargram (B-scan) as result (bottom image). (Fernandes 2006)

When the image is digitalized, it can be then visualized in the various ways:

A-Scans (one-dimensional profiles)

An A-scan is the result of a point measurement. The detected intensity of the reflections is presented as a function of time (Figure 3.2). If the propagation velocity of radar waves in concrete is known, the time scale can be converted into a depth scale. The intensity and the phase of the signal depend on the distance and on the properties of the structures in the concrete.

B-Scans (two-dimensional profiles)

2D vertical profiles are the most commonly used images in GPR survey and further interpretation. The antenna with a transmitter and a receiver is moved along the survey line. If a whole trace was recorded, the plot of these A-scans along a line on the surface in Figure 3.2 is called B-scan (or radargram for radar data). The result is equivalent to a slice perpendicular through the plane in trace direction. In the B-scan the intensities are represented 2 dimensionally in assigned colors or grey scale.

C-Scans (three-dimensional profiles)

3D visualization technique consists in obtaining a 3D volume of the radar data by acquiring a dense subset of parallel 2D radar profiles (Figure 3.3). More in depth information can be obtained in Valle *et al.* (2000), Groenenboom *et al.* (2001) and Kohl *et al.* (2003). Figure 3.3 illustrates how to acquire adequate data in order to allow a precise reconstruction of the 3D body representative of the subsoil features.

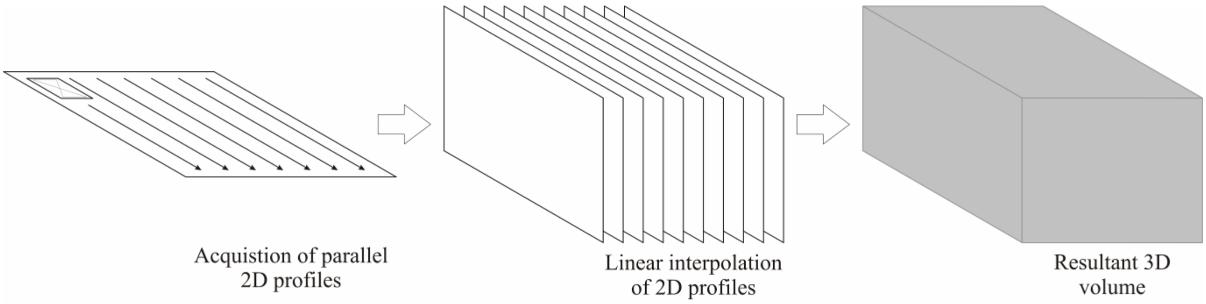

Figure 3.3 - General methodology for producing 3D volumes from field data acquired in reflection mode.

The accurate location of each trace and its parallelism with the adjacent ones is critical to produce accurate 3D volumes. A good control of the starting and end points allows to obtain radargrams with the same length. The separation between each profile is essential to avoid loosing essential information. Although the smaller the separation between parallel profiles the more accurate the final data will be, this can result in a significant amount of data, which processing might not provide useful infromation due to the significant computer resources and time needed for 3D acquisition and processing. Thus, in most practical cases, the Nyquist criterion should be followed (Dokersen 2002) and a separation of 5 cm is usually sufficient to obtain good accuracy. Afterwards, the 3D volume is created by performing a linear interpolation between successive radargrams.

This technique has been successfully applied in numerous applications of NDT investigation of civil structures by providing a visualization of the radar data within the investigated area by showing the results as depth slices (Lualdi *et al.* 2003) or by providing more realistic views of linear objects, such as pipes, cables, rebars and large voids, through isosurfaces (Binda *et al.* 2003). Additionally, it allows non-specialized radar users to better understand radar results by providing more realistic shapes of embedded features. Also use of this technique is one of the topics of that thesis and is presented in the chapters 4 and 5.

Another, more effective 3D data acquisition may be done using orthogonal profile lines. It can enhance the detection of linear and finite-size elements creating images generated from data collected along orthogonal profile lines. This investigation was made by Roberts *et al.* (2002). Results showed that the benefits of using orthogonal profile line data are especially evident when imaging reinforced concrete and utility imaging. In case of concrete imaging the clearest images are obtained by combining x- and y- directed profile line into one coherent image. Also perhaps the most beneficial aspect of using the bi-directional data is the ability to perform spatial filtering operators to improve the detection of linear targets.

For the geotechnical applications, three other ways of performing data acquisition in the reflection mode are possible. Despite the use of those methods has not been reported so far for strictly civil engineering applications, future experiments using those methods are possible. Below short description of Array Beam imaging system, 4D imaging method and Common Mid Point method is given:

Array Beam imaging system

In the ABI 3D method, each discrete point, or cell, in a volume beneath the survey is treated as a reflector (Figure 3.4). A subset of all scans from the survey is combined to obtain a measure of how much electromagnetic energy is reflected from a particular cell in volume, relative to the other cells. The measurement of this reflected energy is provided by combining the signals such energy reflected from particular cell is enhanced and an energy reflected from the neighboring cells is negligible. As a result the coherent signal is obtained, associated with a target cell. A volume image is created by storing the measure of reflected energy from each cell, for all cells in volume beneath a survey. The results presented by Orrey *et al.* (2000) showed that using this technique is very promising, because ABI imaging is not limited to GPR signals. A similar system is being designed for the application to acoustic/seismic data. This kind of system could be very useful in GPR-Acoustic survey.

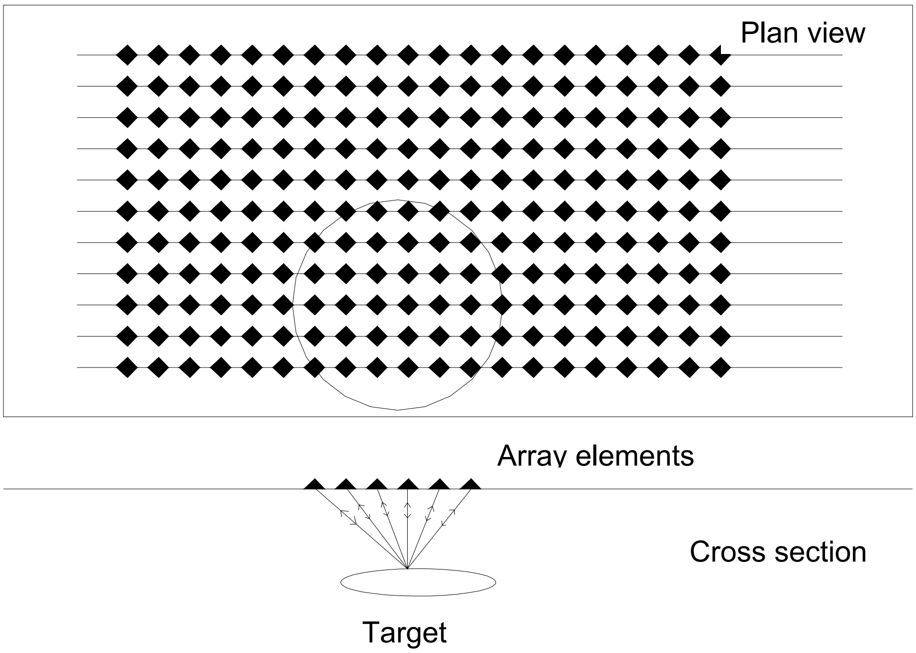

Figure 3.4 - Illustration of ABI method (Orrey et al. 2000)

4D profiles

Four-dimensional or time-lapse three-dimensional ground penetrating radar surveys can be used to monitor and image subsurface fluid flow. This information can be used to create a model of hydro geological properties. In order to obtain quantitative results, tests must be done with a very high positioning precision.

Although the use of 4D profiles is not new (Birken *et al.* 2000), there are still a lot of problems concerning acquisition, data calibration, repeatability and survey frequency, as well as questions on what is really done to observe and to extract of subsurface fluid flow and hydrogeological properties. Also the massive amount of data, which is present in and can possibly be generated from 4D GPR data sets, precludes a manual interpretation. Consequently, 4D data sets have to be processed and visualized in a way that extracts models and allows for data visualization in a semi-automatic way.

Common mid point (CMP) method

The main aim of this method is the collection of data for velocity analysis. The transmitter and receiver are moved in a way that, that the interval between the transmitting and receiving antennas is progressively increased by preserving the mid point between TX and RX coordinates so that the reflections come from the same point in depth provided that reflectors are horizontal planes (Figure 3.5).

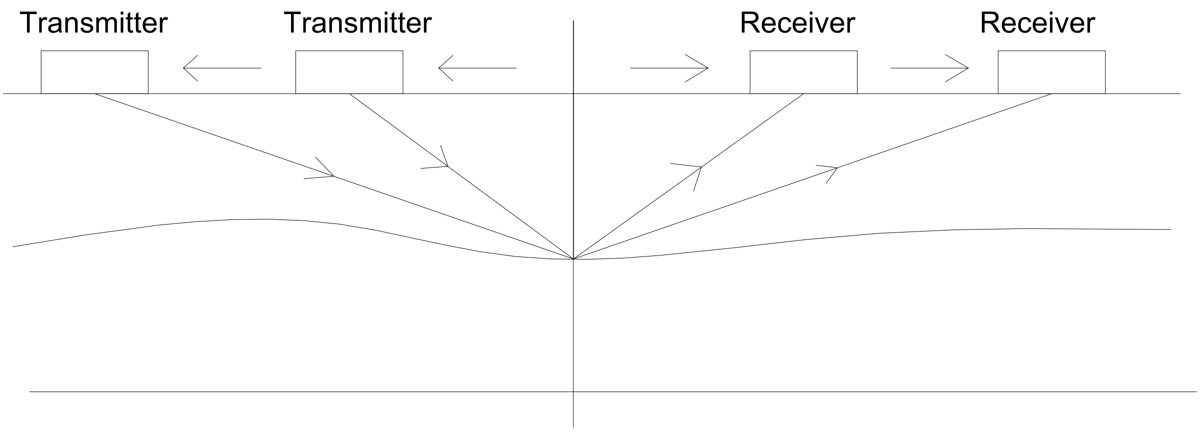

Figure 3.5 - Implementation of CMP method (Reynolds 2002)

The second group of the acquisition methods consists of obtaining the data in the **transmission mode.**

Tomography, which was originally developed in medicine and in several other fields (geophysics) has the aim to reproduce the internal structure of an object from measurements collected on its external surface. Some of the works done for the geophysical applications can be found elsewhere (Becht *et al.* 2004, Brauchler *et al.* 2003, Tronicke *et al.* 2001, Tronicke *et al.* 2002, Tronicke *et al.* 2005). In geotechnical sector, cross-hole tomography is commonly used to check for cracks in rocky ground and to check the state of conservation of deep foundation piles.

In case of structural civil engineering, radar tomography is a quite recent technique. It is generally used to map the interior of objects like columns, walls and other elements that can be accessed from two or more sides. Tomography is a rather distinct processing mode, which makes use of transmission acquisitions. In this acquisition mode, the transmitter and the receiver antennas are separated and located successively in various positions, in order to cover entirely the area under investigation with electromagnetic rays, and the direct pulse is recorded. Figure 3.6 illustrates an example of the tomography of a column where, for each position of the transmitter antenna, the receiver is dragged along the remaining edges of the column in such way that the cross-section of the column covered with radiowaves is maximized. As the distance between them is also known, it is possible to calculate the mean radiowave velocity of the appropriate ray path. Special inversion algorithms (see chapters 3.3.3 and 3.3.4) are used to calculate the velocity or attenuation distributions from the time travel or amplitude information, respectively, to allow the reconstruction of the interior of the column's section, for example (Binda *et al.* 2003). In a radar velocity tomography a typical tomogram shows a velocity distribution inside the cross-section of the structure. In case of electromagnetic waves, areas with high velocity can represent materials with low dielectric constant, while areas with a lower velocity can represent materials with a higher dielectric constant. Areas with a propagation velocity above 0.2 m/ns represent frequently air voids, while areas with a velocity around zero indicate, generally, the presence of steel or of high amounts of moisture.

In a radar attenuation (slowness) tomography operator is able distinguish materials with a high attenuation (e.g. water, sea water, high chloride content, or ferro-magnetic materials) from materials with a low attenuation (air voids, dry timber).

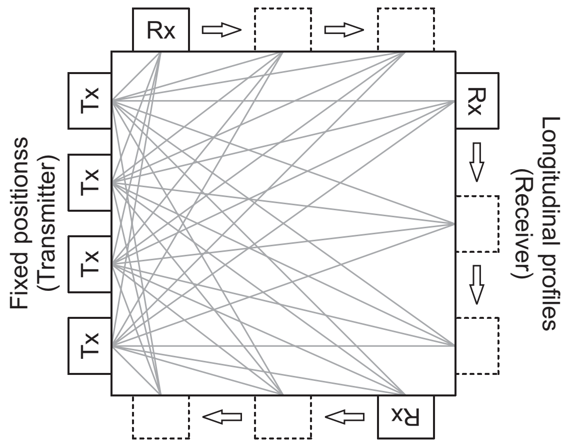

Figure 3.6 - Tomography applied to a square column showing the distribution of transmitters and receivers (Fernandes 2006).

3.3.3 Tomographic Algorithms applied to GPR survey

In mathematical sense, tomography is an inversion procedure that provides for two- or three-dimensional velocity (or attenuation) images between test holes (crosshole tomography) or structural surfaces (crossmedium tomography) from the observation of transmitted first arrival energy. Special inversion techniques are used to reconstruct the hidden structure. In case of civil engineering applications they consist mainly of Travel time and Amplitude Tomography

These techniques are based on the inversion of a single parameter (travel time or amplitude) neglecting other information contained in radar signals. Especially, Travel

Time and Amplitude Tomography, neglecting scattering phenomena and band-limited character of the signals, suffer from low resolution. In general the tomographic problem can be formulated in terms of a line integral:

$$d_i = \int_{T_i(m)} m(x)ds \qquad (3.1)$$

where d_i is the measured data for ray number *i*.

The objective of the tomographic inversion is to estimate the spatial distribution of the property, m(x), characteristic of the medium (x denotes the spatial coordinates). The data is thought being a sum (line integral) of this property along the ray path, $T_i(m)$, from the transmitter to the receiver. The actual ray path is dependent on the properties of the medium, *m(x)*, and is normally the curve which gives the least possible travel time. The complex dependence of the ray paths, T_i, on the properties of the medium, *m(x)*, makes the problem nonlinear. The problem can be linearized by replacing the curves T_i with straight line segments, L_i, connecting sources and receivers.

In a tomography measurement data can be extracted on the travel time and amplitude of the direct wave between transmitter and receiver, e.g. the first arrival. For the tomographic analysis it is assumed that the travel time can be constructed as a line integral of the slowness along each ray.
The problem is then analyzed. The plane between surfaces is divided into a number of cells and the line integral is calculated as a sum where the contribution from each cell is considered in proportion to the length of the ray within each cell. A matrix equation of the following form is then used on the data:

$$d_i = \sum_{j=1}^{M} G_{ij} b_j \qquad (3.2)$$

where d_i represents the data for ray "*i*", G_{ij} the length of ray "*i*" in cell "*j*" and b_j the attenuation or slowness of cell "*j*".

The equation has to be solved with iterative methods:

3.3.4 Algorithms used for solving an inversion problem

To solve non-linear inversion problem for velocity or attenuation tomography, image reconstruction from scattered data must be performed using **iterative algorithms**.

They consist of assuming the object cross-section as an array of unknowns and then solving for those unknowns in terms of the measured projected data. The main shortcoming of these algorithms is that they do not consider diffraction, which can be defined as the interference effects giving rise to illumination beyond the geometrical shadow. Commonly used iterative algorithms are:

1. Algebraic Reconstruction Technique (ART)
2. Simultaneous Iterative Reconstructive Technique (SIRT)
3. Iterative matrix methods (e.g., Gauss-Seidel and Jacobi's method)
4. Conjugate direction/gradient methods
5. Simple iteration
6. A "neural network method"

Those algorithms are mainly used for the travel time tomography. However, these techniques don't consider diffraction. Diffraction becomes important, when the dimensions of the inhomogeneities are comparable to the wavelength of the radiation which is generally the case for microwave and ultrasound NDT in concrete. However if the transmission wave phenomena dominate, in some case it is possible to use algebraic methods. In the other words, algebraic techniques work well for penetrable scatterers. It means that those algorithms are well-suited for the detection of voids or other manmade materials which are transparent for the electromagnetic waves.
Further detailed explanation of different image reconstruction algorithms can be found elsewhere (Berryman 1991; Buyukozturk 1998; Kak *et al.* 1998; Laksameethanasan 2004; Marlekin *et al.* 2002; Meju 2001; Scales *et al.* 2001; Valle *et al.* 1999)

3.4 Propagation of radiowaves in dielectrics

The radar principle is based on the propagation of electromagnetic impulses through a material. Following the Maxwell theory, a dipole excited by a high frequency voltage, generates an oscillating electric field parallel to the dipole (Figure 3.7). The movement of the electrical changes in the electric field generates a magnetic field perpendicular to the dipole.

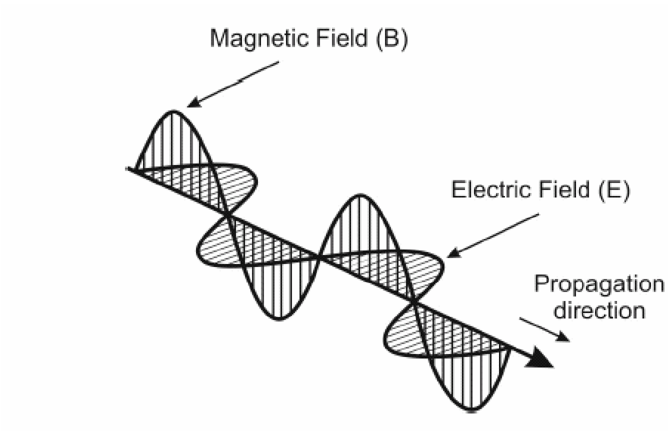

Figure 3.7 - Schematic illustration of the propagation of electromagnetic impulses (Fernandes 2006)

3.4.1 Speed of electromagnetic waves

The manner in which the electromagnetic waves propagate is determined by the physical properties of the material being a medium. The velocity of an electromagnetic wave in free space is equal to speed of light, but the velocity in materials depends on the electrical properties of the material - that is: relative dielectric permittivity *(ε_r),* magnetic permeability *(μ),* and electric conductivity *(σ)* (Neal, 2004*)* and is described with the following equation:

$$w_m = \frac{c}{\sqrt{(\varepsilon_r \frac{\mu_r}{2})(1+\left(\frac{\sigma^2}{\omega^2\varepsilon^2}\right)+1)}} \tag{3.3}$$

The expression w_m for the speed of propagation (equation 3.3) can be simplified when the radio waves propagate through a low-loss material at radar usual frequencies, such as construction materials and most dry soils. This means that the material's conductivity σ is very low and close to zero. Consequently, the term σ / ω, designated by "loss factor", is considered to be null. Moreover, the relative magnetic permeability μ_r is a dimensionless value, defined as the ratio between the magnetic permeability (μ) and the constant of magnetic permeability of free space (μ_0). In non-magnetic materials, μ_r is equal to one. Thus, the general expression for wave velocity can be further simplified for low-loss materials by using (Clark 2003):

$$w_m = \frac{c}{\sqrt{\varepsilon_r}} \tag{3.4}$$

3.4.2 Dielectric properties of materials

The key aspect during many investigations with GPR is to identify the type and state of tested material or to determine the depth of the object found during testing. For that, value of ε_r must be known. Each of the material has its own value of dielectric constant. However, despite the term “constant” in the definition of ε_r, the value of the relative dielectric constant of building materials depends on physical properties (bulk weight and porosity), water content and on the proportion of its constituents.

Table 4 shows typical values of dielectric constant for geological and common building materials. Dielectric constant can reach values of 30 in most dry materials, but rarely exceeds 11 in the case of building materials. In general, ε_r can be taken as an average value from the tables (Table 4) or be determined experimentally. In case of experimental measurements, to estimate ε_r, it is necessary to know the velocity. The velocity in the cross-section can be obtained by the time reflection measurements with a metallic shield (only an average value for the entire tested section is obtained) or by the tomography technique (the values on the entire cross-section are obtained). That technique is one of the topics of that thesis and will be described in detail.

Another important property of each material is its electrical conductivity. As it is shown in Table 4, typical values of electrical conductivity vary from 0 in air to almost 1000. Higher the value of electrical conductivity, higher will be amount of attenuation caused to the propagating waves. For instance in case of fresh water value of conductivity is 1 and in case of sea water is 1000. Salt content and water content are the factors that are increasing the value of conductivity and consequently the value of attenuation of electromagnetic waves.

Table 4 Electrical properties of the materials
(Capinieri et al. 1998, Reynolds 2002, Forde 2004)

Material	Relative Dielectric Constant (ε_r)	Electrical Conductivity (S/m)	Material	Relative Dielectric Constant (ε_r)	Electrical Conductivity (S/m)
Air	1	0	Dry Clay	3	1 - 10
Metal	10^8	1	Saturated clay	15	$10^2 – 10^3$
Fresh water	81	1	Rock	4 - 10	
Sea water	81	$4x10^3$	Dry granite	5	10^{-5}
Dry sand	3	10^{-4} - 1	Wet granite	7	1
Saturated sand	25	10^{-1} - 10	Limestone	4 - 8	0.5 - 2
Soil (dry)	2 – 6		Wet sandstone	6	
Soil (wet)	5 – 15		Dry concrete	6	1
Clays	5 – 40	2 - 1000	Saturated concrete	12	10^8

3.4.3 Penetration depth

Before starting every investigation with GPR, one must be aware of the limitations and possibilities of the penetration depth of the electromagnetic waves in conjunction with the knowledge of the main factors influencing it. It is important to mention, that time spent on careful planning and good data acquisition can be compensated in good, uncluttered data for further post-processing.

The penetration depth is determined by the damping of the electromagnetic waves, which is influenced by three main processes: absorption in the material, loss due to scattering and reflection and loss due to the effective angle of the antenna

Consequently the penetration depth is a function of moisture content, salt content, number of reflection and scattering centres, frequency of the electromagnetic waves and opening angle of the antenna. The typical values of penetration depth for different antenna frequencies are given at Table 3. In the equation 3.5 it is shown that attenuation is directly proportional to frequency. The higher the frequency, the higher will be the amount of attenuation. Also important factor which increases attenuation and highly decreases penetration is conductivity, σ, which is for example

1 for dry concrete and 81 for wet concrete (Table 5).That means that high moisture content decrease the penetration depth significantly, it is a limitation factor using radar measurements in humid environment. Salt content is also one the factors that are increasing the value of conductivity and consequently the value of attenuation caused to the electromagnetic waves.

$$\alpha = \omega\left\{\left(\frac{\mu\varepsilon}{2}\right)\left[\left(1+\frac{\sigma^2}{\omega^2\varepsilon^2}\right)^{0.5}-1\right]\right\}^{0.5} \qquad (3.5)$$

where:

$\omega = 2\pi f$, where f is the frequency, μ – magnetic permeability, σ - bulk conductivity

Material absorption is considered to be the most significant loss mechanism, and causes the conversion of electromagnetic energy into heat energy (Clark 2004). This phenomenon happens generally in materials in which one of the constituents has an elevated conductivity such as sea water.

Another important factor of energy loss is energy scattering and reflection. When an electromagnetic wave hits an object part of its energy is reflected. If there are objects with dimensions of the same order as the signal's wavelength, these objects will cause the electromagnetic energy to be scattered or diffused in a random order (Reynolds 2002). Basic physics behind all used terms is explained in Appendix A.

Moreover, electromagnetic energy can be lost by geometrical spreading of the energy. The radar's signal is transmitted as a conical shaped beam with an angle of 30º to 45º. As the signal travel away from its source, it spreads within a larger area, causing a reduction of the energy density. This loss mechanism increases with the increase in depth of the signal but in shallow measurements that loss can be neglected.

Finally, energy losses can also occur due to the efficiency and equipment electronics. In the first case, during the transmission of the radiowave, losses of the electromagnetic energy can occur between the air and the ground, due to an insufficient coupling between the antenna and the surface (Greenbom *et al* 2001). It means that in such situation the signal intensity can be significantly decreased and consequently penetration depth will be also lower than in normal conditions.

As it was mentioned, antennas signal spreads as a conical shaped beam with certain characteristics (beam width). But when the signal is radiated into tested surface, the electromagnetic field is irradiated in the structure with a radiation aperture smaller than in free space. For example, Shaari *et al.* (2003) showed that the beam width, or angular spread, of the radiowave's signal in concrete was reduced to 60 % of the value found in air. That effect is very significant in the transmission mode, when it is necessary to correctly estimate the maximum angle between transmitter and receiver antennas. When the critical angle between transmitter and receiver antennas is exceeded, refraction of the waves can occur, what can lead to the misinterpretation of the input data. That problem will be further investigated and described in the chapter 7.

Table 5 Values of Velocity, Wavelenght, Resolution and Z_{min} for different types of concrete and different antenna frequencies (Forde 2004)

Material	(ε_r)	Frequency in air [Mhz]	Frequency in concrete [Mhz]	Velocity in concrete [cm/ns]	Wavelength in concrete [cm]	Resolution# [cm]	Z_{min} [cm]
Concrete (very dry)	4	1500	1050	15	14.3	7.2(3.6)	4.8
Concrete (dry)	6	1500	1050	12.3	11.7	5.9(3)	3.9
Concrete (damp)	10	1500	1050	9.5	9.1	4.6(2.3)	3
Concrete (wet)	20	1500	1050	6.7	6.4	3.2(1.6)	2.1
Concrete (very dry)	4	900	630	15	23.8	11.9(6)	7.9
Concrete (dry)	6	900	630	12.3	19.5	9.8(4.9)	6.5
Concrete (damp)	10	900	630	9.5	15.1	7.6(3.8)	5
Concrete (wet)	20	900	630	6.7	10.6	5.3(2.7)	3.5
Concrete (very dry)	4	500	350	15	42.9	21.5(11)	14.3
Concrete (dry)	6	500	350	12.3	35.1	17.6(8.8)	11.7
Concrete (damp)	10	500	350	9.5	27.1	13.6(6.8)	9
Concrete (wet)	20	500	350	6.7	19.1	9.6(4.8)	6.4

Remarks:

1) # - values of resolution in (..) are given for the estimation that depth resolution equals ¼ of the wavelength

2) Highlighted fields represent the typical values for concrete structures

3.4.4 Resolution

The resolution of a particular antenna defines the minimum feature that can be successfully resolved, and, generally, it depends essentially on the central frequency of the antenna. Even if it is widely accepted that resolution increases with increasing frequency, the nonlinearity of the medium in which the electromagnetic waves propagate demands that additional considerations must be made, which are related to hardware characteristics and radiowave properties.
Common materials and configurations that can affect resolution are:

- Metal and closely spaced metallic features
- Water saturated materials
- Wet clay-rich materials
- Materials with high ferro-magnetic content
- Heterogeneous materials

It has to be considered that reflections at metal inhomogeneities or at interfaces to metal plates yield to a reflectivity of 100 %. Thus, investigations of the inner conditions of metallic tendon ducts, of steel fiber reinforced concrete and of concrete structures with a high amount of reinforcement (distance of reinforcing bars is less than 7 cm) are not possible.

Vertical resolution is a measure of the ability to differentiate between two signals adjacent to each other in time. Simplistically, vertical resolution is a function of frequency. Each radar antenna is designed to operate over the range of frequencies (bandwidth) where the peak power occurs at the centre frequency of the antenna. Depth resolution is determined by GPR measurement bandwidth. Maximum vertical resolution can be given as $0.5 \times \lambda$ (Padrataz & Forde 1995), where λ is the wavelength. However, there exist also opinions that maximum vertical resolution can be given as $0.25 \times \lambda$ (Forde 2004). However, it must be noticed that smaller objects can also be detected, such as small metal reinforcement in concrete structures or masonry bed joints, even if nothing can be said about their size. A direct result of this formula is that higher frequencies ensure a better resolution by having a smaller wavelength than lower frequencies.

The wavelength can be obtained from the following equation:

$$\lambda = \frac{V}{f} \tag{3.6}$$

where *V* is a propagation velocity, *f* is the frequency

Even if the bandwidth of the signal can be increased indefinitely, most materials contain water. Increasing bandwidth means using higher GPR frequencies. It theoretically can give higher resolution of the signal. However, the presence of small amounts of water can cause strong signals absorption above 1000 MHz. For most practical situations, GPR bandwidth greater than 2000 to 3000 MHz is usually not possible.

Studies by Padaratz and Forde (1995) showed that the wavelength of the electromagnetic signal decreases with the central frequency and dielectric constant of the investigated material, so in reality, the resolution is less than ½ or ¼ of the wavelength, due to complex nature if the source waveform and the ground responses. Many examples are shown in the Table 5, where it is clearly indicated, that nominal central frequency of the radar signals in air is much higher that in the different materials. For example, for the concrete with ε_r = 10 real signal frequency is 1050 MHz, wavelength is 14.3 cm, and resulting resolution is in reality 3.6 cm, while if we would take the theoretical antenna frequency of 1500 MHz, the wavelength would be 10cm and resulting resolution would increase to 2.5 cm.

Horizontal resolution is inversely proportional to $\sqrt{\alpha}$, where α is the attenuation coefficient (equation 3.5). The horizontal resolution Δx, i. e. the separation of two adjacent reflection centers, is determined by the diffraction phenomena observed during the reflection and therefore depends on the depth in the material, the damping of the electromagnetic waves in the material, the antenna aperture and the frequency. Under optimum conditions a horizontal resolution of 1 cm can be achieved.

3.4.5 Minimum depth of a detectable target (Z_{min})

For radar operators it is important to know, at which minimal depths the targets can be successfully located. Some research was carried out to give an answer to that question. Forde (2004) suggests taking $\lambda/3$ as the depth of the first detectable target, which is useful when targets are located at shallow depths, such as in problems like material detachments, superficial cracks, and thin layered materials. To solve those problems, it is necessary to use antenna with a very high frequencies. However, these antennas are characterized by a rather low penetration. The values of the vertical resolution and minimum depth of a detectable target (Z_{min}) are given in the Table 5.

3.5 Combinations of GPR and other NDT techniques

It has been verified by many authors (Boule-Bodin *et al.* 2003, Derobert *et al.* 2002, Derobert *et al.* 2003, Krause *et al.* 1997, Maierhofer *et al.* 2003, Scott *et al.* 2003, Rhazi *et al.* 2003) that the application of a single NDT technique does not always provide quantitive and reasonable results. It is true almost in all the cases, that NDT engineers have to use the combinations of many different techniques to obtain good results. Because the combined use of GPR and other techniques is one of the most commonly used approaches for bridge non-destructive assessment, some of the most known groups of NDT used for concrete evaluation are presented below:

3.5.1 GPR and thermography

Combination of these two NDT techniques was shown in Maierhofer *et al*. (2003) in the application of detecting shallow voids in concrete structures. Using 1.5 GHz radar antenna voids between 1 and 20 cm were localised. Using impulse thermography, voids up to depth of approximately 10 cm were detected after a heating duration of 5 min indicating that with this method the voids can be detected very fast. From transient curves, not only the depth and the shape of the voids can be determined but also a thermal properties giving information about the material. However, one of the limitations of IR thermography is that it provides no information about the depth of the defects. To solve this problem, it can be combined with a GPR.

3.5.2 GPR and impact echo

After tests on a concrete specimen shown in Krause *et al*. (1997) it seems to be quite clear, that radar and impact echo can be used as the supplementary techniques for detecting voids in a steel tendon ducts. Radar can detect a steel tendon duct, but electromagnetic waves cannot penetrate through metal. In conclusion, it is said, that GPR can be used to primarily localize metallic tendon ducts, while impact echo method can asses voids inside those found metal tendon ducts. Another work reported in Derobert *et al*. (2002) shows that GPR as a fast NDT technique should be implemented first and then in case of detection of doubtful areas Impact echo examination should be preceded on specific points.

3.5.3 GPR, ultrasonic echo and impact echo with data fusion method

To obtain complex image of the internal elements in a concrete structures work led by German research group FOR-384 was presented (Kohl *et al.* 2003). In the referred work, scanning was made using the combination of GPR, ultrasonic echo and impact-echo methods. Each of these methods has its own advantages and disadvantages.

Radar can detect metallic reflectors in concrete (metallic ducts and concrete reinforcement) very well. This method is not able to locate defects behind these reflectors (injecting defects, defects behind close concrete reinforcement), because the electromagnetic waves are completely reflected at the metallic interfaces.

The acoustic methods are able to compensate this deficit i.e. acoustic waves can penetrate through metal. But acoustic waves in the ultrasonic range are completely reflected by air layers. Air layers have smaller influence on radar propagation, so that both methods complement each other. In order to be able to combine the NDT-data from several methods records at the same volume, the different data sets modes of signals must be adapted. Also the different radar antenna frequencies must be used to obtain the best scan results. For example, in the B-scans recorded with the 1.5 GHz antenna, the reinforcement bars and the tendon duct are well recognizable compared to the B-scans measured with the 900 MHz antennas. The resolution of reflections from the tendon duct und reinforcement bars obtained with the 900 MHz antenna is much worse. The advantage of the 900 MHz antenna is the higher penetration depth. Also use of the different antenna polarization (horizontal or vertical) can be used to obtain the best results.

To combine advantages of all these methods and systems (different data sets) data fusion is needed. Data fusion is able to contribute to the improvement and simplification of the interpretation of the experimental data. Some information can be enhanced by visualization data sets recorded with different methods from the same volume. Also the combination of numerical simulations and experimental results of measurements can contribute to a better interpretation. Last but not least the storage requirement for saving data sets is decreased, because only the combined data set with the sum of information is being saved.

3.5.4 GPR and half cell potential

Tests presented in Derobert *et al*. (2003) and also in Rhazi *et al*. (2003) showed that in case of detecting a corroded areas in reinforced concrete a global approach could begin with radar scanning, as a high-speed NDT, and then highlight measurements on a doubtful areas by a punctual measurements (like half-potential ones) for corrosion measurements should be carried out. In case of any doubt, a coring can be proposed.

3.5.5 GPR and Radiography

Radiography is often used in NDT tests as complementary method to the GPR, especially as the tool for the detection of cables in the tendon ducts. Tests results on a Bridge in Farum, Denmark (Shaw & Xu 1997) gave such a conclusion, that x-ray radiography can give more accurate results, than GPR, but of course is much more dangerous, due mainly to a high radiation. It requires safety closures of the investigated area, is much slower in use and requires two-sided access to the test location. Another investigation presented in Derobert *et al*. (2002) on the Pont Neuf Bridge shows undoubtedly, that best combination of current NDT techniques seems to be GPR followed by gammagraphy. While the GPR can rapidly detect the position of tendon ducts, radiographic methods can be applied for the detection of grouting faults or corrosion within the tendons itself.

3.6 Positioning systems applied for the structural inspection

3.6.1 Introduction

As it was mentioned before, during scanning the structure, the exact position of the antenna must be estimated very precisely. In some cases, hand scanning does not provide sufficient accuracy or is just not possible due to the access problems. To overcome this deficit, different positioning or scanning systems are subject of research within NDT community. In this chapter a few positioning systems, both commercial and non-commercial will be presented with their own advantages and disadvantages are shortly presented.

3.6.2 BAM automated scanning system

That scanner it is applicable for the inspection of different bridge types specified in by the end-users; therefore certain adjustments are required, like e.g. work overhead or on inclined walls. Two of five automatic scanning systems available at BAM can be seen in Figure 3.8. It is possible to attach to the scanning head different types of transducers, like radar antennas or acoustic transducers. In case of radar measurements, advantages include millimeter accuracy of the scanned region, constant and quite high speed of scanning, movement of the antennas above the tested surface what can help avoiding the problems with irregularity of the surfaces.

Figure 3.8 - Scanner system under development for automated measurements of radar, ultrasonic and impact-echo in parallel traces (x- and y-direction) at BAM (www.bam.de)

3.6.3 Improved optical positioning for GPR based structure mapping

Typical existing positioning systems generally require some fixed patterns or require automation scanning for obtaining parallel traces; the optical positioning system is capable of transducing movement anywhere on a 2D plane, facilitating arbitrary scanning patterns. An arbitrary scanning pattern is much faster than one that requires the user to stop at each point on a fixed grid and press a button, or even one which involves surveying parallel lines. With such system, the user starts collecting data at a waypoint, periodically moving over another waypoint and pressing a button to add a calibration marker to the data. Typically a roughly serpentine pattern is used to cover the area.

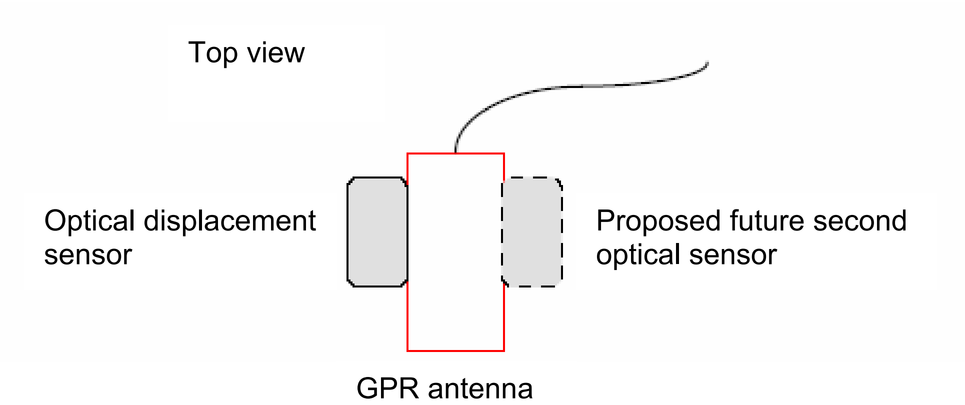

Figure 3.9 - Optical positioning system for GPR (Doerksen 2002)

The proposed system (Figure 3.9) is comprised of an optical computer mouse rigidly mounted to a GPR antenna. Compatibility tests were first performed to ensure that this mounting arrangement did not cause false reflections in the returned radar data. The used optical sensor is capable of capturing over 1500 frames per second, providing a rated accuracy of 450 DPI at a tracking speed of up to 25 cm/s. The sensor's DSP calculates the differences between two frames of the data, and determines the relative displacement along two vectors perpendicular to its axis. Values for Δx and Δy are buffered internally and made available as requested. Position information is indexed by GPR trace number for post-processing. Further information about the system can be found in Doerksen (2002).

3.6.4 Pad System for Georadar (PSG)

Department of electronic engineering, Politecnico di Milano, Italy has developed very simple and easy to use positioning system for the GPR acquisition process (Lualdi & Zanzi 2003). PSG (Pad System for Georadar, patent of Politecnico of Milano) consists of a soft pad whose surface is modelled with parallel tracks that are a few millimetres high. A mate pad must be applied on the bottom of the antenna (Figure 3.10). The total thickness of the mating pads is about half a centimeter to keep the antenna in close contact with the soil.

The GPR antenna is dragged along the tracks so that parallel and regularly spaced profiles are rapidly executed. Moreover, the system presents the important benefit of ensuring that the antenna orientation does not vary during the survey. Thus, during structural inspection, PSG can be placed directly on the inspected surface, allowing to the operator rapid scanning of closely spaced 2D profiles. Just after the testing, system can be easily rolled and moved to the next test location.

Figure 3.10 - Illustration of the PSG system

Chapter 4 - Tests on the concrete specimens

The following tests were performed with cooperation of Federal Institute for Materials Research and Testing (BAM) in Berlin, Germany in the frame of “Sustainable Bridges” European Project. During these experiments, innovative procedures for the radar technique were developed and applied on the laboratory specimens.

Firstly, results from the test specimen constructed at the University of Minho are presented. On that specimen reflection acquisitions were carried out to show the comparison and advantages of 3D imaging over 2D imaging for the verification of structural geometry and integrity inside simulated concrete bridge deck.

Secondly, the results from the tests on the two big concrete specimens at the BAM laboratories are presented. During those measurements, the radar tomography technique was used for the verification of structural geometry and integrity inside concrete specimens.

In the final stage of laboratory tests, more detailed error checking procedures for the tomography technique were developed and significant problems present in the tomography were pointed out. After those calibration measurements, the procedures for the data acquisition and processing were improved and validated during field measurements on the three concrete bridges (see chapter 5).

4.1 Concrete slab built at Minho University

One of the methods for evaluating structural geometry and integrity can be 3D imaging. Previous research carried out, showed that technique is able to detect voids present inside concrete structures. However, use of that technique was not reported so far for the detection of poorly compacted concrete present inside real bridges. Thus the purpose of that testing is to validate the GPR technique with 2D and 3D imaging for the detection of structural geometry and integrity inside simulated concrete bridge deck.

4.1.1 Description of the test specimen and methodology

The concrete specimen was specially built to simulate a part of a typical concrete bridge deck, being square in plan, with dimensions of 2.50 x 2.50 m, and a thickness of 0.32 m. Additional elements were placed inside, chosen from typical elements used in the construction of structural elements in reinforced and prestressed concrete bridge decks. Typical defects and anomalies that may occur during construction were also reproduced in the specimen. A general view of the features inside the slab before being filled with concrete is illustrated in Figure 4.1a, while a general view of the cast specimen is illustrated in Figure 4.1b.

(a) (b)

Figure 4.1 - General view of the concrete specimen. (a) Overview of the features and objects placed inside the specimen (before casting) and (b) final view of the slab after casting

Three PVC tendon ducts (one with 110 mm diameter and two with 35 mm diameter) were placed inside the slab. The larger tendon duct is generally used for the introduction of post-tensioning cables, while the two smaller tendon ducts are simulating simple mono-strands, one being straight and the other curved. The objective was to detect the location of all the ducts by radar with special attention paid to the curved duct. Measurements were initially performed without strands inside the smaller ducts in order to further challenge the technique. Half of the large duct was fully grouted and the other half partly grouted in order to evaluate the difference between fully filled and partly filled tendon ducts. The other simulated defects included a poorly vibrated or lower density concrete, represented by blocks of concrete with insufficient binder, low density concrete (light-weight concrete), large voids and blocks with inclined surfaces. Furthermore, one empty glass bottle, one clay brick, wood and mortar prisms and two metallic bars were also inserted. In addition a precast concrete element (class C30/35; 70 mm thickness) was placed at the bottom of the specimen and occupied half of the total area of the slab test slab (Figure 4.2). The leading edge of the precast element can be seen in the centre of Figure 4.1a.

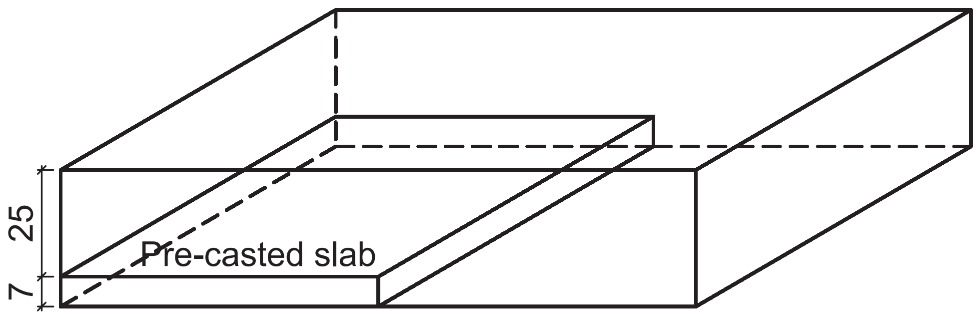

Figure 4.2 - Location of the precast element inside the concrete specimen.

The remaining test area was filled with concrete (class C30/35) without any steel reinforcement bars, except steel grids at the bottom of the specimen and on the upper surface of the precast slab in order to prevent premature cracking and to increase the specimen's resistance. The grid constituted steel wires with 2 mm diameter and square cells with 0.15 m offset. An additional steel part was inserted at the contact area with the precast element in order to be able to easily detect it in the radargrams.

The GPR system used for the acquisition was the RAMAC/GPR from MALA Geoscience. The system was equipped with a high resolution antenna with a central frequency of 1.6 GHz due to the small dimensions of the targets of this investigation. A digital hip-chain was used as positioning system and as pulse trigger.

In order to construct accurate 3D images, longitudinal 2D profiles closely spaced (50 mm apart) were drawn over the testing area (Figure 4.3). Such a density of longitudinal profiles was essential in order to obtain a realistic 3D image and necessary to map all possible internal elements. Two areas of interest have been selected and are reported in Figure 4.3b: one constituted the part of the specimen (Area 1 in Figure 4.3b) where most of the deficiencies were located (poorly vibrated concrete, voids, etc.) and half of the precast slab; another area (Area 2 in Figure 4.3b) considered Area 1 again and also the three simulated tendon ducts. Area 1 was acquired parallel to the tendon ducts, whereas radar acquisition in Area 2 was carried out in the direction perpendicular to the tendon ducts, in order to maximize the return of the signal reflected by them.

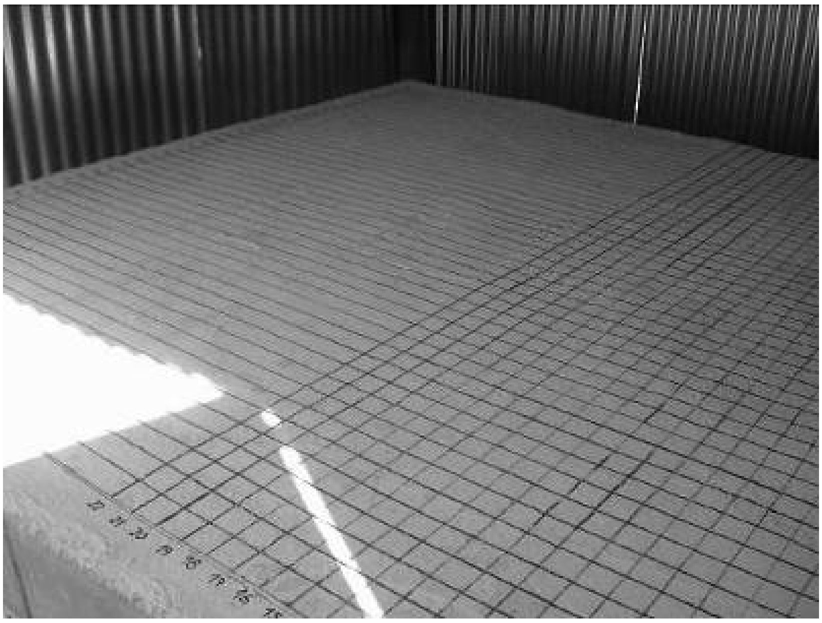

(a)

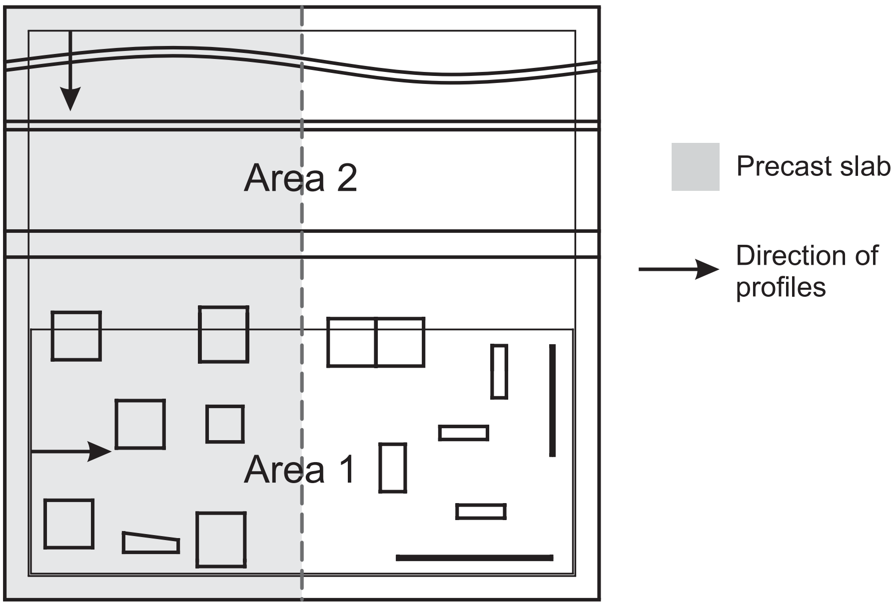

(b)

Figure 4.3 - 3D measurements. (a) Partial view of the grid drawn over the surface of the slab and (b) location of the areas of interest.

4.1.2 Results

2D profiles provided the depth and location information about elements located under each profile. Afterwards, all profiles were merged in a 3D volume, and time slices were extracted at different depths, which provided additional information such as shape and location of elements. The first area to be discussed is Area 1 followed by Area 2, where the results from 3D reconstruction present a clear advantage over 2D profiles in the case of bridge deck investigation.

Results from Area 1

The objective in this test area was to determine the position and shape of all internal elements, position of the opposite surface of the slab and the position of the precast slab. Figure 4.4 illustrates one radargram that shows the opposite surface at 7 ns of depth. The opposite side was detected by means of the hyperbolas reflected by the steel mesh, which was used to prevent concrete shrinkage, located at the bottom of the slab and almost in direct contact with the surface. As these hyperbolas were considered to correspond to the bottom of the slab, the 7 ns were considered to correspond to the 0.32 m of thickness of the slab. This resulted in an average radiowave velocity of 92 mm/ns, which is low for concrete. Typical velocities in dry concrete are 90-130 mm/ns. The precast slab was detected in the first half of the radargram, at 5 ns from the surface, with a thickness around 1.5-2 ns (0.07-0.09 m).

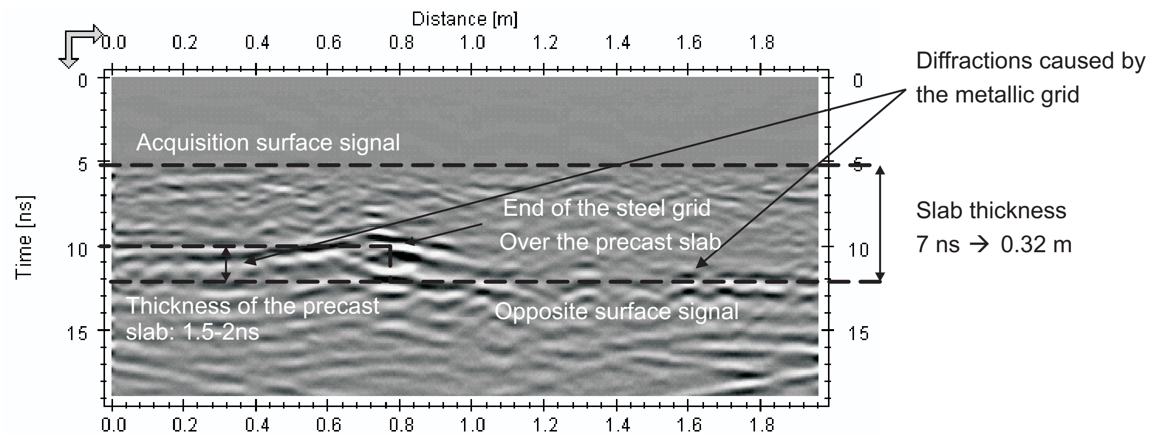

Figure 4.4 - Detection of the opposite surface of the slab as well as the precast slab.

Figure 4.5 shows additional profiles from where poorly vibrated concrete / light-weight hollow concrete elements and the steel bar were successfully detected. From the radargrams, the length of the concrete elements was acquired with a rather satisfactory accuracy (the dashed boxes correspond to the dimensions of those elements). The height computed with the velocity of 92 mm/ns resulted in lower values than the real ones, which seem to suggest that the velocity within these concrete elements is slightly higher than in the rest of the specimen (radiowaves in very porous concrete have indeed a higher velocity than in normal weight concrete). The location of the objects is also accurately described with respect to the central axis in case of the two concrete blocks in the 22nd profile. The radargram reported a depth of 0.125 m, while the accurate value according to the specification drawings was located 0.12 m. However, one element in each profile from lines 4 and 22 was not detected. It must be noted that these elements have a triangular shape (see also Figure 4.1a) and that the incident waves in such surfaces are scattered in a direction far from the receiver position. Thus, they are very difficult to detect.

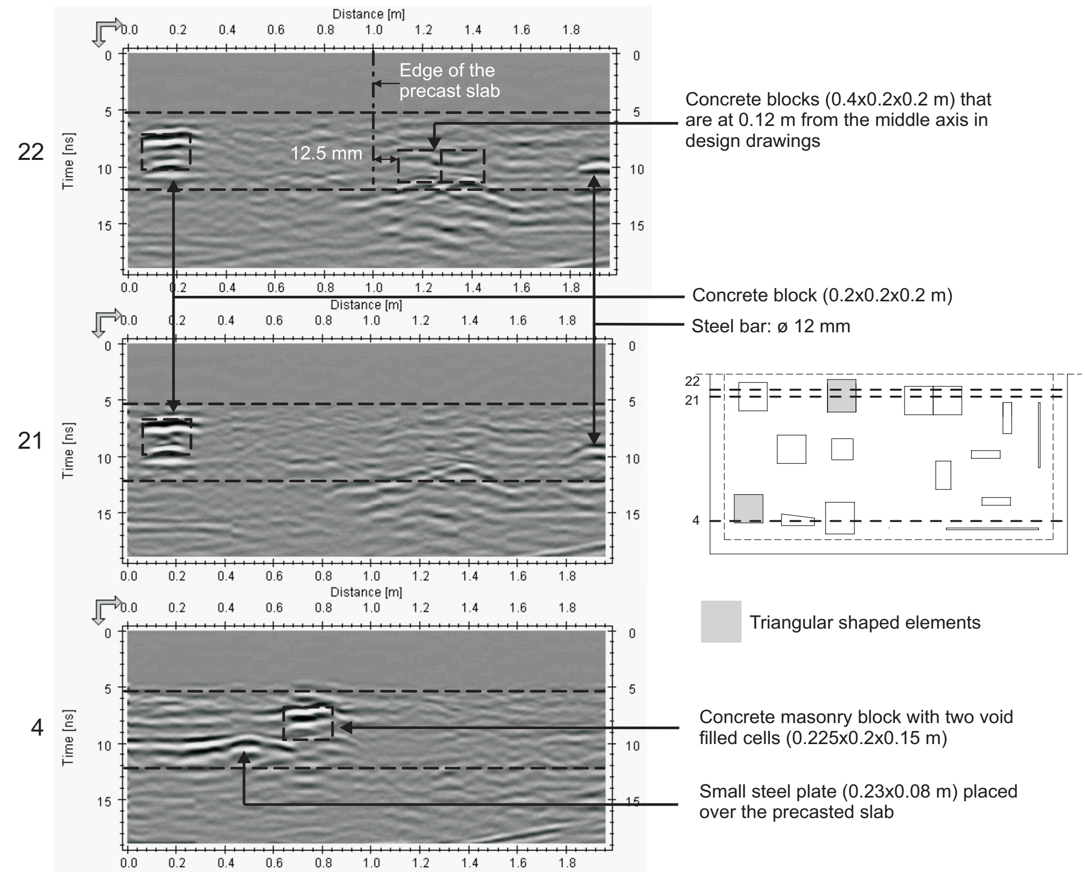

Figure 4.5 - 2D profiles of the 22nd, 21st and 4th acquisition lines, respectively, from top to bottom.

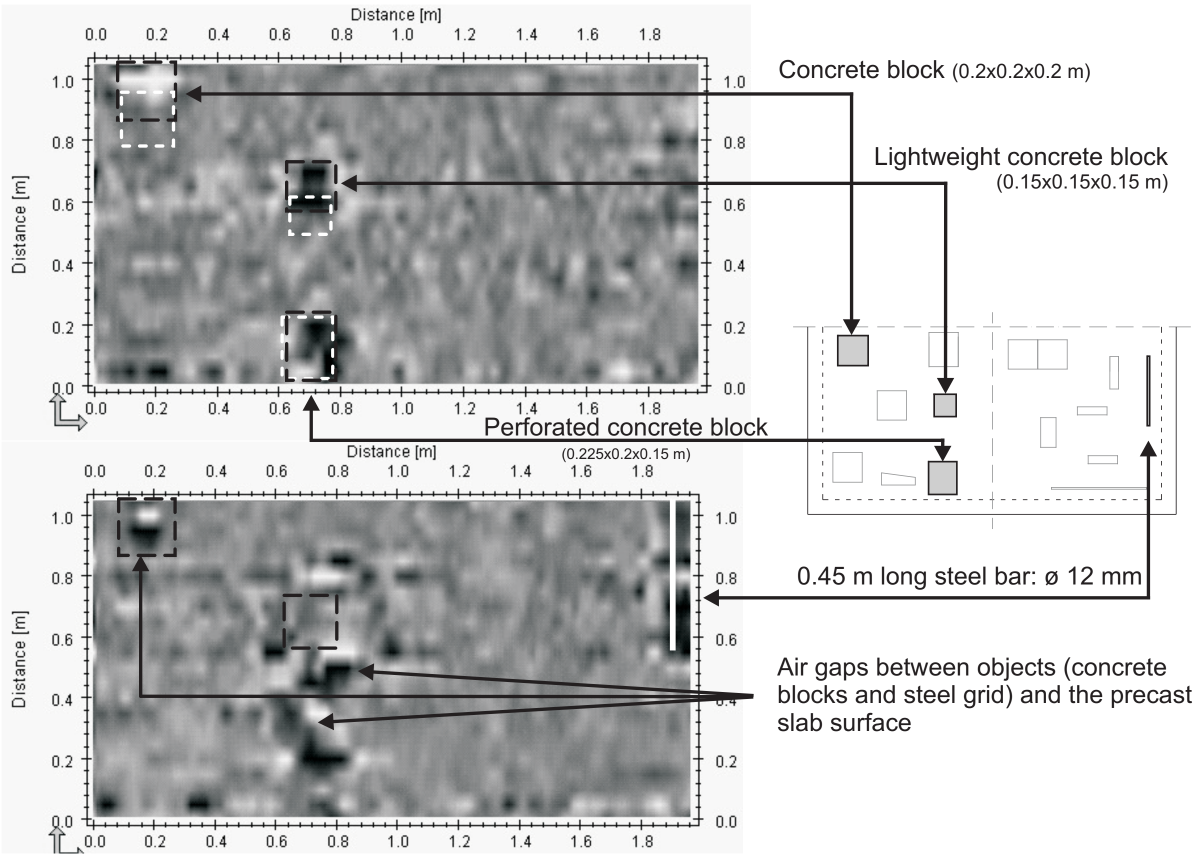

Figure 4.6 - Time slices from the migrated 3D volume with accurately positioned objects that are not in their original location. Depth of the slices: 0.10 and 0.185 m, respectively, from top to bottom.

Results from Area 2

The second test area considered for the investigation corresponded to the whole slab surface (see Figure 4.3), with the objective of mapping the features located in the interior of the slab plus the three tendon ducts. Of particular interest was the correct acquisition of the curved shaped tendon duct and of the larger duct, which had half and fully grouted sections.

The analysis of 2D profiles showed that the three tendon ducts were detected in all cases. The radargram in Figure 4.7 illustrates the three tendon ducts, where it appears that the two smaller diameter tendon ducts (35 mm) were detected by their upper interfaces, while in the case of the larger diameter tendon duct (110 mm), both interfaces were detected. This phenomenon is associated to the short wavelength (λ) of the 1.6 GHz antenna, which is 187.5 mm, from where an expected resolution of 47 mm, taken as $\lambda/4$ (Forde 2004). Because the diameter of the smaller tendon ducts is lower than 47 mm, the signal from the upper interface of the smaller tendon ducts covers the lower interface signal. Only the signals reflected by the boundaries of the largest tendon duct were visible due to the fact that the distance between them was longer than the signal's expected resolution. However, this depends on the contrast between the tendon duct and the infill material (air, grout or steel bar).

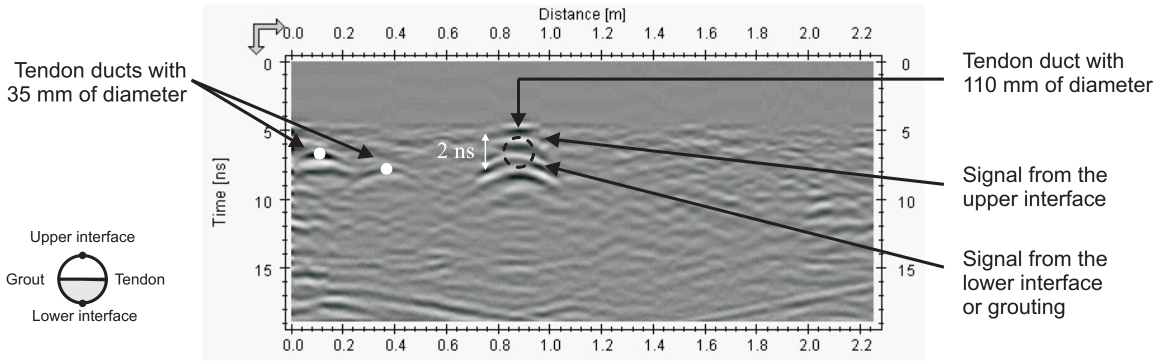

Figure 4.7 - First profile from area 2 at 0.10 m from the border.

The analysis of the time slices illustrates the adequacy of the results. It was possible to identify the three tendon ducts, as well as the position and shape of most of the other targets. The radargrams illustrated in Figure 4.8 clearly show several concrete blocks as well as the steel reinforcement bar that was perpendicular to the direction of radar acquisitions. The square/rectangular shape of the objects was quite reasonably detected after the migration of the data. However, some of the objects placed in the interior of the concrete specimen could not be identified because they were oriented parallel to the radar profiles (the plastic bottle and the clay brick) while others were too small or too deep to be reached by the radiowaves (lightweight concrete cube, mortar and wood prisms), and another had insufficient contrast (concrete cube with 50 mm edge).

The mapping of the three tendon ducts is shown in Figure 4.9. All ducts were correctly detected and the curved duct was also well defined. Regarding the largest tendon duct, although it had been correctly detected, the intensity of the signal amplitude was not uniform along its entire length. As it can be seen in the 2nd and 3rd radargrams, the radiowave energy seems to be higher in the bottom part of the section, where the tendon duct section was half grouted. The air in that area could explain the higher energy due to the higher contrast between dielectric constants of concrete ($\varepsilon_{r,\ concrete}$ = 6) and air ($\varepsilon_{r,\ air}$ = 1), which does not exist between concrete and grout. Thus, it seems also possible to detect differently filled tendon duct sections by analyzing the amplitudes of the reflected signals.

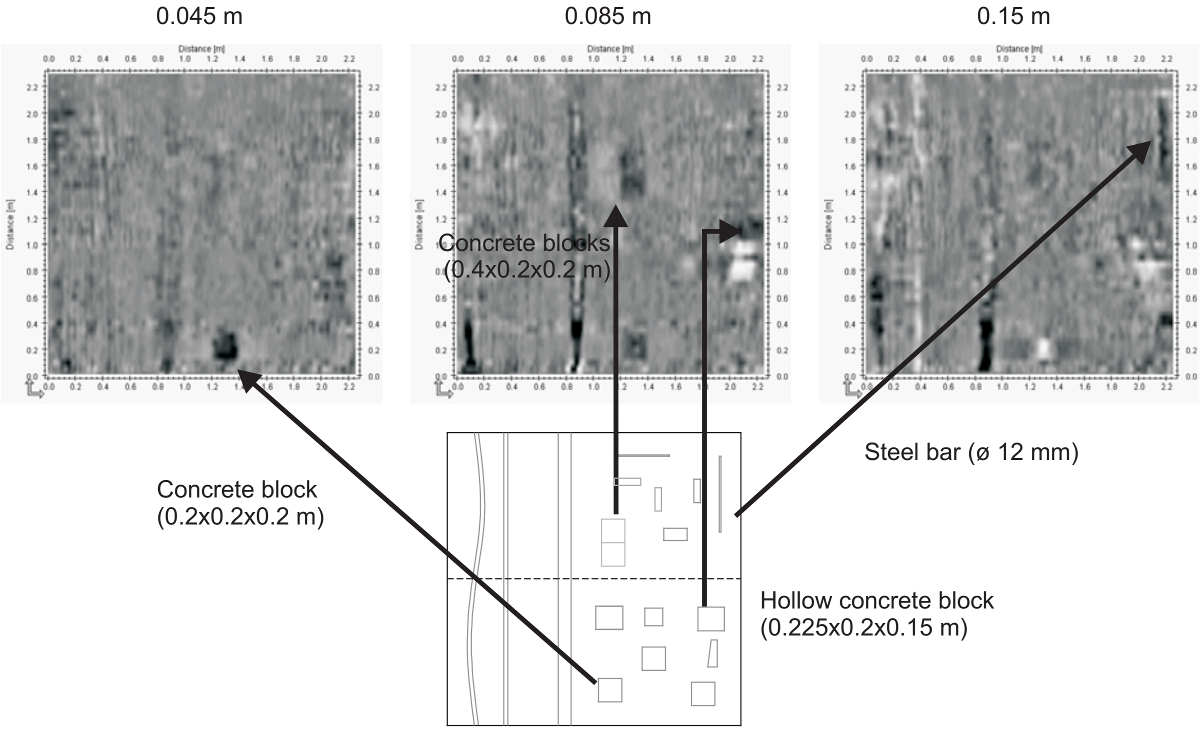

Figure 4.8 - Time slices after migration where are observed some of the concrete blocks and the steel bar perpendicular to the acquisition direction.

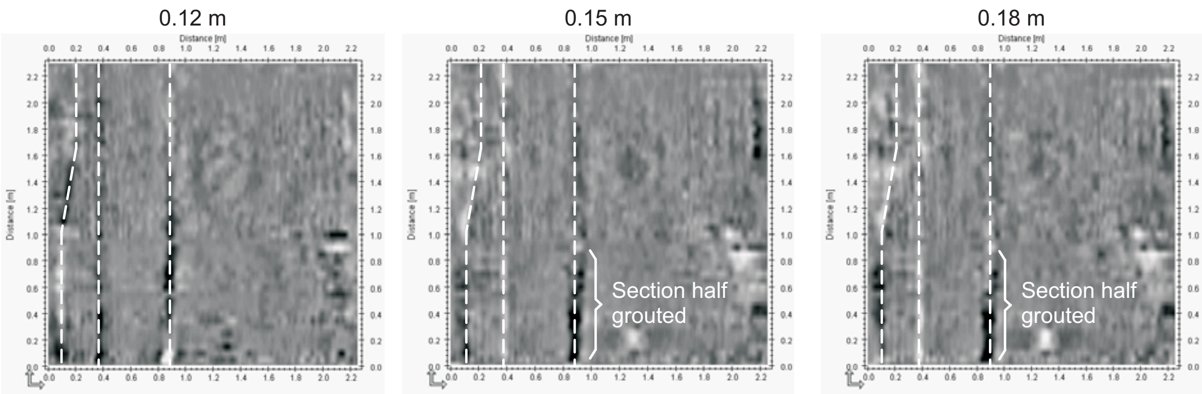

Figure 4.9 – Time slices showing the three tendon ducts.

4.1.3 Summary

The use of GPR with 3D reconstruction showed good potential in geometrical evaluation of structural elements as well as in the mapping of typical defects and inclusions frequently found in structures. In the case of prestressed concrete elements, the location of tendon ducts, including the curvature of a curved tendon duct, was correctly assessed.

Nevertheless, not all targets could be resolved due to their unfavourable orientation with respect to the direction of the profiles. Because the profiles started and ended 0.10-0.15 m after and before the specimen end, some objects located very close to the edges of the specimen were also not detected. Moreover, the poor contrast between materials resulted in poor reflectivity and thus weak detection, particularly in the case of a lightweight concrete specimen placed inside a concrete mass. Finally, triangularly shaped inclusions did not reflect favourably for detection by the radar signals.

The adopted antenna, with a central frequency of 1.6 GHz, exhibited very good resolution and high accuracy for 3D reconstruction. This advanced technique can be already used competitively by construction companies, design offices and structure and infra-structures owners that seek accurate geometrical and condition information by using cost-effective solutions, at a moderate budget when compared with construction, repair or rehabilitation costs.

4.2 Concrete slabs built at Federal Institute for Materials Research and Testing (BAM), Berlin, Germany

The second way to perform GPR surveys is to provide the cross-sectional velocity or attenuation image of the tested structure. That information can be used for determining material properties and thus giving information about structural geometry or integrity. For that purpose number of tests was carried out in BAM laboratories to evaluate performance of GSSI system for tomography measurements and data analysis.

4.2.1 BAM.NB.FBS.1 concrete specimen

Description of test specimen and methodology

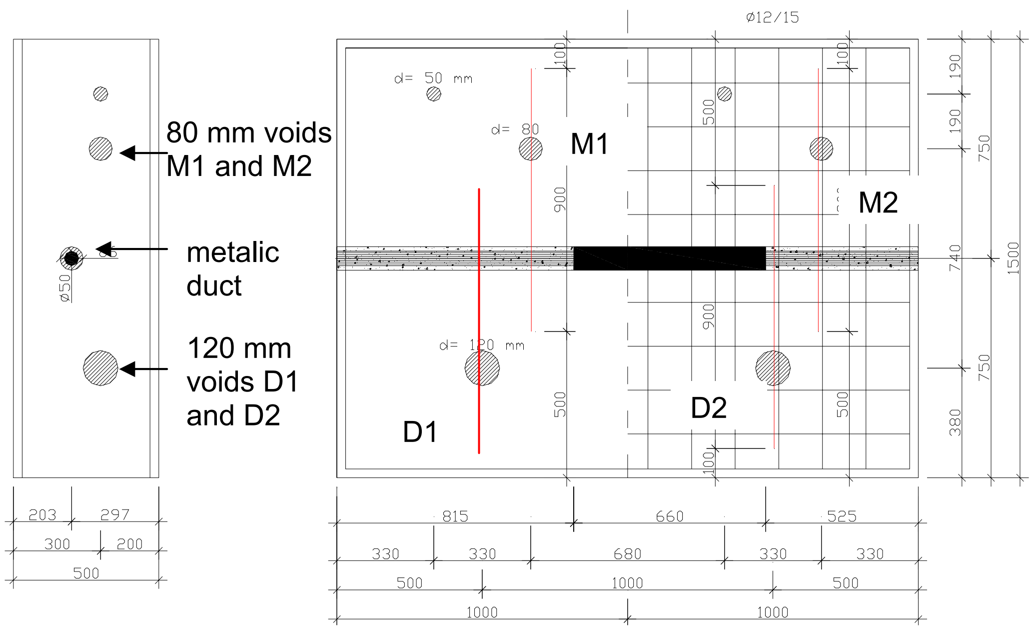

Figure 4.10 - Drawing of a BAM.NB.FBS.1 concrete specimen with marked 4 positions of transmission measurements.

Test specimen BAM.NB.FBS.1 was constituted of concrete class C50 and has the dimensions 2 m x 1.5 m and 0.5 m of thickness (see Figure 4.10). Number of objects was placed inside the tested specimen, like one metallic tendon duct, and 3 types of voids constituted of polystyrene with different diameters (50 mm, 80 mm and 120 mm – see Figure 4.10). Objective of the measurements was to locate the metallic tendon duct and polystyrene balls (diameter 120 mm – voids D1 and D2) behind and without reinforcement grid.

Tests were performed using SIR-10 radar system with two antennas with central frequency of 1.5 GHz in the transmission mode, one acting as a transmitter and second as a receiver (Figure 4.11). Each of the measurements was done using 50 mm offset between transmitter positions. While the transmitter was remaining stationary, the receiver was moving on the second side of the specimen. When all transmitter – receiver combinations positions were accomplished, positions of transmitter and receiver were changed and second scan was performed. Each of the tomograms has 0.9 m length and 0.5 m width (see Figure 4.12). The detailed methodologies for the data acquisition and processing in the tomography mode are presented in chapter 7.

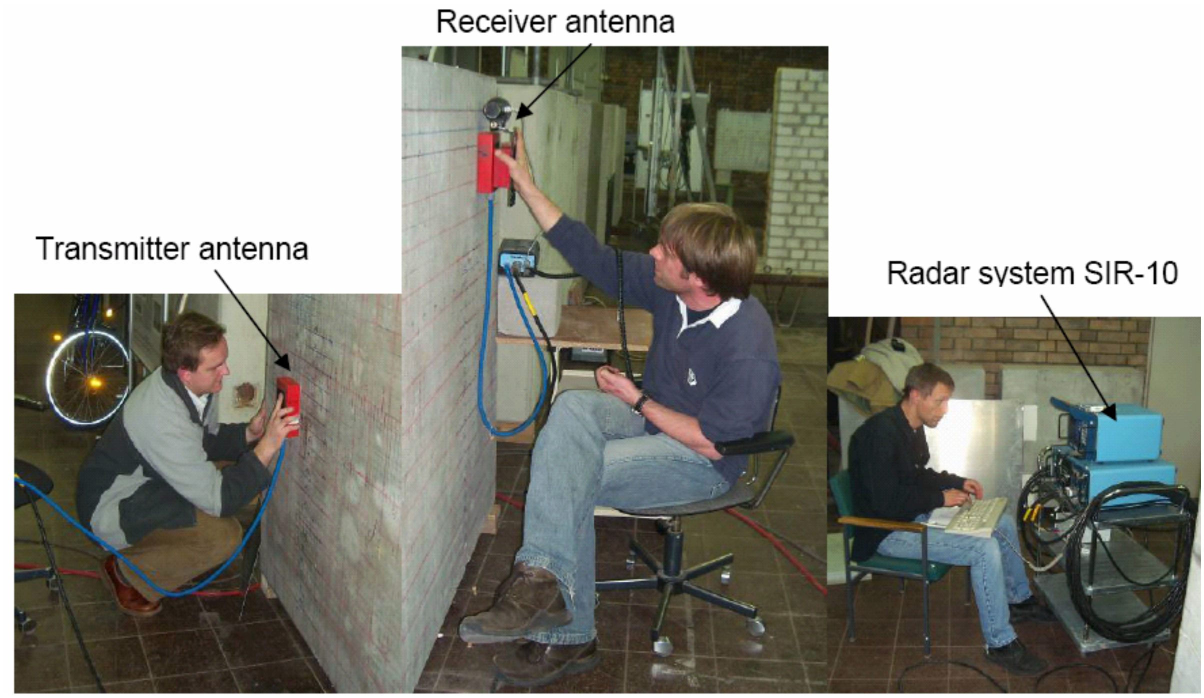

Figure 4.11 - Hardware set – up for the transmission measurements at BAM

Results and interpretation from the voids D1 and D2

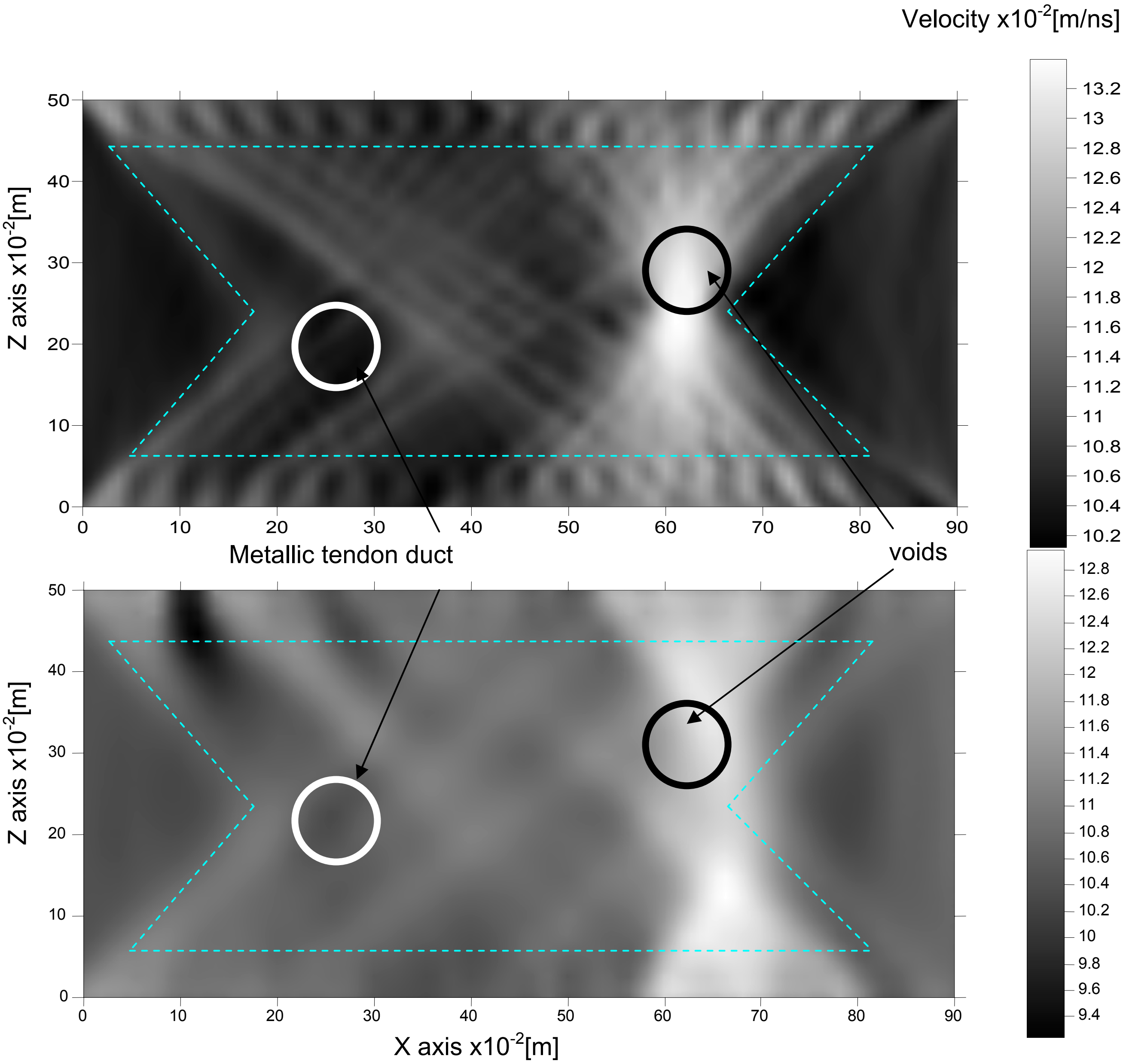

Figure 4.12 - Two tomograms with voids D1 –without reinforcement grid (top) and D2 –with reinforcement grid (bottom). Tomograms were processed with GeoTom CG software.

Investigated area is placed inside dashed boundary (Figure 4.12). Due to artefacts and different edge effects area behind this line was not taken into consideration. Grid size for the inversion was set to 25 mm, which is half of the distance between transmitter antennas. Different grid sizes were considered. However, even with a presence of inversion artefacts images have much better quality than with 50 or

100 mm grid. Inversion artefacts were caused also by presence of big void, which concentrated much of electromagnetic energy and thus resulting radargrams for travel time picking were little bit confusing. Presence of steel close to boundaries had also significant influence on a final result what can be clearly visible on a bottom image. Part of the electromagnetic pulse was reflected and thus in obtained travel times a lot of uncertain values can be found. In Chapter 7 explanation for artefacts and edge effects can be found. There in Figure 7.6 is visible how many rays are passing through void and how many areas are almost not covered by rays. All investigated area was covered by substantial number of crosses of unknown origin. Although calibration of the signal was done every 10 minutes and detailed data quality checks were applied, there was not possible to filter the data from those unwanted artefacts. However, even with those problems metallic tendon duct was correctly detected in both cases. Void D2 was not as clearly visible as void D1 because of reinforcement presence on boundaries of tested specimen.

To complement the results on the big voids, additional tests on the same specimen were performed. This time the objective was to locate the metallic tendon duct and polystyrene balls (diameter 80 mm – voids M1 and M2) with and without reinforcement grid (see Figure 4.10). Tests were performed using SIR-10 radar system with two antennas with central frequency of 1.5 GHz in the transmission mode, one acting as a transmitter and second as a receiver (see Figure 4.11). Each of the measurements was done using 50 mm offset between transmitter positions. While the transmitter was remaining stationary, the receiver was moving on the second side of the specimen. When all transmitter – receiver combinations positions were accomplished, positions of transmitter and receiver were changed and second scan was performed. Each of the tomograms has 0.9 m length and 0.5 m width (Figure 4.13).

Results and interpretation from voids M1 and M2

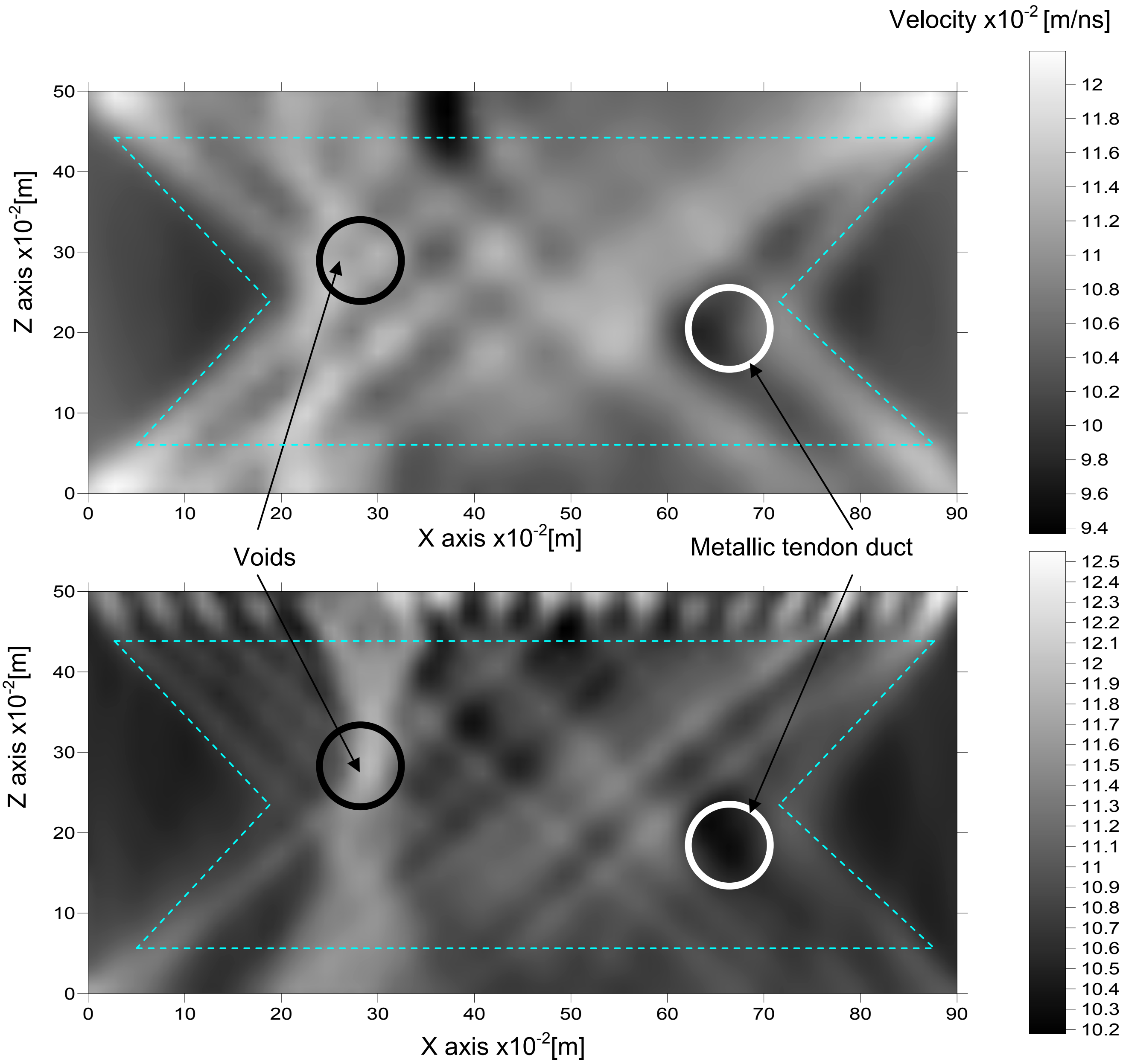

Figure 4.13 - Two tomograms with voids M1 – without reinforcement grid (top) and M2 –with reinforcement grid (bottom). Data were processed with GeoTom CG software.

Investigated area is placed inside dashed boundary (Figure 4.13). During those measurements influence of steel was not as visible as in case of voids D1 and D2. In fact, results obtained from void M2 (bottom image), which was placed behind reinforcement grid are much more clear and with less artefacts than those from void M1 (upper image). It was caused by very noisy and difficult to pick radargrams what resulted mainly in low quality output which is visible on a top tomogram with void M1.

In case of void M2 quality of input data was much higher what resulted in better output after the inversion. In case of metallic tendon duct, in both situations it was possible to identify it correctly. Because of the smearing effect visible on tomograms problem with right positioning of the voids can occur. Similarly as in case of experiments performed on voids D1 and D2, all investigated area was covered by substantial number of crosses of unknown origin. Although calibration of the signal was done every 10 minutes and detailed data quality checks were applied, there was not possible to filter the data from those unwanted artefacts.

4.2.2 BAM.NB.FBS.2 concrete specimen

Description of test specimen and methodology

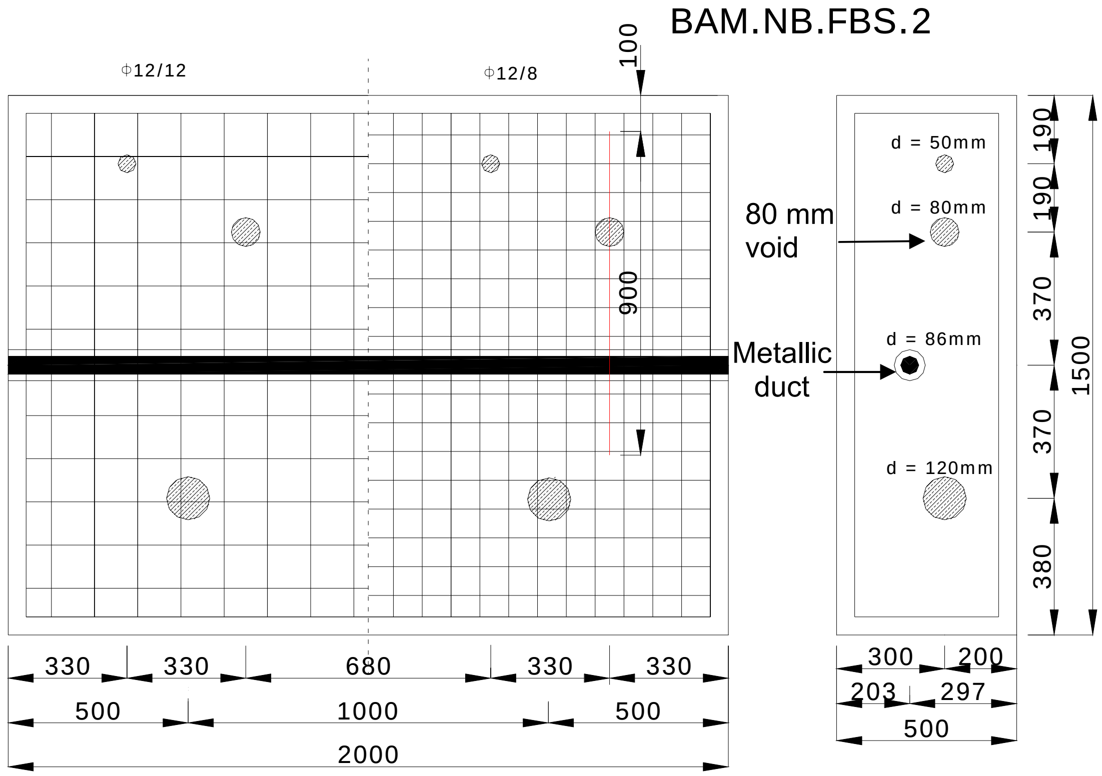

Figure 4.14 - Drawing of a BAM.NB.FBS.2 concrete specimen with marked position of transmission measurements.

Test specimen BAM.NB.FBS.2 was constituted of concrete class C50 and has the dimensions 2m x 1.5 m and 0.5 m of thickness (see Figure 4.14). Inside of specimen a number of objects were placed inside, like one metallic tendon duct, and 3 types of voids constituted of polystyrene with different diameters (50 mm, 80 mm and 120 mm – see Figure 4.14). Objective of the measurements was to locate 80 mm void and a metallic tendon duct behind a very dense reinforcement grid (80 mm) in the horizontal and vertical antenna polarisation. Tests were performed using SIR-10 radar system with two antennas with central frequency of 1.5 GHz in the transmission mode, one acting as a transmitter and second as a receiver (see Figure 4.11). Each of the measurements was done using 50 mm offset between transmitter positions. For each trace 2 measurements were performed: first transmitter was on one side of tested specimen and after completing a scan, positions of transmitter and receiver were changed and second scan was performed. Each of the tomograms has 0.9 m length and 0.5 m width (see Figure 4.15). The detailed methodologies for the data acquisition and processing in the transmission mode are presented in chapter 7.

Results and interpretation

Investigated area is placed inside dashed boundary (Figure 4.15). Due to artefacts and different edge effects area behind this line was not taken into consideration. Presence of inversion artefacts is quite similar in both examples and thus quality of data input was also similar. A lot of uncertainties during interpretation were caused mainly by presence of very dense of reinforcement grid and thus large amounts of lost signals. Despite presence of more dense reinforcement grid that during previous examples it was possible to identify voids more easily. It was caused mainly by better quality of input data (better final model for inversion, better time picking, and better selection of data sets for inversion). However, the same situation as in case of tests on the previous specimen occurred. All investigated area was covered by substantial number of crosses of unknown origin. Although calibration of the signal was done every 10 minutes and detailed data quality checks were applied, there was not possible to filter the data from those unwanted artefacts.

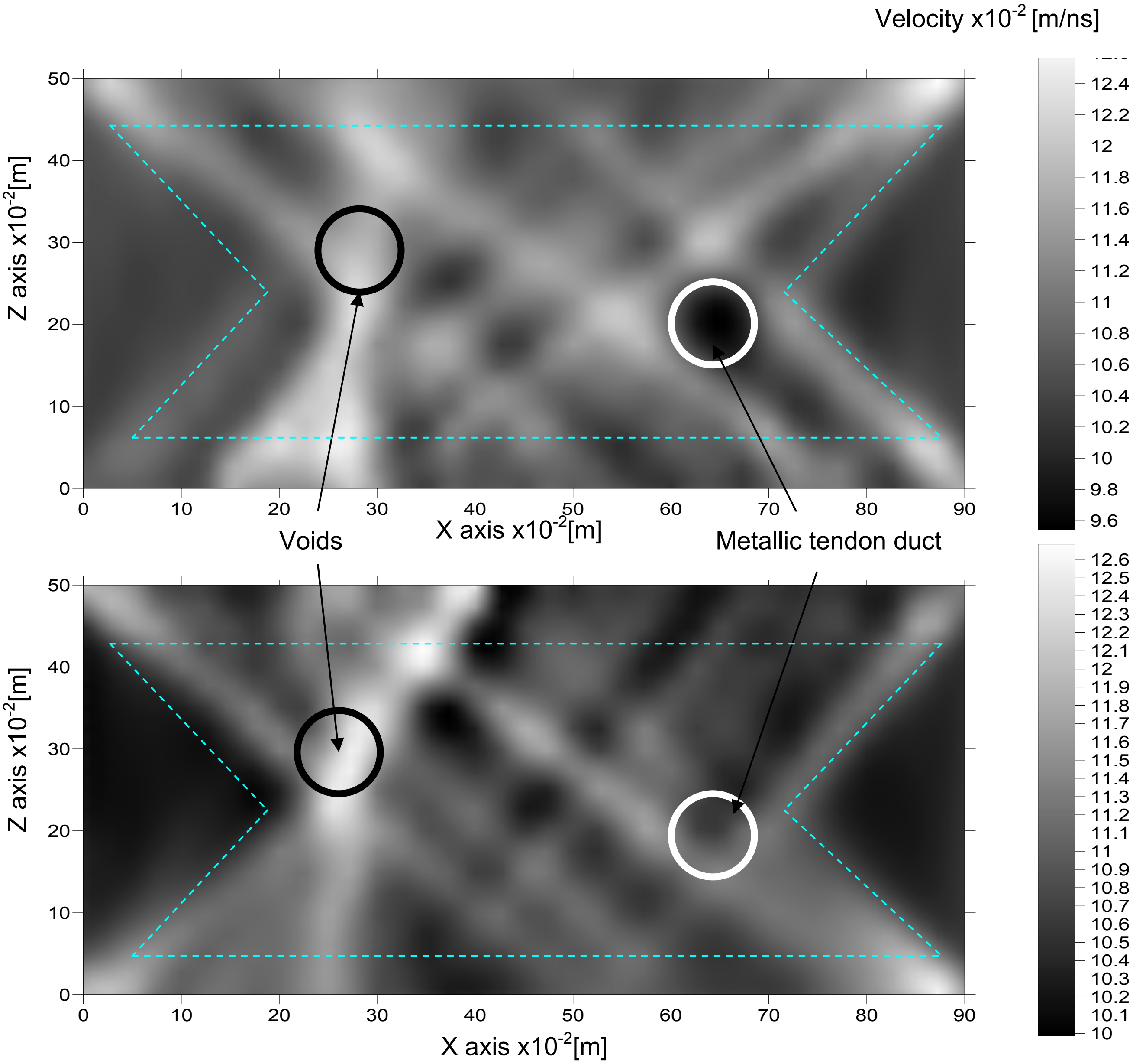

Figure 4.15 - Two tomograms with void M2 (top – horizontal antenna polarization) and (bottom – vertical antenna polarization). Data were processed with GeoTom CG software.

4.2.3 Summary

To check the accuracy of the transmission measurements, series of measurements was done in BAM laboratories on two large concrete specimens. Voids and a metallic tendon duct inside both tested specimens were successfully detected using GSSI system with two 1.5 GHz antennas and the GeoTomCG software. Antennas proved their usefulness and very good penetration. However, the results were far from being perfect. Detection of small voids (diameter 80 mm and smaller), in case of concrete structures was very difficult and required very precise time picking and less noise and errors. In case of metallic tendon duct it was detected even behind the very dense reinforcement grid, but velocity on the final tomograms was never zero (image was represented as an area with much lower velocity than a surrounding areas).

Also another significant conclusion was drawn. Although the voids and metallic tendon ducts were detected, significant number of artefacts was present in the final results. Detailed quality checks of input data strongly indicated, that significant time variations are present and the source of them was unknown. It led to the conclusion that additional tests are needed for checking of the time axis stability. The results from those tests are presented in the chapter 4.3.

4.3 Examples of tests using tomography method for the calibration purposes

4.3.1 Introduction

The main motivation of this sub-chapter is to provide the information about how important is deep understanding of the behavior of the radar equipment. Electronics in the modern radar systems is still far from being perfect and if some effects present in every commercial radar system are not known, it can cause very serious problems during data interpretation, what was already shown in the results from the BAM specimens in the previous chapter or in Topczewski *et al.* (2006). Not stable signal can introduce many artifacts (crosses) in the final data. That problem was already reported by other researchers from the geophysical field (Tronicke *et al.* 2002) and is shown in the Figure 4.16c. There can be seen that any traveltime delay can lead to unwanted artifacts and make the final interpretation of the data difficult or almost impossible. The problem is even more serious if in the signal are constant variations in the traveltimes, what can completely disort the data and even with filtering make them impossible to interpret.

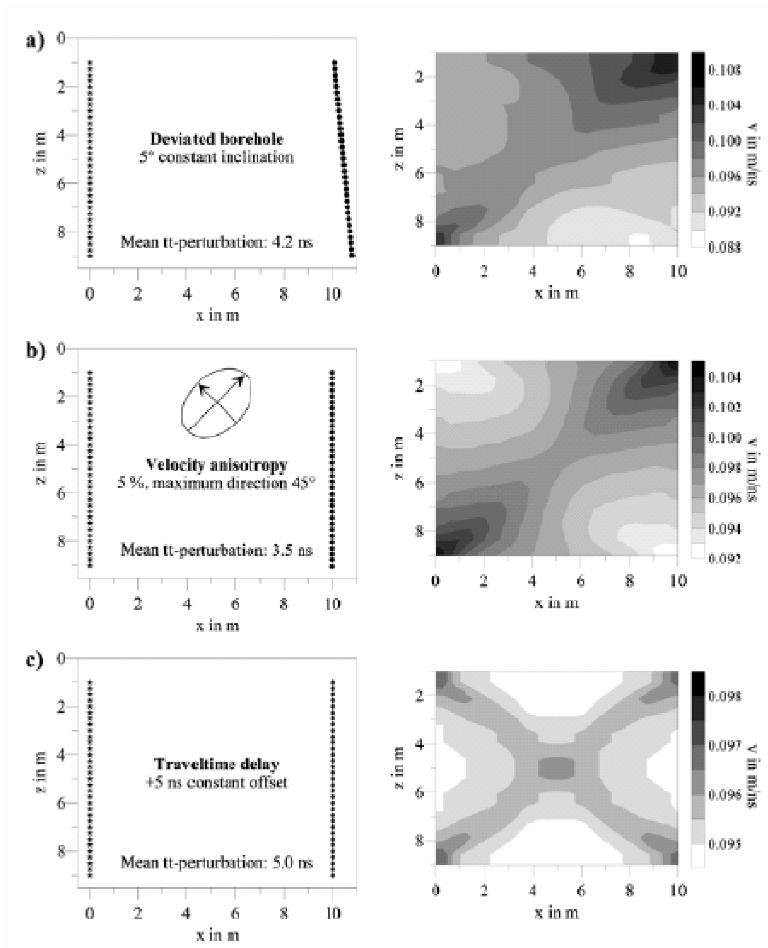

Figure 4.16 - Three possible errors in tomographic inversion and their images (Tronicke et al. 2002).

In case of all radar tomography systems, the real "time zero" signal needs to be calibrated by performing series of air transmission measurements every 5-10 minutes (see Figure 4.17). In case if time axis is not calibrated, the final images can be totally covered by substantial number of artifacts (like crosses shown in Figure 4.16). They can mask partially or totally the real information from the test location and lead to the misleading interpretation of the data. Detailed description of the standard time calibration procedure is provided in Chapter 7.

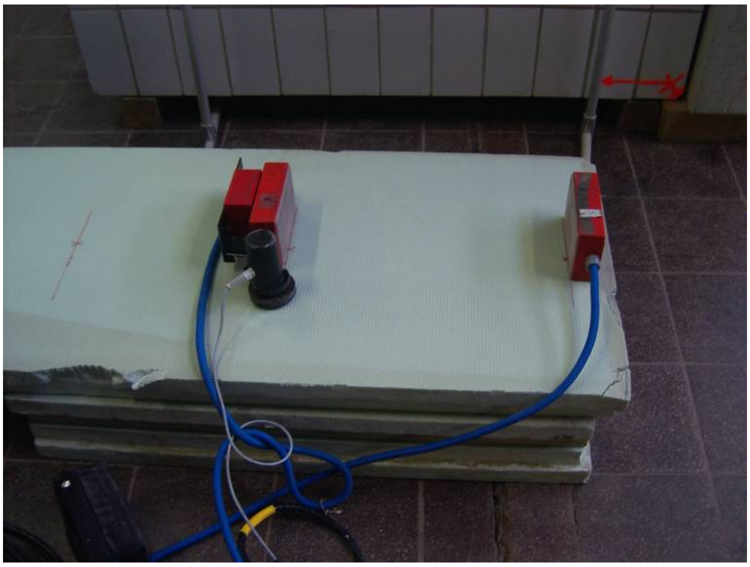

Figure 4.17 - Illustration of time axis calibration with two 1.5 GHz antennas.

4.3.2 Problems with warming up of the antennas

After obtaining many not satisfactory results from the concrete specimens (see chapter 4.2) even using standard time calibration procedures signal seemed to be still not stable and the final results were far from desired. Also results from the masonry specimens reported in Topczewski *et al.* (2006) indicated that signal have significant variations that may cause unwanted artifacts in the final images. It gave to the author an idea that during some period of time just after starting up of the radar system signal can have the tendency of jumping or to present other not stable behavior. Thus experiments in the BAM and UMinho laboratories were proposed and performed to prove that theory and to show that the same problem occurs in two completely different radar systems (GSSI and MALA Geoscience). In the case of GSSI system, experiment was performed during around 1.5 h with two antennas of 1.5 GHz in the transmission mode and SIR-20 Radar system. Antennas had an offset of 30.9 cm and were remaining stationary. Experiment started 10 minutes after starting the radar system. Signal started to be stable only after 45 minutes but still small not significant variations were present (see Figure 4.18).

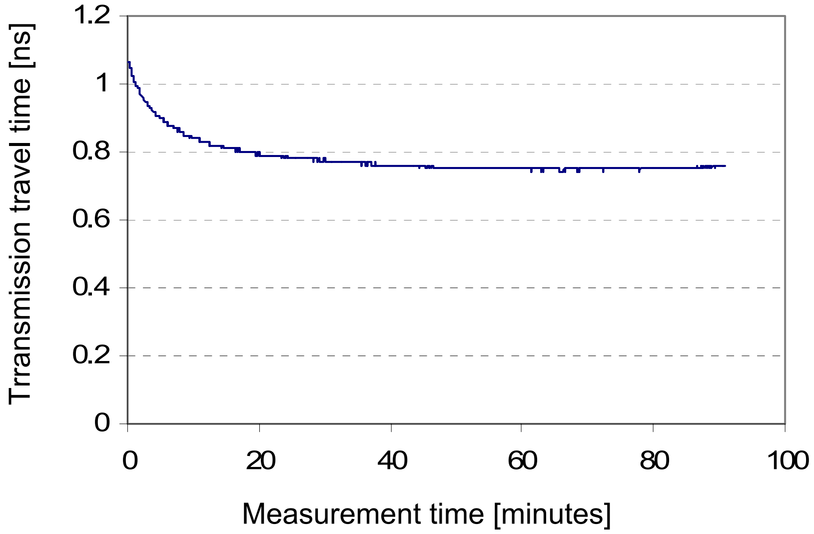

Figure 4.18 Graph representing time drift effect in the GSSI antennas

To verify those results, the second tests at University of Minho with MALA Geoscience radar system and two 1.6 GHz antennas in the transmission mode were performed. The procedure was the following one. The 1.6 GHz antennas were fixed in the ground, separated by 60 cm and the transmitter of the first antenna was aligned with the receiver of the second antenna (see Figure 4.19).

Figure 4.19 - Configuration of the MALA antennas for the air measurement

They were connected to the control unit through the special cable the University asked MALA to develop to carry out tomography measurements. The measurements started 2-3 minutes after system boot. During the entire measurement, the antennas and the cables remained untouched and no object crossed between the antennas.

The first measurement lasted 2 hours, approximately (see Figure 4.20) and the system was shutdown after. In this first measurement, from the beginning to the end, a difference of 0.5 ns in the duration of the transmitted signal occurred. Stability of the signal was reached only after 70 minutes. Also during first 30 minutes signal presented very significant drift.

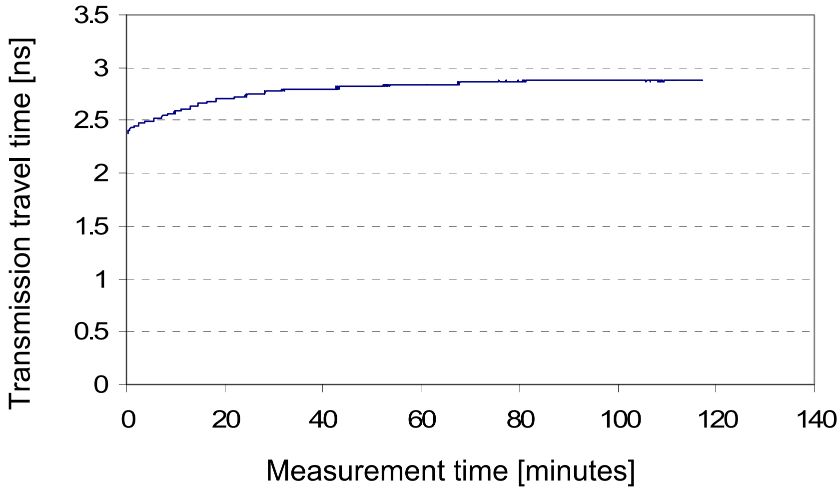

Figure 4.20 - Graph representing time drift present during first time measurement just after starting up the MALA system

A second time measurement started 5 minutes after previous one and lasted 10 minutes and gave the results that can be seen in Figure 4.21. Although the antennas were supposed to be stable after the two hour warm-up period, restarting the system caused the similar time drift effect like during the first time.

A third measurement started 10 minutes after the second one and the results can be seen in the Figure 4.22. During this measurement, signal started reaching its stability faster, but still the stability of the time axis was far from desired.

It seems that there is some instability in the signal that only is dissipated after a long period of warming up (see Figure 4.20). Also, after shutting down and restarting the system, the signal was instable again, like if it needed another warm up period.

After those measurements some important conclusions were drawn. Firstly, the results have shown that both systems (GSSI and Mala) represent high instability of signal for at least one hour after the system starts. Also in case of system reboot during the measurements, another warm up period was needed, what made difficult to apply standard time calibration procedures (see chapter 7) during the warm-up period, because air calibration would have to be done or after the warm up period or during the warm up period but with much higher frequency than normally (for example every 5 minutes). Even then the results could contain bad data for the final inversion.

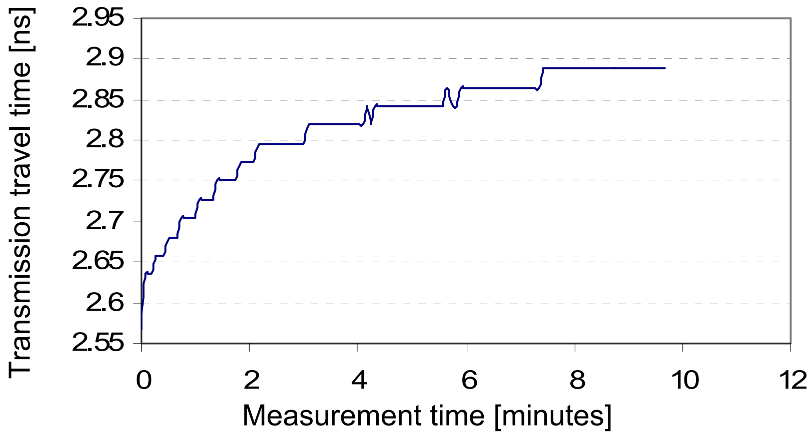

Figure 4.21 - Graph representing time drift present during the second time measurement 5 minutes after restarting the system

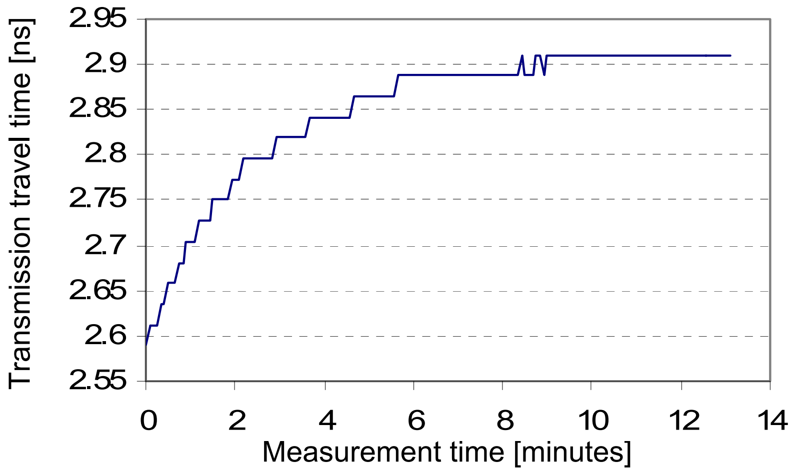

Figure 4.22 - Graph representing time drift present during the third time measurement 10 minutes after restarting the system

4.3.3 Advanced time calibration procedures

To overcome problems with not stable signal, advanced solution for the time axis calibration was proposed and applied at BAM by Dr. Christiane Trela. The solution is now under patent phase at BAM, so any details cannot be given at the time of writing of this thesis.

4.3.4 Summary

The last stage of laboratory tests consisted of calibration tests of MALA and GSSI antennas in the BAM and UMinho laboratories. The tests indicated that in the every Radar equipment time drift problem is present and that effect cannot be compensated by traditional time calibration procedures. To control that effect, advanced calibration procedures were proposed and applied in the BAM laboratories.

After the stage of experimental testing, validation tests of the radar technique in transmission and in the reflection mode were proposed and applied on three big prestressed concrete bridges in the north of Portugal. Those results and conclusions are presented in the next chapter.

Chapter 5 - Validation through field testing

5.1 Introduction

In the particular case of prestressed concrete bridges, which is addressed in this chapter, the location of the tendon ducts and ordinary reinforcement was fundamental in rehabilitation works. In addition, the verification of the quality of work during the execution of the works and initial life is absolutely necessary in order to prevent the occurrence of early deterioration, such as reinforcement corrosion.

In this research, GPR inspections were carried out on three large concrete bridges located in the northern part of Portugal. These applications clearly illustrate the potential to obtain the information necessary to design strengthening, namely, to locate the exact position of tendon ducts and reinforcement using 2D and 3D imaging techniques. In addition, in one of those examples, the application of tomographic techniques made possible the assessment of the concrete quality and the comparison with the information obtained with sensors installed inside these elements. Additionally, the improved radar tomography system showed its reliability during field testing for the verification of concrete integrity, what was one of the issues within Work Package 3 of Sustainable Bridges European Project.

5.2 Main characteristics of the inspected bridges

5.2.1 Lanheses Bridge

The Lanheses Bridge crosses the Lima River and was designed by the most famous Portuguese bridge engineer, Edgar Cardoso, in the seventies and was built in 1981. Currently, it suffers from significant deterioration after more than 30 years of service life.

Figure 5.1 – Overview of the Lanheses Bridge.

The Lanheses Bridge is illustrated in Figure 5.1. It is a cantilever bridge with a total length of 1218 m between abutments and a width of the bridge deck of 11.5 m. The superstructure, in reinforced and prestressed concrete, is constituted by four longitudinal beams with variable inertia, connected superiorly by the deck's slab and transversally by beams located over the columns and at thirds of the spans. The bridge presents along its length typical spans of 30.0 m, with the exception of the approach spans, with a length of 24.0 m.

The columns, in reinforced concrete, have a large slenderness, a rectangular cross-section, and are rounded at the extremities. They are articulated at the top and at the base, which allow a pendulum movement that does not resist any horizontal force. The abutments are constituted by walls in harmonium and extend for 10.3 m. The complete bridge deck works as a cantilever deck, which is fixed in the South margin of the River and free in the North margin. The columns extremities' supports are ball-and-socket joints, constituted by lead plates and bolts. In the North margin, the mobile extremity of the bridge deck is made with pinned steel bearings.

5.2.2 Barra Bridge

Figure 5.2 – Overview of the Barra Bridge.

The Barra Bridge, which crosses the delta of the Vouga River (“Ria de Aveiro”), in Ílhavo, was also designed by Edgar Cardoso in 1972 and was built in 1978. Currently, this bridge suffers from significant deterioration caused by the contact with seawater, aggressive environment and nearly 30 years of service-life. Figure 5.2 illustrates a general view of the structure. The bridge total length is about 620 m between the abutments and the width of the bridge deck is 15.9 m. The bridge deck is constituted by reinforced concrete, being supported by four longitudinal beams of variable inertia and box-girders over the bridge supports. These beams are prestressed longitudinally, are connected in the top face by the deck slab and are connected transversally by reinforced concrete beams located over the support columns. The distance between columns is 32.0 m, with the exception of the approach spans, with a length of 25.0 m. The columns, in reinforced concrete, possess a large slenderness and a rectangular cross-section. They are connected through transversal beams at the top and at the base, in the foundations. The transversal beams are connected to the longitudinal beams through neoprene supports. Finally, the abutments are constituted by walls in harmonium and extend for 20.9 m.

5.2.3 Bridge over Ave River

Figure 5.3 Overview of the Bridge over Ave River.

The bridge over the Ave River was constructed during 17 months beginning in 2001, and was opened to traffic in July 2003. The bridge is located close to Guimarães, in Portugal, at the A11 highway. The general view of the bridge is illustrated in Figure 5.3. The bridge consists mainly of three parts: two access viaducts characterized by a continuous bridge deck supported by circular columns and a central rigid frame constituted by a prestressed bridge deck supported by box-girders, with V-leg piers at the extremities of the single span. The bridge total length is about 280 m between the abutments and the width of the main bridge deck is 120 m. In case of access viaducts, they have 128 (8x16 m) and 32 m (2x16 m) of length, respectively.

5.3 Application to detect tendon ducts and ordinary reinforcement

The rehabilitation and structural strengthening currently being carried out in the Barra and Lanheses bridges include the addition of external strengthening through longitudinal external prestressed cables and prestressed threaded iron bars transversally on the bridge supports. The strengthening devices will be fixed through steel devices, directly tied up to the longitudinal beams.

As soon as the works began, designers noticed the fact that the tendon ducts were not located in the positions defined in the original design plans. Without this information, a real risk of damaging the prestressed cables existed. Thus, it was fundamental to assess the exact localization of the ordinary reinforcement and the tendon ducts in several specific locations. Figure 5.4 illustrates examples of some damages and the consequences of semi-destructive techniques typically employed to locate essential structural elements such as tendon ducts. In fact, in this particular bridge, the holes for the external strengthening were drilled without prior knowledge or true assessment of the real position of the tendon ducts. Figure 5.4b shows that the initial design position of the strengthening elements would have caused damage to the existing tendon ducts.

(a) (b)

Figure 5.4 – Example (a) of corrosion of the reinforcement in the Barra bridge and (b) window opened in a longitudinal beam for the detection of tendon ducts in the Lanheses Bridge.

The detection of the metallic elements was carried out with a commercial GPR system from MALA Geoscience. The field acquisitions are mostly constituted by 2D radargrams carried out in the longitudinal beams of the two bridges with the objective of detecting the ordinary reinforcement and the steel tendon ducts in the inspected area. The antenna used for these surveys was a 1.6 GHz high frequency antenna. The area of interest is constituted by panels with 2x1 m^2 or 1x1 m^2. In each position a set of parallel and vertical lines was defined to perform accurate GPR acquisitions (see Figure 5.5). The distance between consecutive lines was 20 cm, and, in some cases, 5 cm (used for subsequent three-dimensional processing). In general, the speed of propagation of the electromagnetic wave was estimated to be around 10.2 cm/ns, which was determined by calculating the time needed by the electromagnetic pulse to travel from the antenna towards a metallic shield, located in the opposite side of the beam.

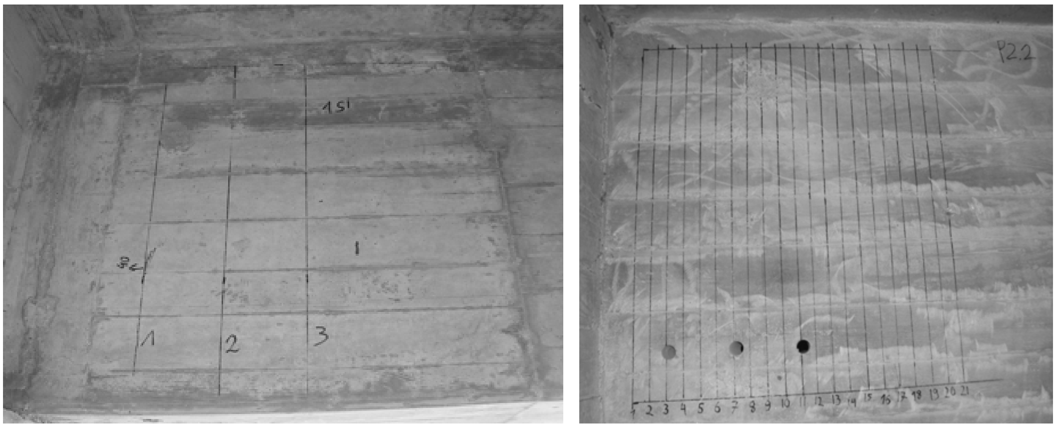

(a) (b)

Figure 5.5 – Examples of measuring vertical and horizontal lines in beams: (a) at the Barra bridge with a line separation of 20 cm and (b) at the Lanheses bridge with a line separation of 5 cm.

5.3.1 Lanheses Bridge

In the Lanheses Bridge, all the radar acquisitions were performed over support columns. As such, the examples shown refer to two of those tests locations. The first example was acquired in a beam in the middle of the width of the bridge deck and was acquired in both sides of a transversal beam. The area of interest was constituted by two 1x1 m^2 panels, with vertical profiles distanced by 20 cm. Figure 5.6 illustrates the procedure for the general interpretation of the GPR radargrams, where the characteristics signals from the detection of linear objects such as bars and tendon ducts can be observed. The results, illustrated in Figure 5.7, depict the positions of the steel reinforcement bars of Ø 32 mm and the tendon duct. Thus, it is possible to predict with sufficient accuracy the path of the tendon duct and the main reinforcement bars, to plan the location of the strengthening without harming the existing structural elements.

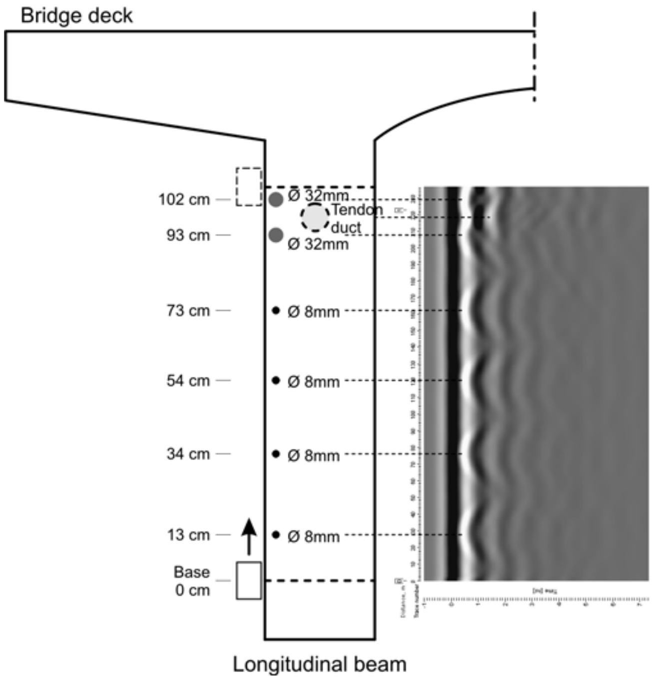

Figure 5.6 – Schematic exhibiting the interpretation of a common 2D radargram.

A second example was located in the external surface of a beam located in the extremity of the bridge. At this position, two small windows were opened to verify the real location of the tendon ducts. As a result, it was not possible to carry out continuous acquisition, and the area was split into four smaller areas. The distance between the profiles was 5 cm, which allowed to obtain sufficiently accurate data for three-dimensional subsequent processing.

The elements detected were the following ones: four reinforced bars of Ø 8 mm spreading along the entire length investigated with GPR and separated by 20 mm, which is corroborated by the original design plans, two reinforced bars of Ø 32 mm at the top of the beam and the presence of two tendon ducts. Figure 5.8 illustrates the position of the ordinary reinforcement and the prestressed cables in the tendon ducts. It must be noted that the lower tendon duct was not detected in the in the right superior corner due to difficulties related to steel concentration above the tendon.

These results were further processed in 3D with the objective of improving the interpretation of the previous results and assess the usefulness of 3D reconstruction for these tasks, see Fernandes (2006) for further details on 3D reconstruction techniques. Partial results for the tested area are shown in Figure 5.9, which illustrates one depth slice from the 3D volume, at about 15 cm of depth, shows the tendon duct located between the Ø 32mm bars at the top of the beam. Another one, at about 5 cm of depth, shows the disposition of the Ø 8 mm and Ø 32 mm reinforcement (not illustrated). The 3D volume reveals also the presence of vertical reinforcement in some points, although its identification is not accurate due to the fact that the methodology used in this case was not favorable for the detection of such bars, being necessary the acquisition of additional horizontal profiles in the same area for this purpose.

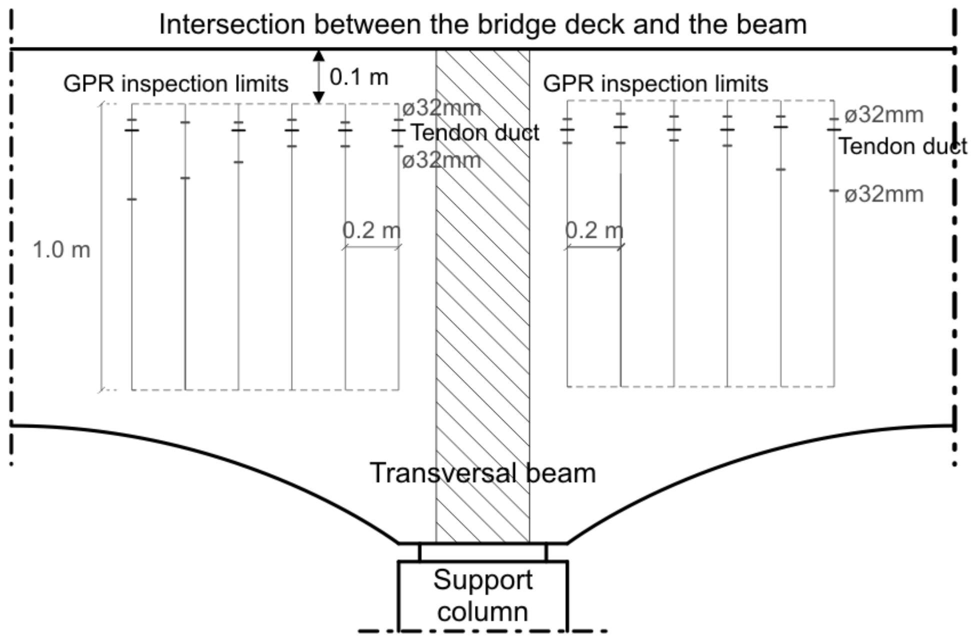

Figure 5.7 – Graphical representation of the detected reinforcement and tendon ducts from one of the two internal external beams. The presence of the transversal beam prevented the continuous acquisition of data.

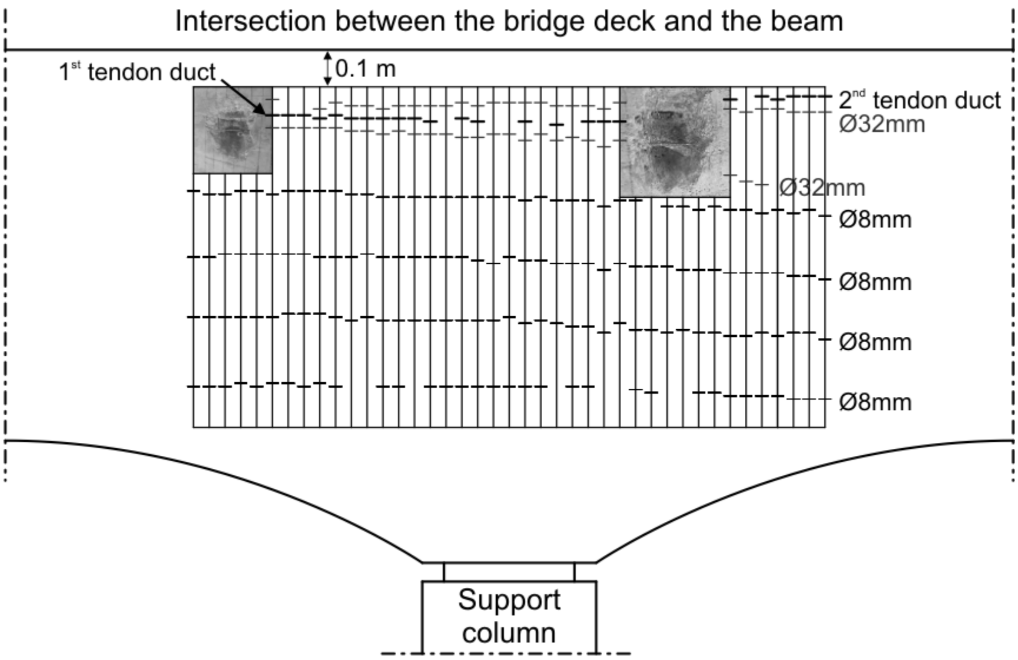

Figure 5.8 – Graphical representation of the reinforcement and tendon ducts from the external beam. The data was obtained from 2D radargrams and from the 3D volume.

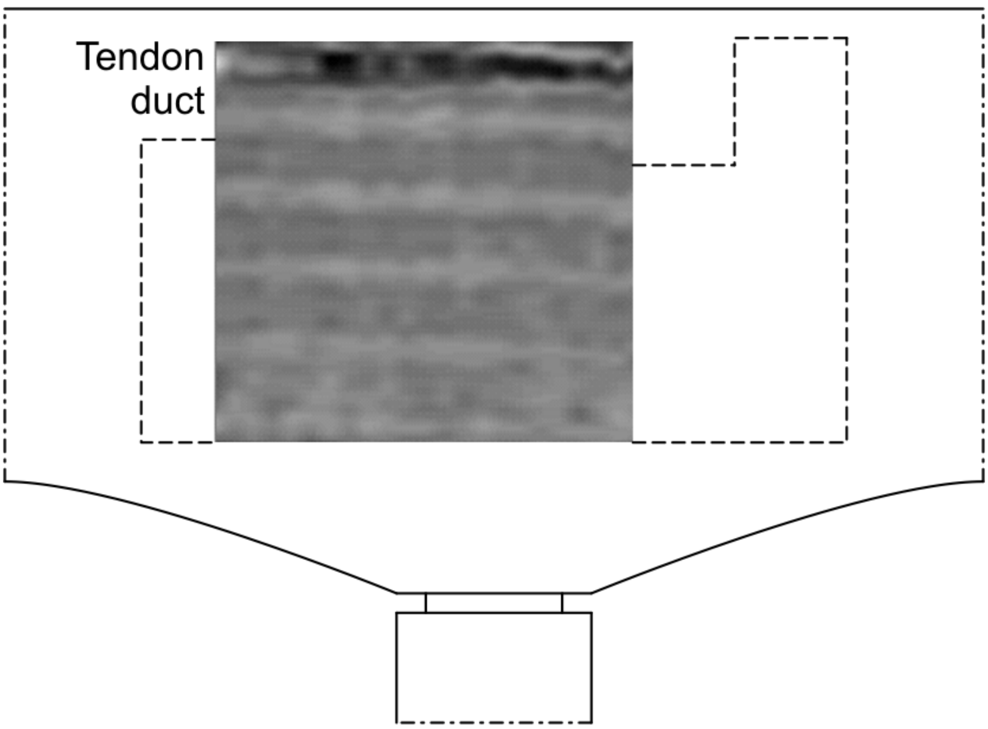

Figure 5.9 – Example of a depth slice taken from the main 3D volume with the indication of the tendon duct between the Ø32 mm steel bars, at 15 cm of depth.

5.3.2 Barra Bridge

(a) (b) (c)

Figure 5.10 – Example of the way of accessing tests sites: (a, b) from an articulated mobile platform and (c) over a continuous scaffolding system.

In this bridge GPR acquisitions were carried out in 21 locations. Of those positions, 13 were accessible through a fixed platform under the access viaducts of the bridge, while the remaining positions were located over the water and, thus, were only accessible with a mobile platform. Figure 5.10 illustrates examples of both situations.

In each position two to five vertical lines were carried out, according to the accessibility, the surface's nature and geometrical characteristics of the testing area. The vertical lines were executed with the maximum possible length (between 1 and 1.5 m). However, there were cases where it was not possible to reach the entire height of the longitudinal beam, especially when access was made through the mobile platform. Thus, in order to have a reference point that would allow the correct introduction of the location of the tendon ducts during design, the acquisition has always stopped at 10 cm from the edge between the bridge deck and the longitudinal beam.

It must be noted that the different smoothness of the surface influenced significantly the field acquisitions and conditioned the normal working of the antennas. Generally, the surface of the beams were rough and exhibited sharp edges of concrete in the surface due to the type of formwork used in the construction period. Thus, in the cases where the surface was not in adequate condition for the test execution, and if concrete drips and roughness were detected, a preliminary cleaning and leveling was usually carried out.

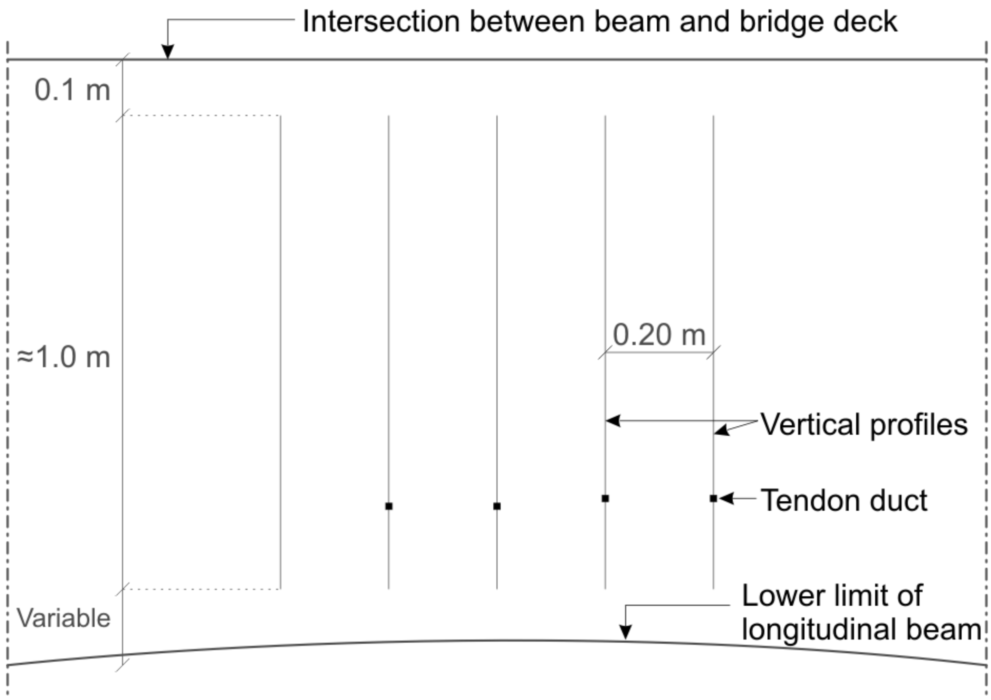

Figure 5.11 – Location of the tendon duct in a position that corresponds to a cross-section at the mid-span of the beam.

Due to the large number of testing sites and the vast amount of data, only two examples located in characteristic places of the bridge will be presented here, located in the first span of the bridge located above firm ground. Figure 5.11 and Figure 5.12 illustrate, respectively, examples of the localization of the tendon ducts: at mid span between supports and over a support column. The results are presented in such a way that, for each vertical radar profile, the location of the tendon duct is done through a small and thick horizontal line. As expected, the tendon ducts are localized in the bottom of the beam, when the radar acquisition is carried out in the mid span of the beam. The tendon ducts are localized in the top of the same beams when the radar acquisition is performed directly over a support column.

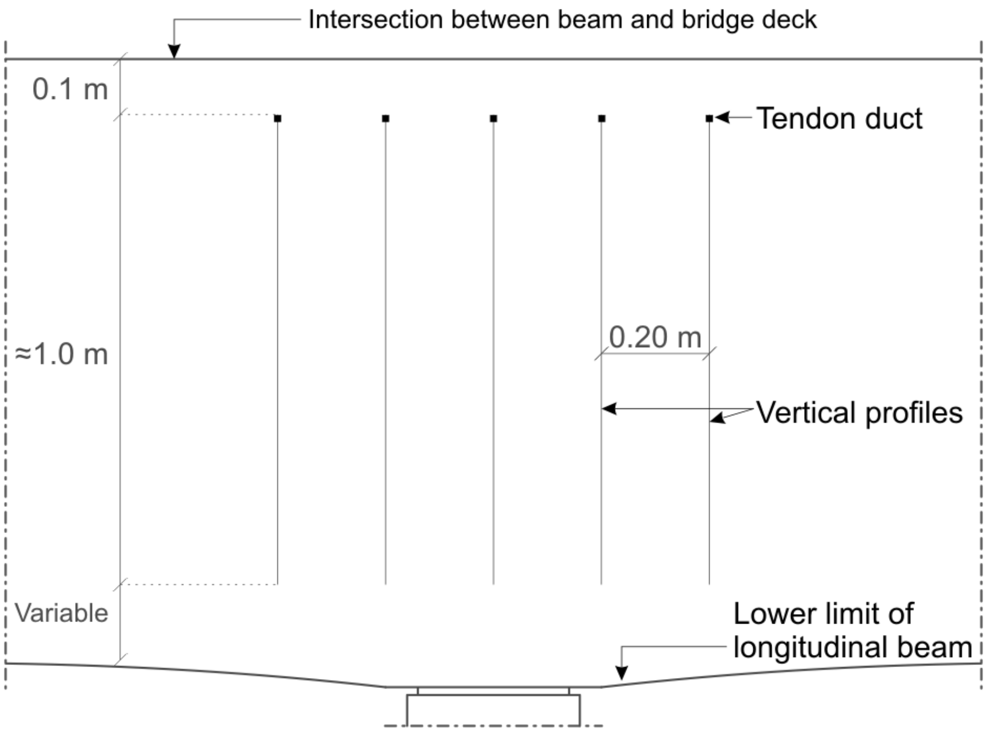

Figure 5.12 – Location of the tendon duct in a position that corresponds to a cross-section over a support column.

5.4 Application to construction and concrete quality control

During the construction of the concrete bridge over the Ave River, a significant number of different sensors were installed to monitor corrosion, humidity, temperature, etc. (Cruz & Wisniewski 2004). Shortly after the end of the construction, some of the corrosion sensors indicated large corrosion values in some structural elements. The largest values were located in two of the columns located in the access viaduct and inside one of the box-girders supporting the bridge deck. In order to assess the possible deterioration inside the elements that exhibit corrosion, a throughout GPR survey was carried out in two circular columns on the access viaducts. Two different equipments were used: one from MALA Geoscience with one 1.6 GHz antenna for reflection measurements, and a second one from Geophysical Survey Systems, Inc. with two 900 MHz antennas for transmission measurements.

Two columns were then chosen. In the first column (A), the embedded sensor did not indicate any signs of corrosion. In a second column (B), the sensor indicated the occurrence of corrosion in the metallic reinforcement.

5.4.1 Intact column – column A

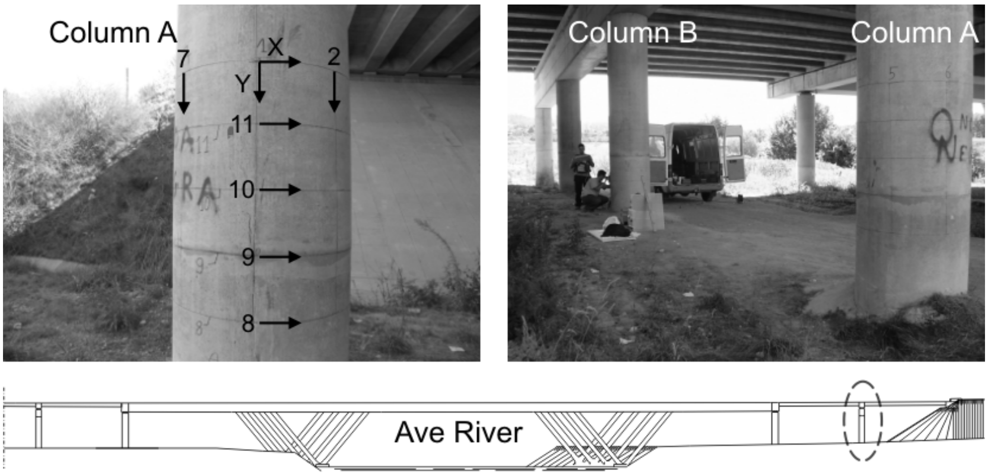

Figure 5.13 – On the left, view of the column A, the used coordinate system and the alignment of the horizontal and some of the vertical profiles. On the right, overview of the two columns tested.

The location of the test object is illustrated in Figure 5.13. The measurements were carried out with the 1.6 GHz antenna in reflection mode around the entire circumference of the column, around the location of the corrosion sensor. These measurements resulted in the following profiles: seven vertical profiles carried out from top to bottom, with 1.2 m of length and performed every 45 cm; and five horizontal profiles, carried out counter clockwise with 3.15 m of length and performed every 40 cm (see Figure 5.13).

The vertical profiles show, basically, the presence and frequency of stirrups (secondary reinforcement). According to the design drawings, these stirrups should be placed every 15 cm. Typical radargrams such as the one illustrated in Figure 5.14 shows that the secondary reinforcement was placed correctly.

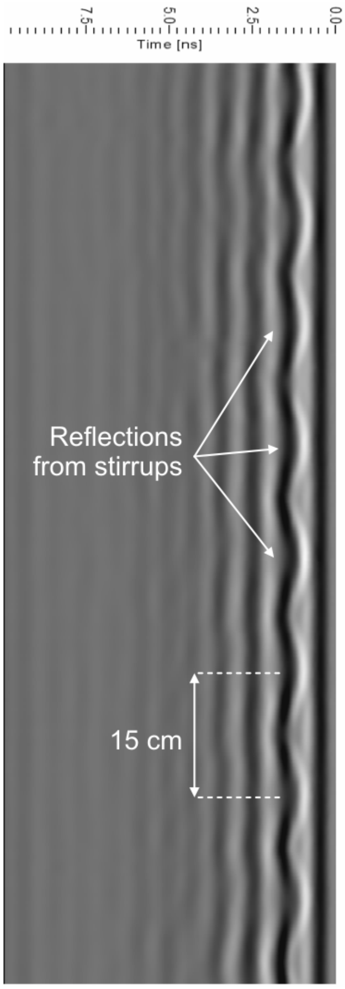

Figure 5.14 – Example of one radargram from vertical lines with marked reflections from the stirrups (column A).

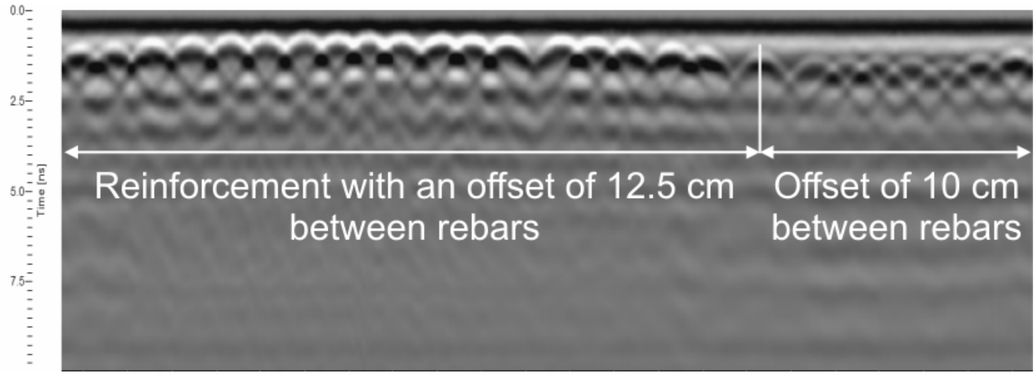

Figure 5.15 – Radargram showing different offsets between rebars.

The horizontal profiles were acquired from the same starting point and following the same direction as the vertical ones and as illustrated in Figure 5.13. Two main situations occurred in all the profiles acquired. Firstly, the offset between reinforcement bars is changing, having been observed distances ranging from 10 to 12.5 cm. This phenomenon is clearly observable in Figure 5.15, which shows, for example, the point where that offset between reinforcement bars occurred. Secondly, the concrete cover is changing along the circumference of the column. Generally, a difference of time of around 0.5 ns is observed in most radargrams, which means a difference of around 2.5 to 3 cm in depth. This difference means that some of the reinforcement bars are located very close to the surface, which can cause an earlier occurrence of corrosion.

5.4.2 Column with corrosion activity – column B

The location of the column B, the measurements and processing steps were identical to those carried out in the column A and follow the same rules as in Figure 5.13. This column was chosen because the embedded sensor (sensor C41) indicated the occurrence of corrosion.

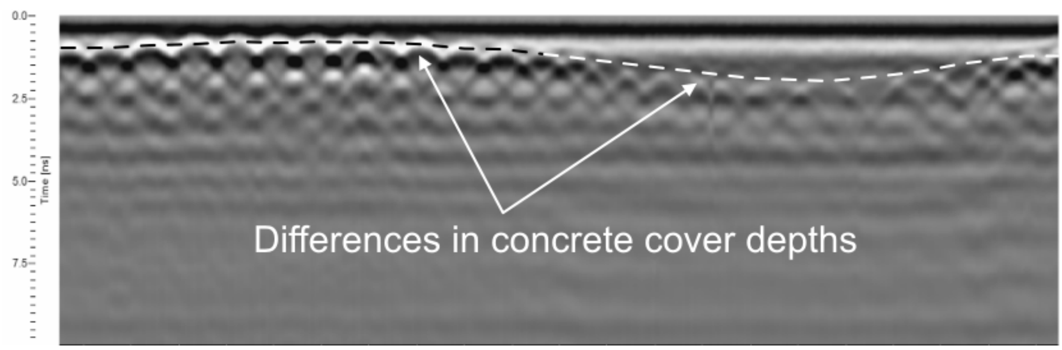

Figure 5.16 – Radargram from a horizontal profile of column B showing large differences in the cover layer of reinforcement.

The vertical profiles show the location of the secondary reinforcement and the results showed that this reinforcement was placed correctly, like in the case of the column A. Regarding the horizontal profiles, it can be observed that in the bottom part of the column there is a significant deficiency in the positioning of the main reinforcement, which shows a tendency to deviate towards the centre of the column. This phenomenon is well illustrated in Figure 5.16, which illustrates a profile located below the construction joint, where a difference of up to 8 cm between the different cover depths is detected.

Figure 5.17 – Radargram located at the top of the area investigated in column B showing the smallest differences in the cover layer of reinforcement.

On other profiles, this shift is progressively reducing. In the profile illustrated in Figure 5.17, there is almost no deviation of the main reinforcement towards the centre of the column, which suggests that in the part of the column above the construction joint, the construction's quality is higher. The distance between primary reinforcement is around 12.5 cm, matching the original design drawings. Figure 5.18 shows a sketch of the probable real position of the main reinforcement, and illustrates how the main reinforcement is possibly distributed along the column.

This situation requires further investigation of the entire columns and of the remaining columns as well, in order to assess the real position of the steel bars, as it can affect the resistance and durability of the columns.

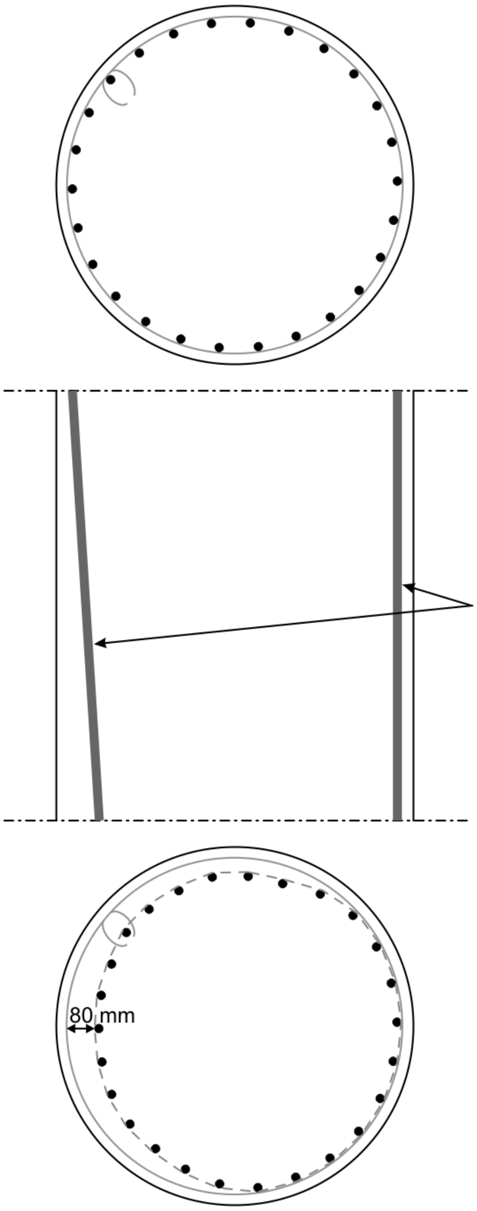

Figure 5.18 – Design drawing of the column indicating the real position of the main reinforcement, in the top, with respect to the original design, in the bottom. A deviation up to 8 cm is found. Correct position of the primary reinforcement (estimation) along the tested length.

5.4.3 Transmission measurements in column B

Transmission measurements were additionally performed around the construction joint. Due to the fact that this is a time consuming methodology, this technique was only applied in the column B, where the corrosion sensor indicated the occurrence of a very large value of the current resistance, which indicated that the steel were severally corroded. The objective was to detect deteriorated areas that could explain those high values. Due to the lack of sufficient penetration of the antenna of 1.6 GHz, the antennas of 900 MHz were used instead. The main acquisition mode is illustrated in Figure 5.19.

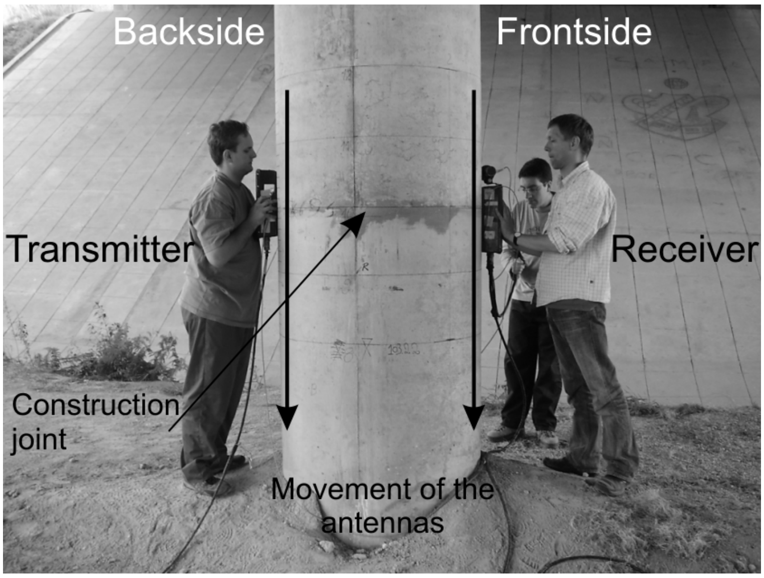

Figure 5.19 – Acquisition of the transmission measurement with transmitter and receiver antennas at opposite site at the column B. Positions of the transmitter antenna and profile length of 1.2 m of the receiver at the column B.

The measurements were carried out with the antennas in the vertical position. At each position, each 5 cm, the transmitter antenna was fixed, while the receiver was moved along the entire length, from top to bottom, which resulted in 25 profiles of 120 cm of length (see Figure 5.20). For error checking purposes a second identical measurement was performed, changing the transmitter and receiver antennas' position.

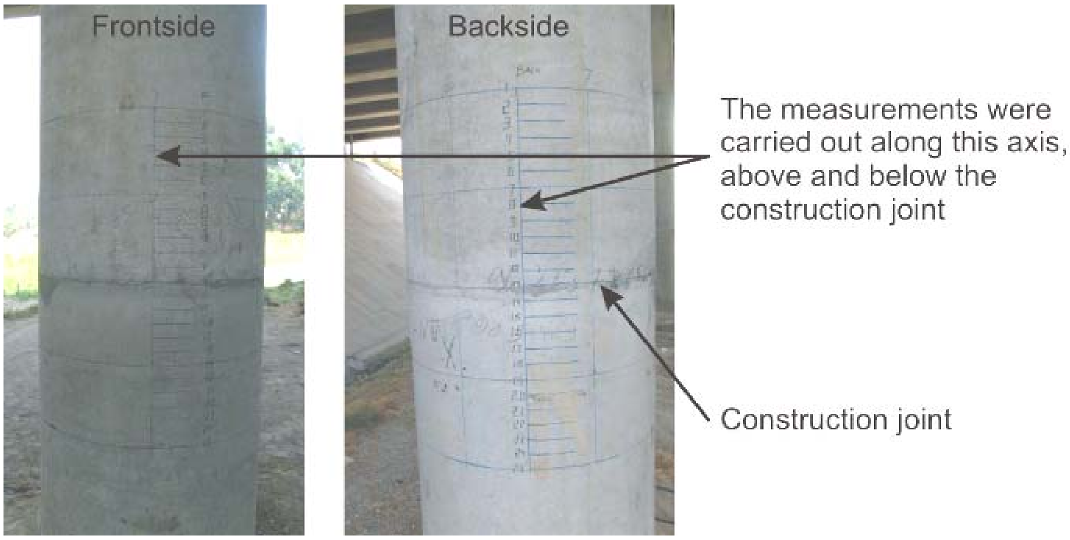

Figure 5.20 – Positions of the transmitter antenna and profile length of 1.2 m of the receiver at the column B.

The data processing was carried out in various steps. Firstly, the length of the various profiles was adjusted and the data input prepared and properly checked. Afterwards, the data was introduced in the inversion program and various tomograms were obtained, representing a map with the distribution of the velocity of the electromagnetic waves along the tested cross-sectional area. In this case, velocity maps such as those illustrated in Figure 5.21 and Figure 5.22 were obtained.

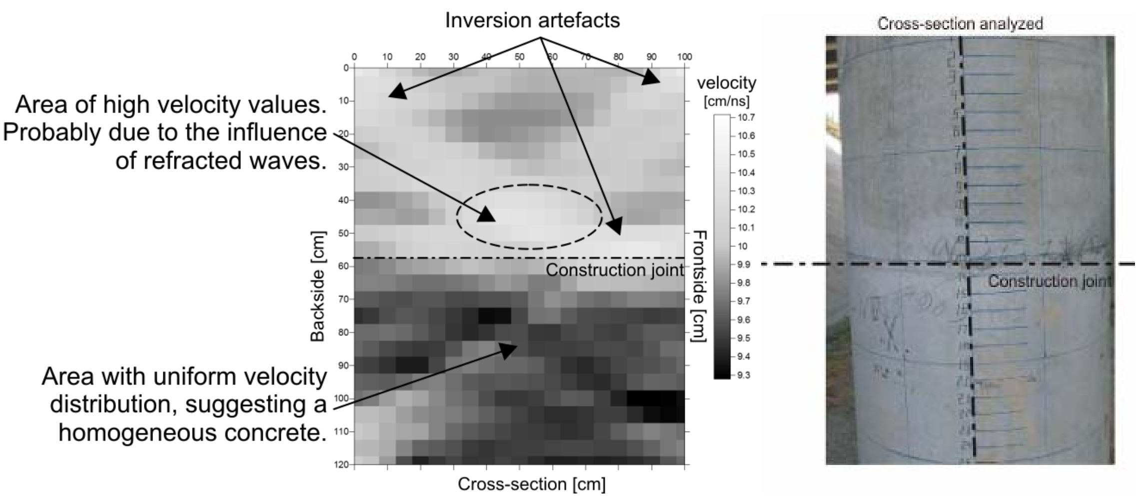

Figure 5.21 – Velocity tomogram showing the velocity distribution (left) in the cross-section of the column B (right). Data were processed with GeoTom CG software.

The entire dataset of profiles was used to produce the velocity tomogram illustrated in Figure 5.21. From this tomogram, it is possible to observe that the column can be divided in two regions, above and below the construction joint, that exhibit different velocities. The concrete above the construction joint presents a higher velocity with respect to the concrete below the joint (10 % larger, in average). This result strongly suggests that the concretes used in this column are different. Generally, areas of higher velocity values indicate the presence of concrete deterioration, which can be caused by an effect of the corrosion or by poor compaction during the construction phase.

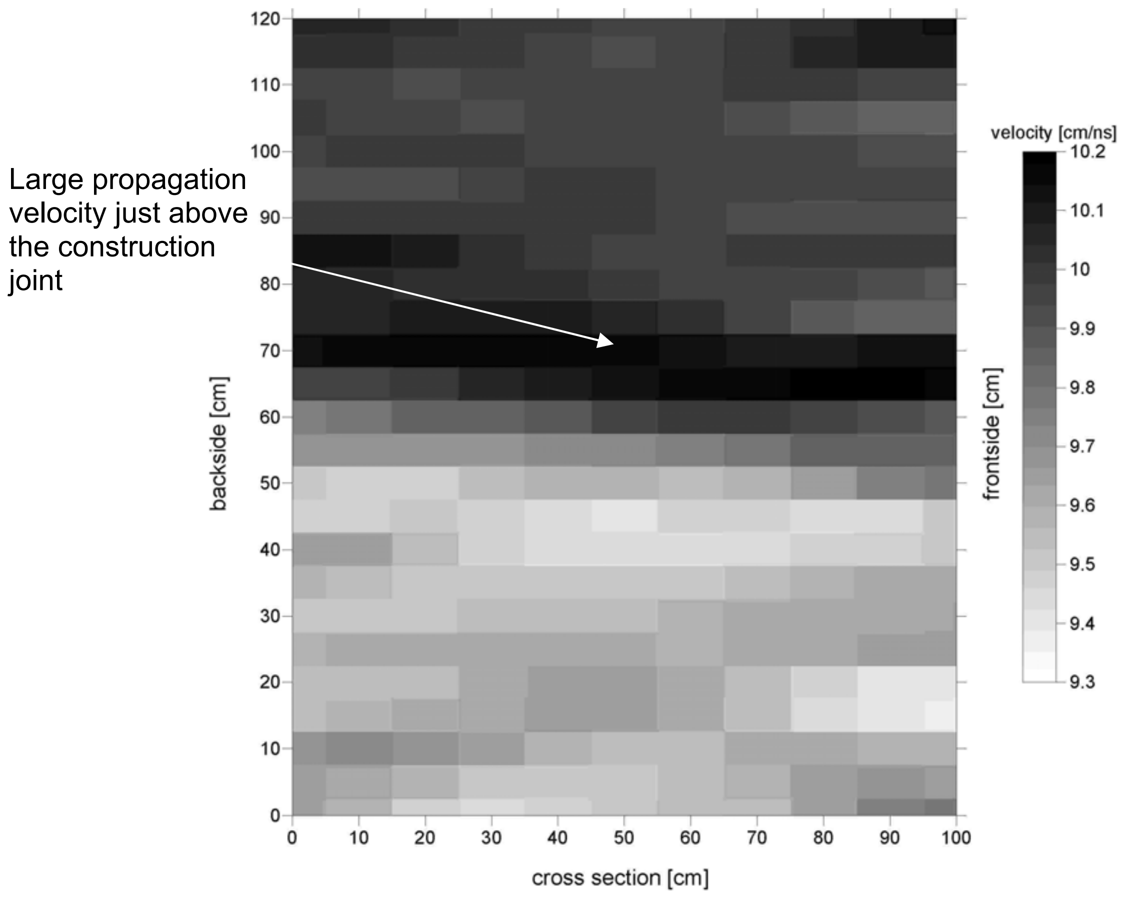

Figure 5.22 – Velocity tomogram showing the velocity distribution of the cross-section of the column B. This tomogram was produced with the profiles that had a ray inclination between ± 20 º and represent the final result. Data were processed with GeoTom CG software.

However, a significant number of artefacts (which can be defined as false, multiple or misleading information introduced by the imaging system or by the interaction of the electromagnetic waves with the adjacent materials) and the presence of refraction effects in the travel time data (see Chapter 7) resulted in a rather poor quality tomogram. To overcome this situation, new velocity tomograms were produced, with the profiles where the transmitter-receiver angle was between ± 20 º. The result of this new tomogram is illustrated in Figure 5.22. Just above the joint, a noticeable change of the velocity is confirmed, which can indicate the presence of very poorly vibrated concrete or deterioration in the column at the level of the construction joint. Due to the different time periods of construction, the most probable is that the concrete above the construction joint shows the result of insufficient vibration.

5.5 Summary

GPR is a fast and reliable technique to inspect concrete structures, which is being used recently to inspect bridges for locating deterioration and non-visible information, such as tendon ducts and the true location of reinforcement. This chapter focuses on three case studies in major bridges in Portugal and clearly illustrated the potential of this NDT technique, when combined with powerful signal processing tools.

In the first two case studies bridge inspection using GPR system with high frequency antennas allowed to accurately detect the position of the tendon ducts, which is a fundamental element for the safety of bridges. The inspection concluded that the tendon ducts were, in some cases, shifted with respect to the original design location. This information is important for efficient structural assessment and strengthening design. First, the information allows taking into account the real contribution of existing structural elements in the numerical and analytical models for strengthening design. Secondly, by determining the true position of tendon ducts and most important steel bars, the strengthening with external prestressing can be better planned and damage of the existing elements can be avoided during rehabilitation works. It must be noted that with the results of this work, the engineers responsible for the strengthening design were able to change the previous design in order to avoid drilling in locations where this would cross through existing tendon ducts.

In the last case study, GPR was used for the early detection of material and construction defects. The early detection of defects can help to adopt corrective measures (if necessary) to prevent further damage and to understand early occurrence of deterioration. The inspection of the support columns in a recent highway concrete bridge, which seems to register the occurrence of high levels of corrosion, allowed to detect deficiently positioned steel bars. Some of those bars were located very close to the surface, favoring the early occurrence of corrosion, while other bars where positioned deeper towards the centre of the column, affecting the design stresses, which can cause cracking and deformation of those structural members. Additionally, the application of advanced GPR tomography allowed to characterize the quality of the concrete, indicating the presence of execution defects. Radar tomography system has showed its usefulness and the data for the final inversion was almost free of not reliable signals, what made the interpretation of the tomograms much easier. Also successful combination between radar reflection profiling and radar tomography was successfully applied.

Chapter 6 - Methodologies for radar in the reflection mode while applied for the inspection of bridges

Although some of the procedures presented in this chapter were shortly mentioned in the previous parts of this thesis, it is necessary to clarify all aspects of radar inspection in reflection and in transmission mode and to present them in a systematic way. That is because testing using radar technique is a very expensive and complex process and requires deep explanation of all aspects of radar investigation on concrete bridges to the bridge owners, design offices, or radar operators. Only carefully planned NDT inspection using radar technique with deep understanding of its advantages and limitations can make the inspection worth its price. Thus detailed methodologies for radar in reflection (chapter 6) and in transmission modes (chapter 7) are presented. It is also important to mention that those techniques can't be treated as separated methods. They have to be applied together to give as much as possible information about geometry or integrity of tested structure. Those conclusions are based on authors own experience taken from the laboratory and on-site measurements in Portugal, Germany and Poland.

6.1 Planning an NDT investigation

6.1.1 Limitations and practical requirements

Before applying radar technique in reflection or transmission mode, one should be aware of the specific requirements of these techniques and should analyze the parameters involved in the investigations which might affect the data acquisition and processing. Non-Destructive Techniques can be expensive, despite their advantages. In the case of GPR, the following items must be considered in the process of selecting the technique:

- Type and nature of the materials to be investigated, as electromagnetic waves propagate at different speeds in different kinds of natural and man made materials.

- Nature of the targets of the investigation (reinforcement, moisture, voids, etc.). Generally, a very dense grid of reinforcement produces poor or no results at all.
- Preliminary assessment of the presence of moisture (e.g. due to rain or rising damp), as it affects severally the GPR performance and can prevent the acquisition of suitable data.
- Careful choice of antennas needed to perform the task. It must be based on operator's individual expertise taking into account over mentioned remarks. In general terms, choice of antennas depends on requested depth resolution and required penetration depth. It must be remembered that high frequency antennas have very low penetration depth but have quite high depth resolution (see Chapter 3)
- Carefully assessment of the time needed to acquire sufficient data to obtain the requested results. Too much data can increase processing time and costs unnecessarily.
- Careful assessment of time needed to perform the testing. Irregularities of the concrete or masonry surfaces can make the data acquisition very difficult due to possible malfunctioning of survey wheel of the antennas. Also time needed to access the test sites can be much longer that time for testing itself. Good scaffolding systems or movable platforms must be chosen very carefully and correspond to each particular test site.

6.1.2 Possible areas of applicability for radar reflection profiling using 2D and 3D image visualisation techniques

All possible applications of radar reflection profiling were widely described in chapter 3, and validated experimentally in chapter 4 and chapter 5 of this thesis. They include mainly the use of 2D and 3D imaging for the verification of structural geometry (like detection of rebars or tendon ducts) and integrity (like location of voids or areas with poorly compacted concrete).

6.2 Testing

6.2.1 Accessing the test site

As it was mentioned in the chapter 5, good and safe access to test site is the key to successful GPR investigation. If the scaffolding system is not covering well the test area, or the height needed to reach the test location requires use of additional ladders or platforms, the duration of GPR investigation can be significantly extended. In Figure 6.1 an example of access platform is shown. Because of the wrong height of the platform itself, to test internal beams, additional stairs had to be used, what significantly extended testing time. Also because the scaffolding system was not placed all over a bridge, equipment had to be transported down and upstairs several times to access consecutive pillars. That caused unnecessary time loss and implied additional costs.

Figure 6.1 - Example of scaffolding system used to access the test site

6.2.2 Selection and marking of test grids

Once the test location was safely reached, operator need to make the decision concerning density of the test grid. Operator should have the prior indication of the position and size of test location. It means that when entering to the test site, objectives and coordinates of the test should be clearly indicated.

The size of the grid strongly depends on the test objectives. If for instance design office requires the information about the location of embedded objects in plane only, and the objects are not expected to have complicated shapes, less dense grid can be advised. According to the author's experience, to search for tendon ducts, grids with 20 - 40 cm of spacing between parallel profiles can be successfully applied. Profiles should be performed in the perpendicular direction to the expected embedded elements (like rebars or tendon ducts).

In case if 3-dimensional information about location and shape of embedded elements or anomalies is required, more dense grids can be strongly advised. According to author's experience, 5 cm of spacing between parallel profiles is sufficient to obtain realistic 3D information about embedded structural elements or anomalies (see Chapter 4.1 and 5). That method is required only in very specific situations to solve specific problems. 3D image visualization is especially useful while searching for areas with poorly compacted concrete, like indicated in Chapter 4.1.

The grids should be marked with waterproof marker, using the levelling rod. Vertical and horizontal reference lines should be indicated very clearly. Examples of test grids are shown on Figure 6.2.

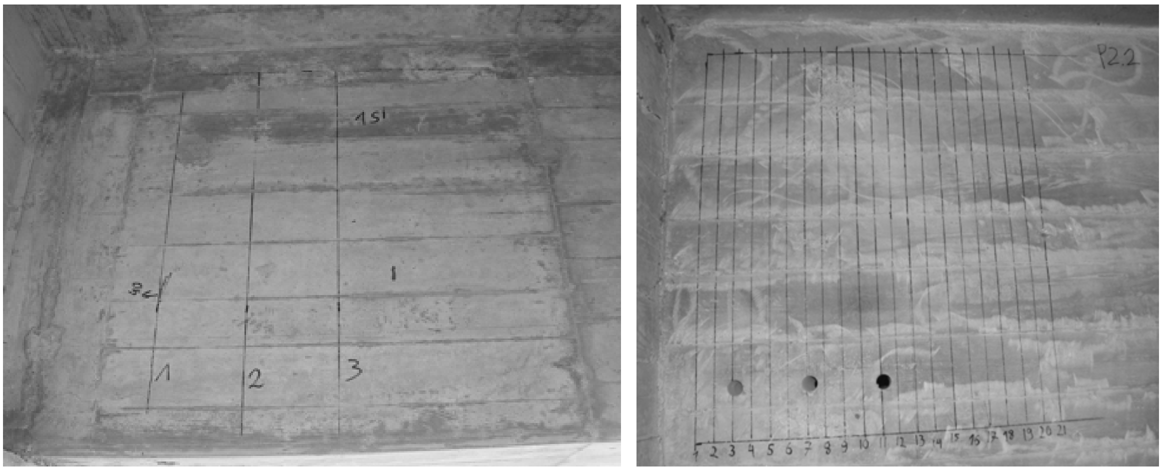

(a) (b)

Figure 6.2 – Examples of measuring vertical and horizontal lines in beams: (a) at the Barra bridge with a line separation of 20 cm and (b) at the Lanheses bridge with a line separation of 5 cm.

6.2.3 Performing data acquisition

Data in the reflection mode should be acquired on the smooth, dry surface, with previously prepared test grid. Length of the acquired profiles should be controlled during the measurement, so no misleading distance information is obtained. Operator should pay attention if no traces are lost, and if so, repeat the measurement (see Figure 6.3). Antenna should be moved with constant speed and remain as close as possible to the tested surface. To ensure exact distance information, position of the centre of the antenna should be clearly marked on the antenna itself so the operator can start or end the measurement on an exact reference line marked on the tested surface.

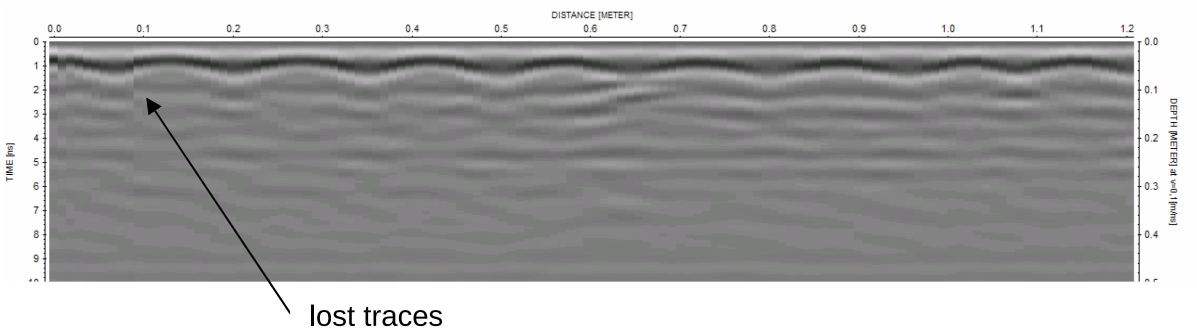

Figure 6.3 - Example of radargram where some traces were lost

During the measurement, time calibration measurements with metallic shield on the opposite side should be performed for the estimation of the average propagation velocity within the cross section of tested structure. Typical result from such calibration is presented in Figure 6.4. When the velocity information is given, time axis can be converted easily into the depth scale to measure the depth of targets. Typical measurement procedure consists of placing metallic shield on one side of tested structure and moving an antenna on another. Also opposite procedure is possible, when the antenna is remaining stationary and metallic object is moved with constant speed on the opposite side.

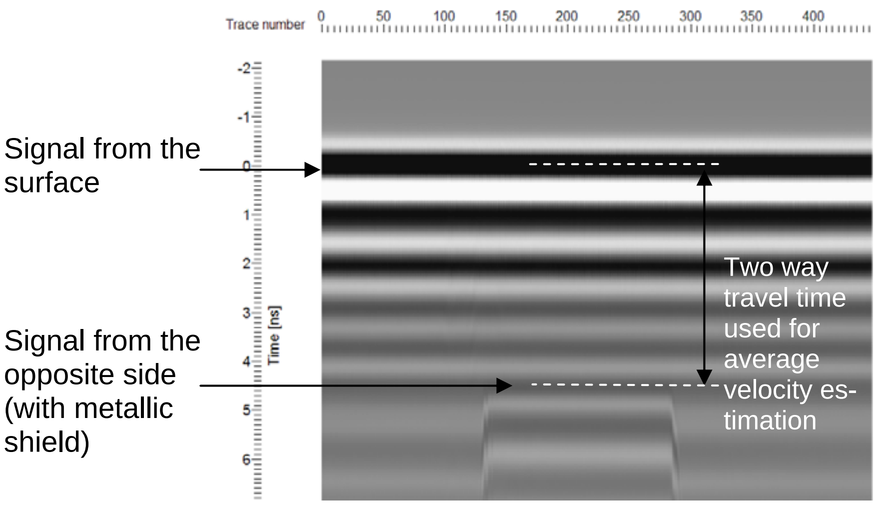

Figure 6.4 - Radargram from the time measurement

6.3 Data processing and analysis

6.3.1 Data processing

Raw data recorded by each radar system contain a lot of noise and they need to be filtered by specialised software. Detailed processing procedures for data acquired in reflection mode are presented widely in Fernandes (2006).

6.3.2 Data interpretation

In general terms, data interpretation from the 2D radargrams is known and is based mainly on the identification of the peaks of the hyperbolas for determining of the position of embedded structural elements or recognition of the layers within the structure. Also interpretation of 3D data is quite easy, because information about embedded structural elements or anomalies is provided as isosurfaces or depth slices, so the shape and coordinates can be quite easily interpreted.

However there exist some situations, where data interpretation can be quite difficult. They consist mainly of:

1. Shielding of the electromagnetic waves caused by closely spaced reinforcement

There exist two cases where shielding effect can be visible or not visible for the operator. In the first case, when the reinforcement grid is very dense, there will be no observable signal below (see Figure 6.5). In the second, more complicated case, due to low aperture of the cone of the electromagnetic waves, objects directly behind the metallic grid remain not detected, especially when they are the similar size to the grid itself (see Figure 6.6).

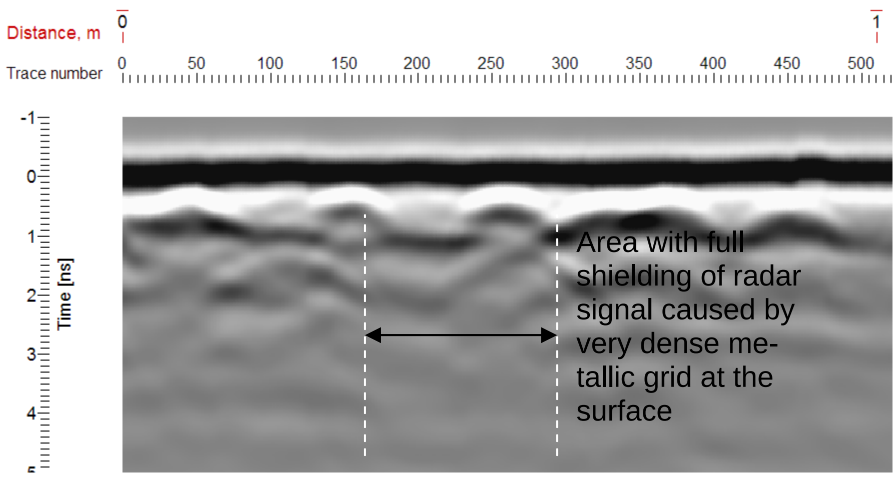

Figure 6.5 - Example of the full shielding effect behind very dense reinforcement grid

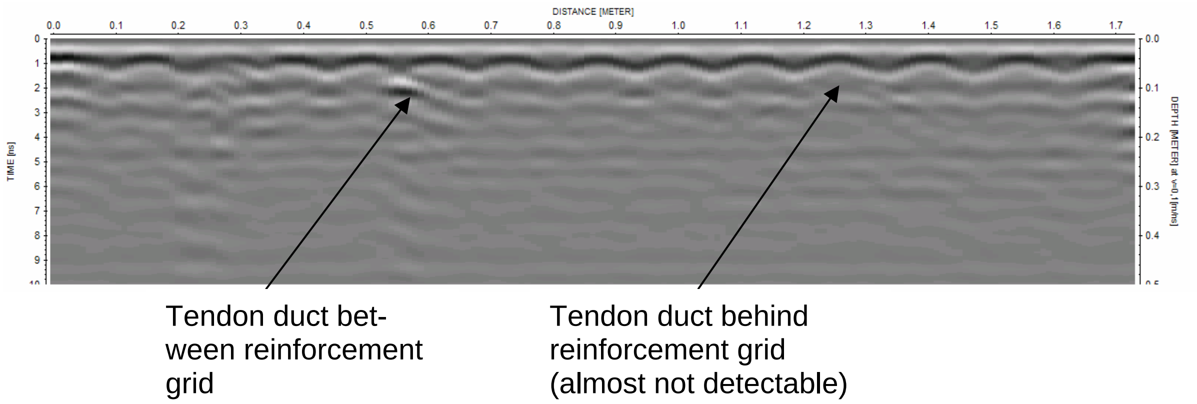

Figure 6.6 - Example of partial shielding effect

2. Presence of different concrete qualities (different vibration or presence of high amount of water)

In that particular case, presence of salty water inside the structure can be identified by observing the changes of signal from the backside of the tested structure. If the signal is uniform along its entire length, the structure can be considered more or less homogenous. But if signal from the back side is changed (like indicated in Figure 6.7), and time needed to reach the back side is longer that usually for the specified depth, it can indicate presence of very wet concrete.

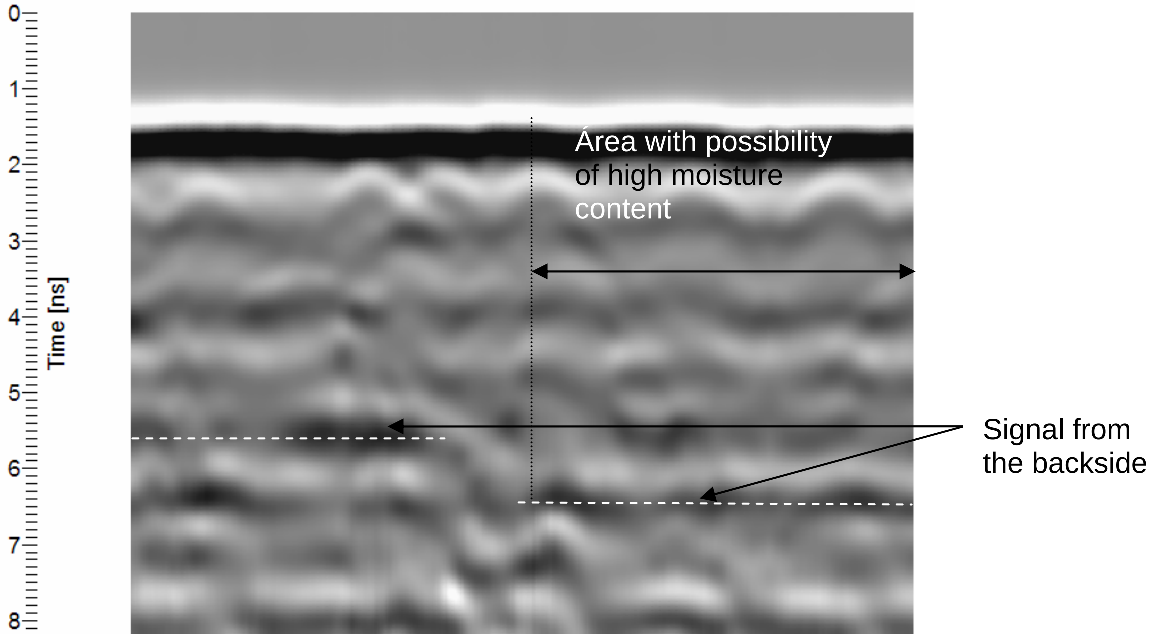

Figure 6.7 - Example of radargram with indication of high moisture inside the tested structure

6.3.3 Data visualisation

After processing, data can be visualized in several ways for final reports. The most common is to present them as 2D or 3D image of the tested structure. Further description of those visualization methods can be found in chapter 3 of this thesis. However, the most adequate way of presenting the results for the end –users is to show them as AutoCAD drawing with coordinates to the reference lines (vertical and horizontal). In that way, bridge owners having marked grids on the test sites, can easily identify location of rebars, tendon ducts or deteriorated areas. Numerous examples of such results are presented in chapter 5 of this thesis.

Chapter 7 - Methodologies for the radar in the transmission (tomography) mode while applied for the inspection of bridges

7.1 Introduction

In this part of the thesis detailed guideline for end-users concerning use of radar tomography technique are presented. Because use of this technique is very complex, this chapter will be considered as the integral part of the thesis. Before reading this chapter, it is advised especially for non-expert readers to read carefully previous chapters and Appendix at the end of the thesis about wave propagation phenomena.
Contents of that chapter is based on the input from Deliverable 3.8 “Radar Tomography” from the “Sustainable Bridges” European Project and presents current most up-to-date achievements done in that technique at an international level.

7.2 Planning an NDT investigation

7.2.1 Limitations and practical requirements

As it was mentioned before, tomography is really complex and expensive technique and its use should be well-planned in all aspects. All mentioned in Chapter 6.1 limitations and practical requirements apply also to the transmission measurements. In case of tomography measurements, additional requirements need to be addressed, namely:

- The necessity of access from two or more sides. The reconstruction algorithms used for data processing are most suitable in cases where two or more sides of the structure are accessible and covered by electromagnetic rays.
- The higher qualifications and experience of the radar operator, especially for data processing.

7.2.2 Possible areas of applicability for tomography

Tomography can be used in numerous applications (see Figure 7.1). Mainly it can be applied to evaluate general structural integrity or geometry of civil structures providing information about material properties inside. As it can be seen from the flowchart, a transmission measurement is not a separate technique itself, but it can be applied, when the reflection methods fail due to various reasons.

1. General problem

- 2D or 3D image does not provide enough information about the geometry or integrity
- Penetration is not sufficient in reflection mode
- Reinforcement grid is very dense

↓

2. Tools to solve a problem

Tomography measurements and data analysis – imaging of general structural geometry and integrity inside tested structure.

↓

3. Possible areas of applicability for tomography measurements

Concrete structures

1. Precast structures
   - To detect areas of voiding in the connection of 2 or more precast elements
2. Monolithic structures (bridge abutments, pillars, beams)
   - To detect areas with different concrete compaction quality
   - To detect areas with high porosity, and thus high possibility of presence of water inside the structure
   - To detect areas with high chloride content (in amplitude tomography)
   - To localize plastic or metallic tendon ducts located behind very dense reinforcement grid

Masonry structures

- To estimate material properties inside old masonry arch bridges
- To detect possible losses of mortar by water and to monitor fluid injections
- To detect areas with high water or chloride ingress

Figure 7.1 - Flowchart showing possible areas of applicability for tomography

7.3 Testing

Once decisions concerning choice of tomography as an investigation technique, hardware, software and qualified staff have been made, detailed testing procedures with some hints will be introduced in this chapter. It would seem that performing an acquisition in the transmission mode should be relatively easy. That is the case, but only in theory. In practice, NDT specialist must have a proper experience to choose the best set-ups and to have deep knowledge about behavior of the antennas in case of radar tomography. Additionally, good data acquisition is necessary to obtain reliable results, which can be a subject for analysis and final interpretation. Because the only parameters, which are used during travel time tomographic inversion, are the travel times and coordinate input, operator must be ensure that they are correct. Most of the testing procedures are similar as in case of reflection measurements (see Chapter 6.3). In case of transmission measurements additional requirements have to be addressed: Types of acquisition methods for transmission measurements are described in chapter 3 of this thesis.

7.3.1 Grids for transmission measurements

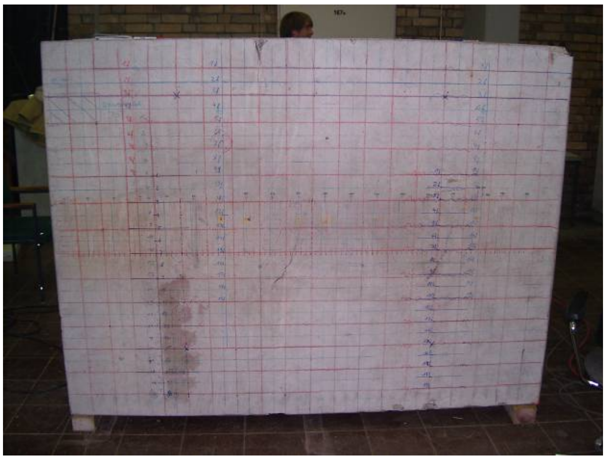

Figure 7.2 - An example of a grid on BAM concrete specimen.

Good grid or good positioning system for transmission measurements is one of the most important things to be done before performing an experiment (Figure 7.2). Coordinates of each point or trace must be very precisely specified (position of a transmitter and receiver at each time must be known). Accuracy of 1-5 mm should be used. Even small deviations from a specified coordinate system may cause serious disturbances during tomographic inversion (see Figure 7.15).

Depending on the size of tested structure and antennas used size of grid may vary. The choice of grid size and depends on the expertise of the operator. In general terms, size of the grid strongly depends on the required resolution needed for solving particular problems – denser the grid, higher the resolution. Also time needed for the acquisition is an important factor – denser grid means more time spent onsite and more processing time what increase the testing costs. For the concrete or masonry structures with thickness up to 0.2 – 0.8 m preliminary tests can be done with 1.5 GHz antennas and 0.1 m grid. If necessary, the grid can be denser. However, grids less than 50 mm are not advised. If the thickness exceeds 0.8 m or the penetration is limited due to very dense reinforcement (50 – 80 mm between rebars) lower frequency antennas must be used (e.g. 900 MHz).

7.3.2 Choosing maximum angle between transmitter and receiver antennas (refraction effect)

If the angle between transmitter and receiver antennas will be higher than critical angle, refraction effect can occur. Critical angle is the maximum angle between transmitter and receiver antennas where the first recorded wave by the receiver antenna is a direct wave (see Figure 7.4). That effect is caused mainly by the fact that velocity in the air is much higher than velocity in the medium, so the refracted wave will move faster than direct wave. For the input data for the inversion algorithms, only direct waves are needed (Figure 7.3). If other kinds of waves are picked (reflected or refracted), additional steps in the data filtering must be taken into consideration (see Figure 7.13a). For those reasons, to avoid problems during processing phase, experiments should be performed to have angles between transmitter and receiver antennas up to 30 degrees.

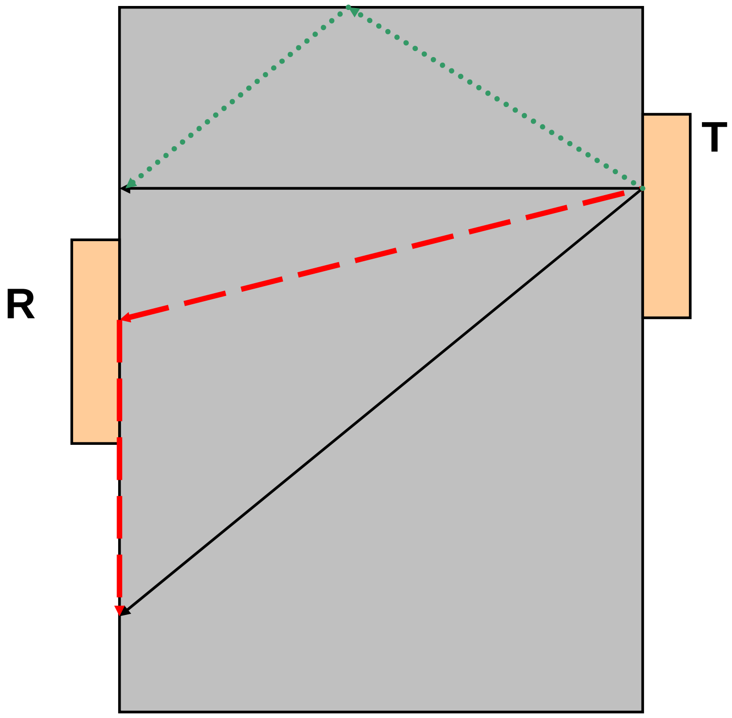

Figure 7.3 - Example of direct (black, continious line), reflected (green, dotted line) and refracted waves (red, dashed line)

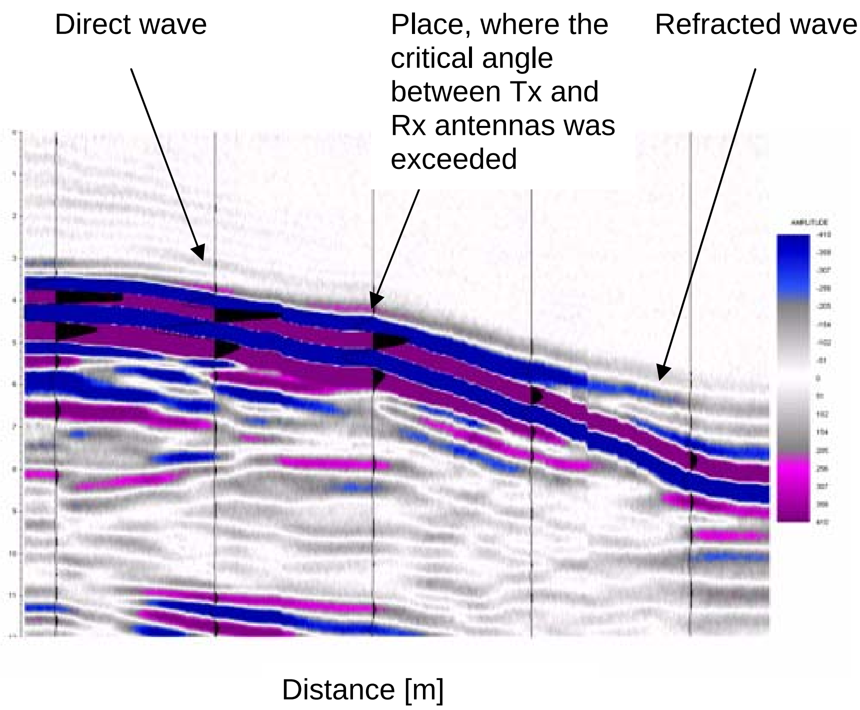

Figure 7.4 - Resulting radargram from the transmission measurement showing the refraction effect

7.3.3 Air measurements

In chapter 4.3, general problems concerning time axis calibration were indicated and main procedure for air measurements was shown. Further information about details behind that procedure is provided in the chapter 7.4.

7.4 Data processing and analysis

Once data has been acquired, it has to pass through many steps of processing, quality checking and finally through the main part, inversion algorithms, which will reconstruct travel time information into velocity map. When final tomograms are available, they are subjected into final interpretation and, if necessary recognition of many possible artefacts, which can occur during the inversion process. Only data with calibrated travel time, coordinate input connected with careful quality checks and artefacts recognition can be subjected into final interpretation. Flowchart showing overview of the processing procedure is shown in Figure 7.5.

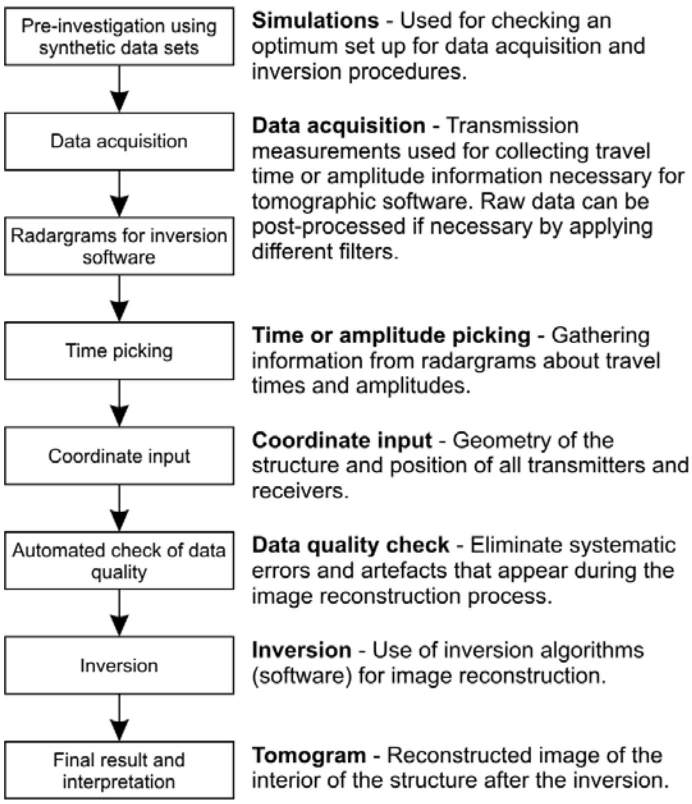

Figure 7.5 - Flowchart showing general idea of steps for data acquisition and data processing.

7.4.1 Preliminary planning

Before starting a measurement on for example a concrete specimen it is advisable to perform some simulations in available commercial software (e.g. Reflex) to have an idealised image of a tested structure. For known geometry (including the anomalies) there is the possibility of solving the questions by creating synthetic data set. For the real situations model used for those simulations must be based on the parameters obtained in-situ by other methods (like radar in the reflection mode or for example visual inspection). Those simulations are used only as a complementary tool, and can be also applied during the data processing and interpretation (after the experiments) for better understanding of the results.

Main steps for preliminary planning/analysis of synthetic data set have the following aims:

1. To estimate the maximum expected travel time / velocity difference for a given investigation problem
2. To choose an optimal measurement configuration (distance of transmitter / receiver)
3. To predict resolution of the tomographic reconstruction for an ideal case

The resolution of the tomographic reconstruction for a specific measuring set-up and specific mesh size can be done by so called “chequerboard” check. In the Figure 7.6 one example of simulation done in Reflex commercial software is given. The aim of this simulation is to explain the results from the BAM concrete specimens presented in chapter 4.2. In the Figure 7.6a it is visible, that most of the rays were passing through an air void. It happens when wave encounters material with very low dielectric constant and most of the energy is accumulated by this material. It is also visible that that concentration of rays passing through an air void caused presence of inversion artefacts as shown in the results from real measurements in chapter 4.3 and in Figure 7.6b. In case of steel (high dielectric constant) waves are passing around the object. Areas with low ray coverage had edge effects after the inversion. Thus only area inside dashed line was taken into consideration (Figure 7.6b).

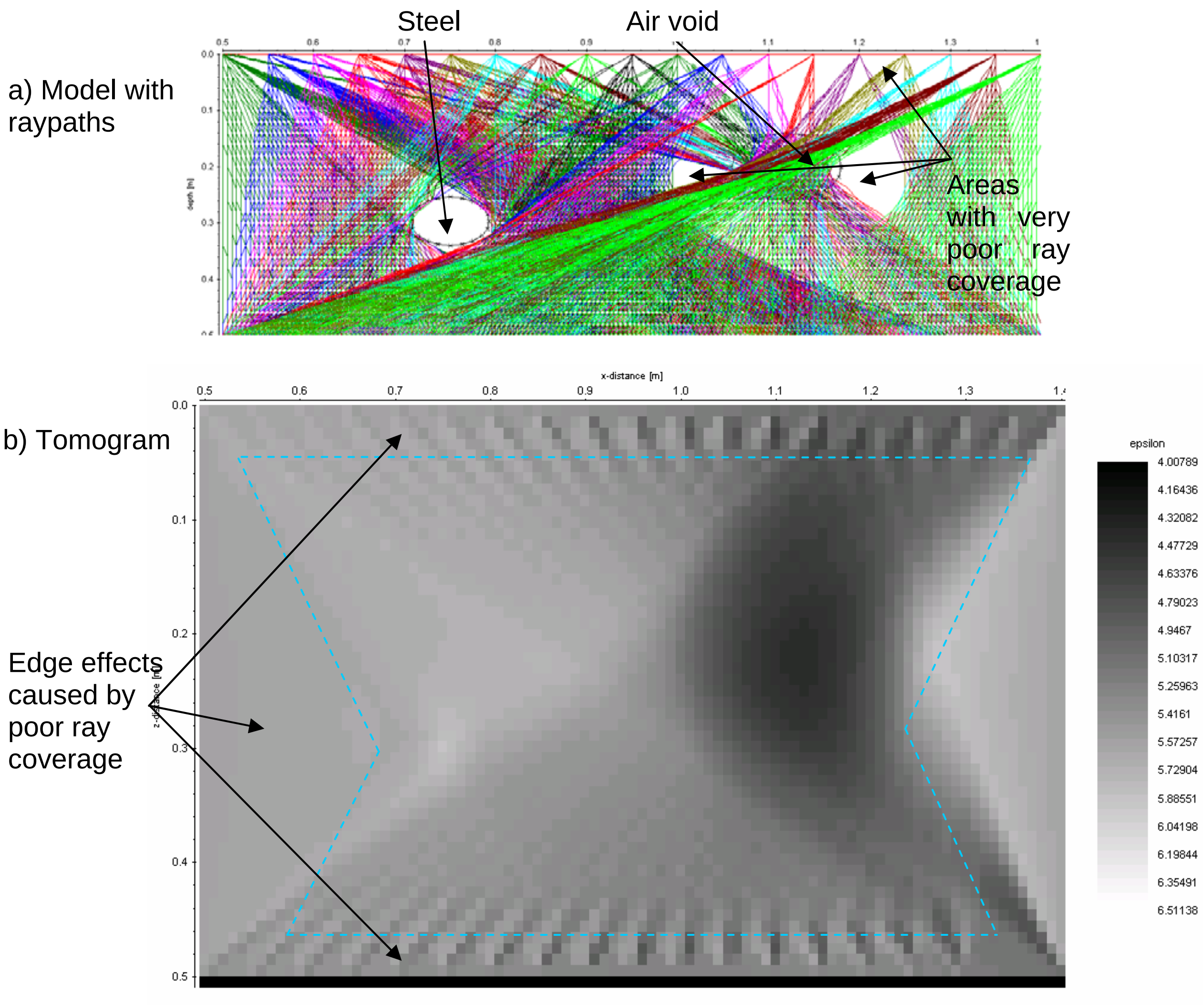

Figure 7.6 - An example of synthetic data set created in Reflex commercial software and a result of a simulation (a) raytracing, b) tomographic inversion of first arrival times).

7.4.2 Coordinate input

GeoTom CG

The first step to prepare the data to most programs that are making an inversion is to give them 3-dimensional coordinates of each transmitter (Tx) and receiver (Rx) positions. An example of data for GeoTom CG commercial software is shown in Figure 7.7. There should be in general columns with: transmitter and receiver numbers; numbers of each ray; 3D coordinates of Tx and Rx; estimated travel times and travel times after calibration; and other additional columns which could be useful for further data quality checking (T-R distance, difference between measured travel times, Tx-Rx angle, straight ray velocity, etc.).

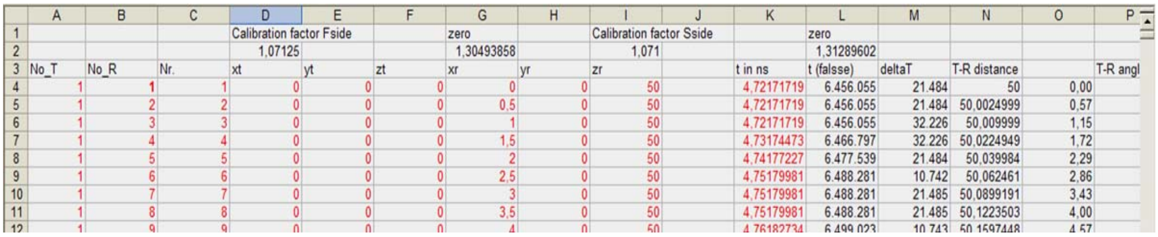

	A	B	C	D	E	F	G	H	I	J	K	L	M	N	O	P
1				Calibration factor Fside			zero		Calibration factor Sside			zero				
2				1,07125			1,30493858		1,071			1,31289602				
3	No_T	No_R	Nr.	xt	yt	zt	xr	yr	zr		t in ns	t (falsse)	deltaT	T-R distance		T-R angl
4	1	1	1	0	0	0	0	0	50		4,72171719	6.456.055	21.484	50	0,00	
5	1	2	2	0	0	0	0,5	0	50		4,72171719	6.456.055	21.484	50,0024999	0,57	
6	1	3	3	0	0	0	1	0	50		4,72171719	6.456.055	32.226	50,009999	1,15	
7	1	4	4	0	0	0	1,5	0	50		4,73174473	6.466.797	32.226	50,0224949	1,72	
8	1	5	5	0	0	0	2	0	50		4,74177227	6.477.539	21.484	50,039984	2,29	
9	1	6	6	0	0	0	2,5	0	50		4,75179981	6.488.281	10.742	50,062461	2,86	
10	1	7	7	0	0	0	3	0	50		4,75179981	6.488.281	21.485	50,0899191	3,43	
11	1	8	8	0	0	0	3,5	0	50		4,75179981	6.488.281	21.485	50,1223503	4,00	
12	1	9	9	0	0	0	4	0	50		4,76182734	6.499.023	10.743	50,1597448	4,57	

Figure 7.7 - An example of a coordinate input in Excel done for GeoTom CG files.

WinTomo

Input of coordinates consists of the following steps:

- definition of 3-dimensional coordinates of transmitter and receiver positions.
- creating a scan list (the scan list describes the positions of the antennas in the boreholes and provides a link between the ray, defined by the geometry and the trace, being the actual data recorded).

This input can be done manually or automatically. Input is very fast and allows user full visual control (see Figure 7.8).

Number	Depth	X	Y	Z
1	0,000	0,000	0,000	0,680
2	0,010	0,010	0,000	0,680
3	0,020	0,020	0,000	0,680
4	0,030	0,030	0,000	0,680
5	0,040	0,040	0,000	0,680

Figure 7.8 - An example of coordinates input done at WinTomo.

7.4.3 Travel times picking and time axis calibration

Travel times picking

The most critical moment during tomographic data analysis is the accuracy of picking the right travel times. Travel time inversion software, which is making an inversion bases on an input of transmitter and receiver positions and picked travel times. The higher error will be done during time picking the worst will be the results of tomographic inversion. Only direct waves must be picked (see Figure 7.3 and Figure 7.4). Depending on which signal position was chosen to pick (at the first arrivals or first maximum or minimum), the proper way of picking must be defined. During experiments at BAM always the first maximum or first minimum was picked (see Figure 7.10). Physically the best would be to pick the first arrival, but usually because of presence of high noise first maximum or minimum is picked.

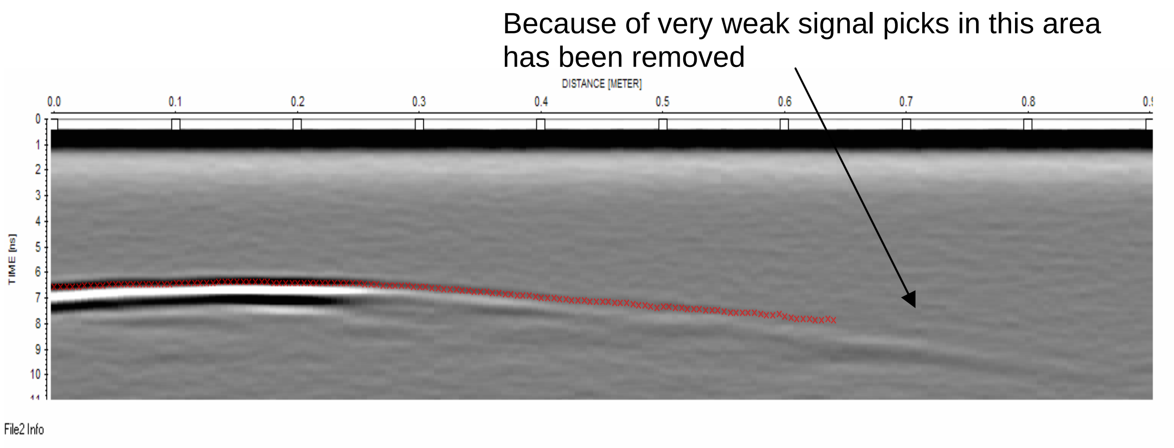

Figure 7.9 - An example of Time Picking done at Reflex commercial software

Every operator has to remember that when a signal is very weak an accurate time picking is almost impossible. Then those doubtful picks should be removed (see Figure 7.9).

Sometimes, however it is quite difficult to know which travel times we have to pick. In the following examples possible difficulties will be explained (see Figure 7.10 and Figure 7.11). On these radargrams (see Figure 7.10 and Figure 7.11) a second maximum would be chosen for picking. Usually in such case, void would be not detected. However, it has to be always remembered to pick the first maximum (minimum) or the best would be first arrival. Following that suggestion it is possible to enhance the reliability of the results.

However, sometimes results from measurements can be even more confusing. When investigation is performed very close to an air interface and antennas are situated parallel to an air interface, interferences of waves can occur, what can lead to misinterpretation of radargrams. Because of that it can be advised that during data acquisition operators should avoid areas very close to interface with air. Experiments on concrete columns with air joints and also results from simulations suggest that acquisition should be made 150 mm from concrete (masonry)/air interfaces to avoid possible high influence of air in the recorded data.

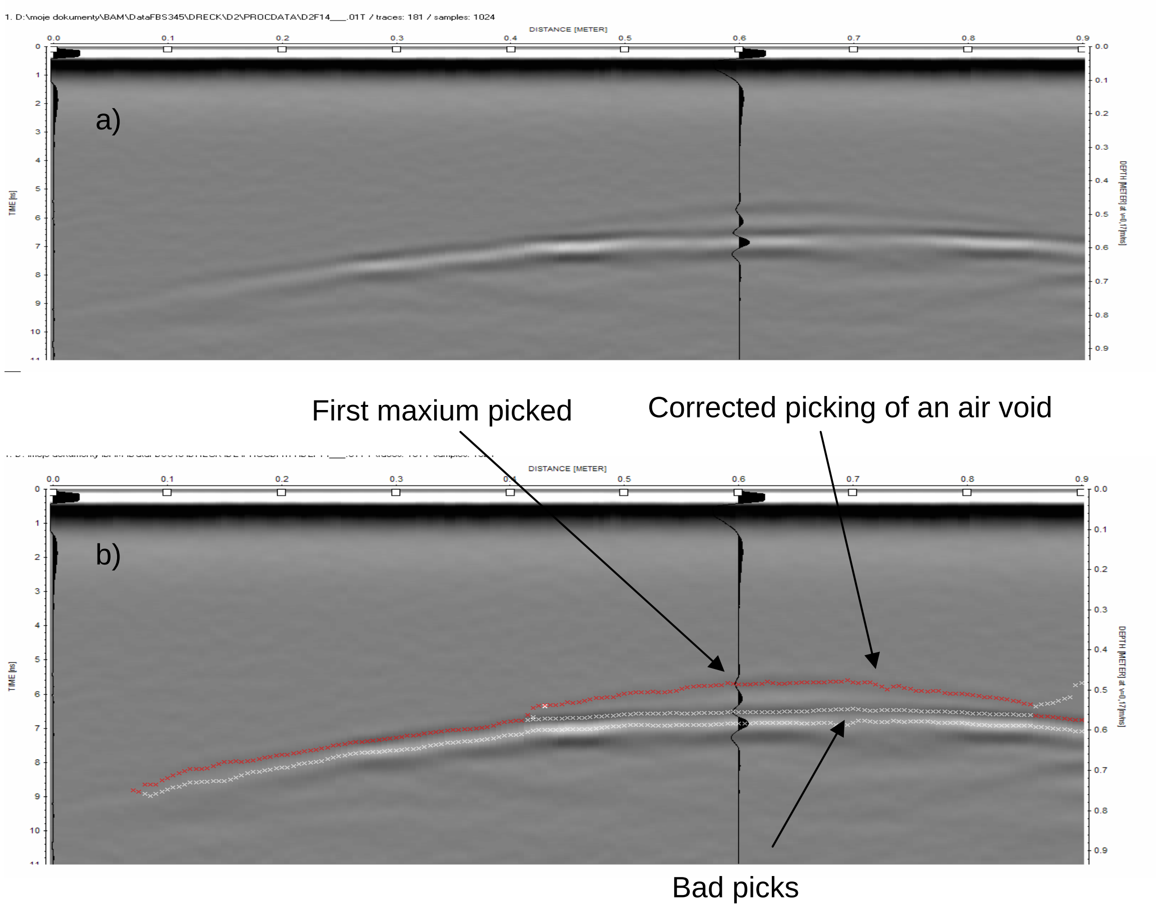

Figure 7.10 - An example of corrected Time Picking done at Reflex commercial software.
a) before picking b) after picking

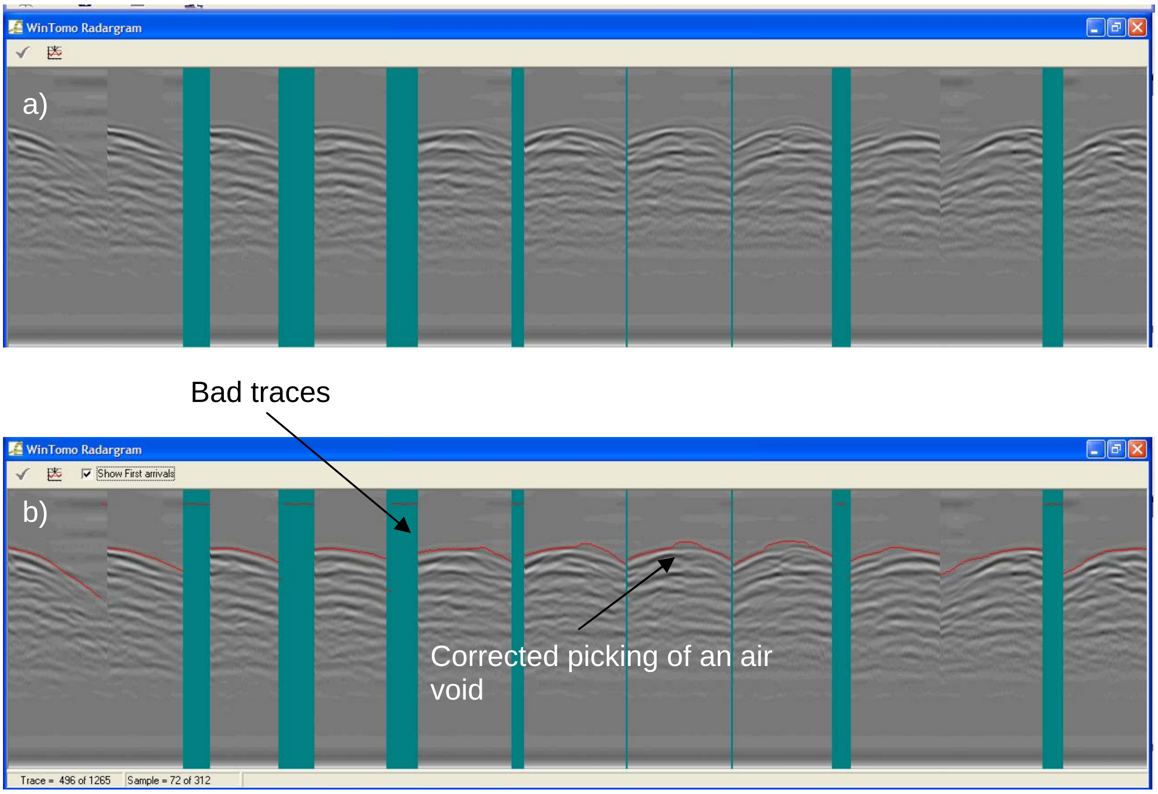

Figure 7.11 - An example of corrected time picking done at WinTomo commercial software:
a) before picking b) after picking

Time Axis Calibration

After travel times are obtained the nest step is to calibrate them into correct values. Those values can be obtained by using standard time calibration procedure. The procedure main idea is to make the series of time measurements between transmitter and receiver antennas. Result is the plot showing transmitter – receiver distance (x) versus corresponding travel time (y). After linear interpolation straight line is obtained:

$$y(x) = A \times (x) + B, \qquad (7.1)$$

where:

$A = \frac{1}{v}$, $B = t_0$, $v = \frac{s}{t}$, *s* – distance, *v* – velocity, *t* – travel time, t_0 – travel time offset

Having travel time offset, it is possible to calibrate the measured travel times into correct values. That procedure is only valid, if the radar signal is considered stable.

7.4.4 Procedures for check of data quality for travel time tomography data

After coordinate input and time picking overall quality of data need to be checked before performing an inversion. Also after inversion systematic errors need to be identified and preferably eliminated. These procedures are in most cases iterative, they need to be repeated until final tomogram will be ready for final interpretation. These procedures can be applied for data from both programs: WinTomo and GeoTom CG. However, in GeoTom CG some procedures for automated data quality check are already included in the software (e.g. residuals vs. Tx-Rx distance plot). Data sets used in this chapter are not used for the particular case. They were taken from different measurements.

In general data quality check can consist of the following steps:

1. Pre-investigation of data sets to improve a data quality
2. First tomographic calculation with a homogenous starting model and different meshes
3. Recognition of the artefacts in tomogram after the inversion
4. Choice of the most capable mesh for the final inversion
5. Check of the stability of tomographic calculation
6. Second tomographic calculation using data subsets
7. Final tomographic calculation

1. Pre-investigation of data sets to improve a data quality

Certain physical conditions have to be fulfilled e.g. the law of Fermat and Snellius. In this case for the repriprocal position of the transmitter and receiver the travel time for both ways has to be the same. The first step during pre-investigation of data gives an overview of the data quality (Figure 7.12). Usually on these graphs we should see a pattern and usually symmetry. If the signal is spread without any sense it could be advised to evaluate such data with high attention. Every discontinuity is quite visible and possible areas with voids can be easily detected as well as the quality of our data being easily evaluated.

The second step during pre-investigation of data specifies the error (Figure 7.13a and b). Attention should be paid firstly to time offset value (Figure 7.13b) and secondly to see if data are not depending on a transmitter-receiver angle (Figure 7.13a). In an ideal case there should be no offset and there should be no data dependence on a T-R angle (only in case of homogenous media like concrete. In masonry data can have strong angle dependence. But then quality of the data can be good. Such dependence can mean an air void). In case of significant increase of velocity at the extremities of the plot, it can mean presence of refraction effect in the recorded data. Then those data sets must be excluded. Bad data sets usually are spread randomly. Very important is to plot these graphs to all data sets and see if lines have comparable inclination and offset (see Figure 7.14). On Figure 7.14 are shown two completely different data sets with different offset and inclination of trend lines. These data sets can not be joined for inversion

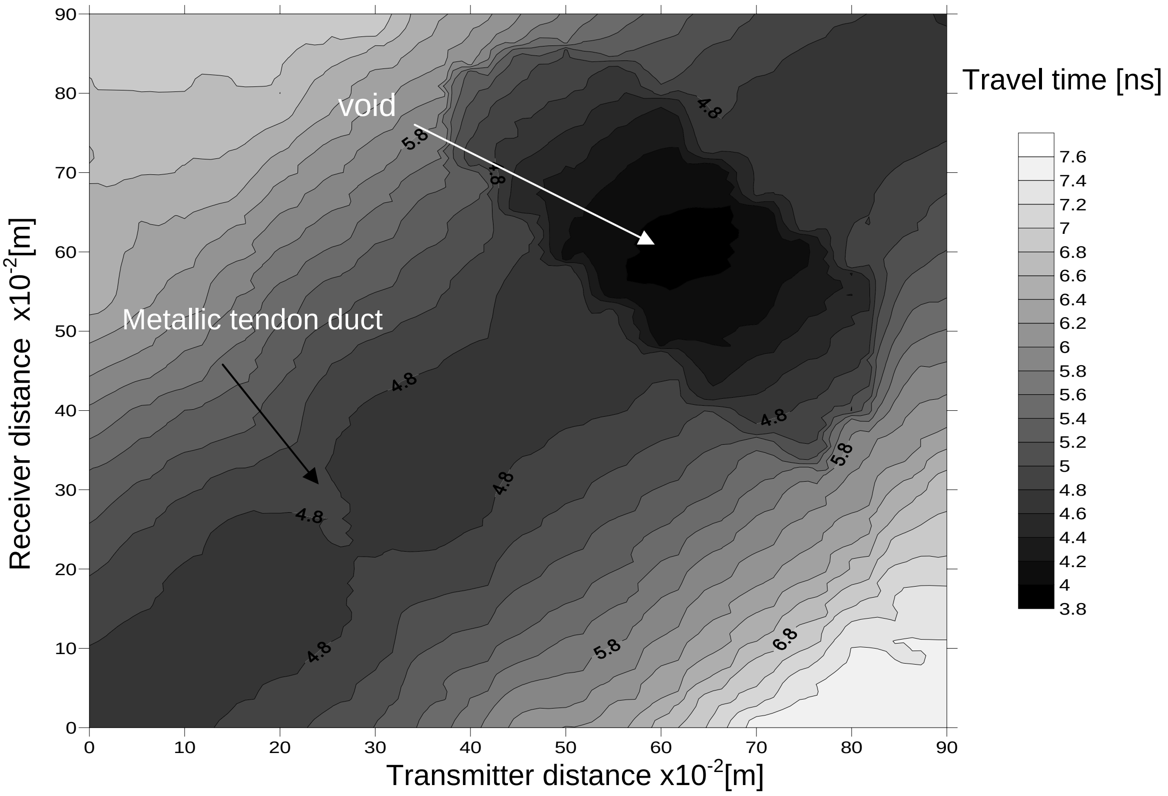

Figure 7.12 - 3D plot of travel times respectively to belonging transmitter and receiver positions (with void and metallic tendon duct)

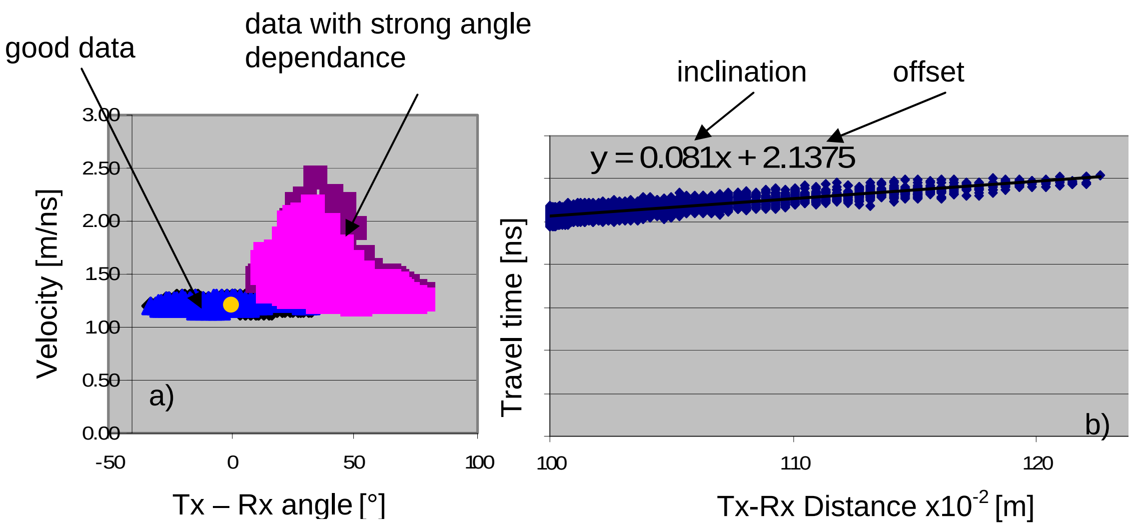

Figure 7.13 - a) 2D plot of T-R angle respectively to belonging straight ray velocity;

b) 2D plot of the T-R distance respectively to belonging travel time

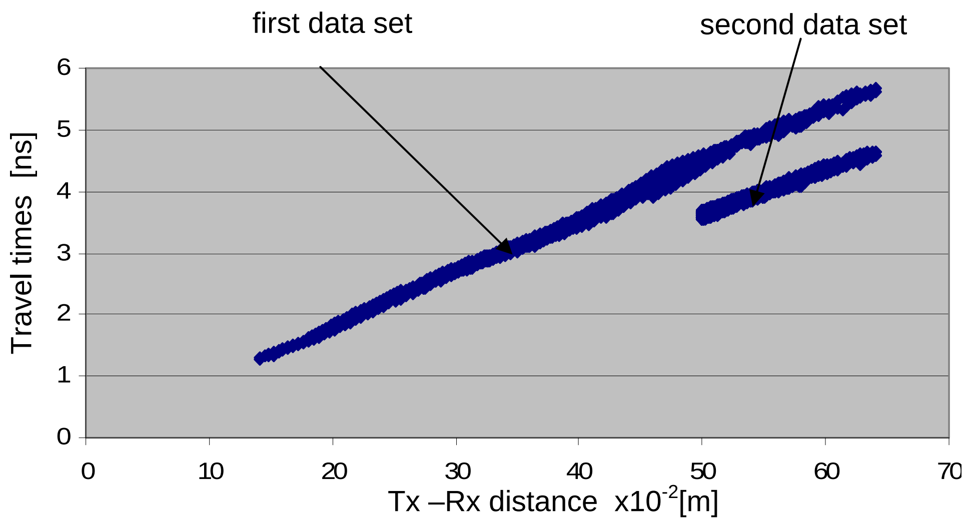

Figure 7.14 - An example of an error when after offset correction we have suddenly 2 completely different data sets. In this case these two data sets can not be analyzed together.

2. First tomographic calculation with a homogenous starting model and different meshes

Resulting from the first inversion of the travel times a velocity distribution at each element is obtained. With use of iterative algorithms different iteration steps are applied. The iteration cycle shall repeat as often as is necessary. This means the residuals (difference between the measured time and the calculated time of the algorithms) of one iteration to another should not have significant differences. One criteria to cancel the iteration cycle are the divergence of the residuals (see Figure 7.16). The absolute value of the residuals of each T-R combination of the last iteration should be less or at least a similar size to the travel time difference caused by the expected anomaly. Another criterion is the average (RMS) of all residuals at one specific iteration step shall be in range of the total accuracy of the measurement and time picking and/or the standard deviation of reciprocal measurements.

3. Recognition of the artefacts in tomogram after the inversion

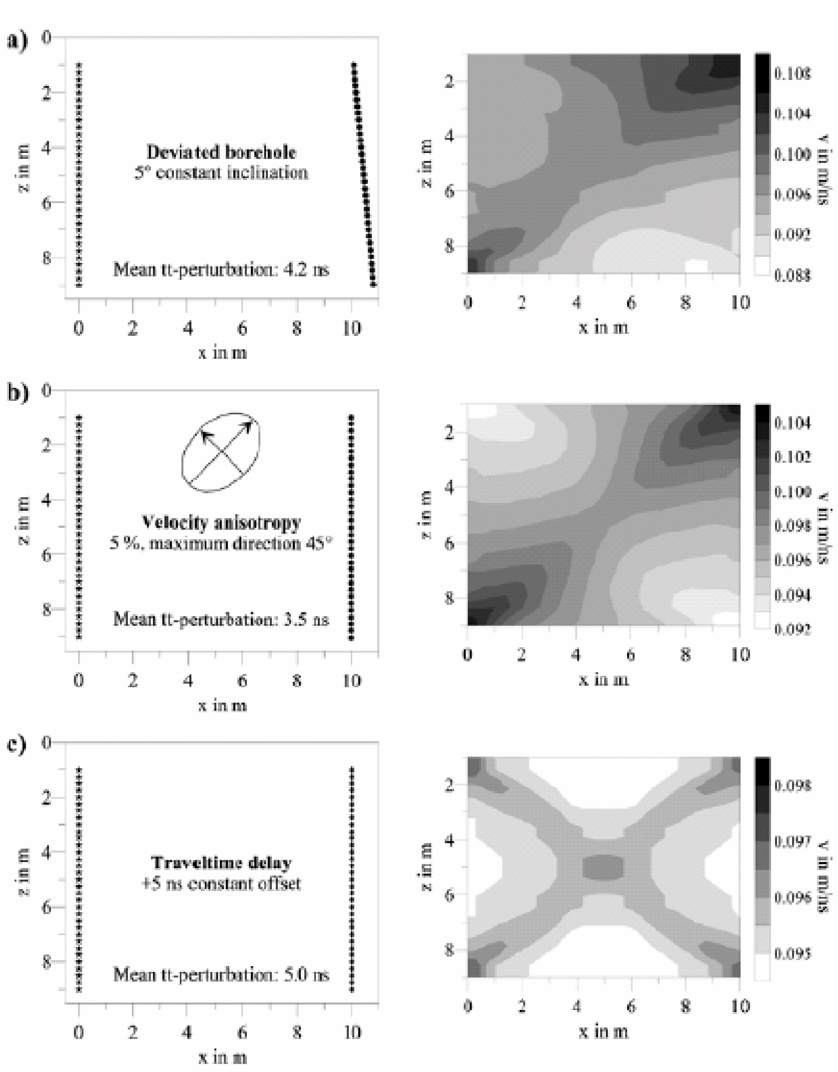

Figure 7.15 - Three possible errors in tomographic inversion and their images (Tronicke et al. 2002).

Data sets of transmission measurements can contain systematic errors. Such errors can be caused by unconsidered faulty positioning of the transmitter and/or receiver;

unconsidered anisotropy and/or a travel time delay. If they are not eliminated they can cause characteristic artefacts at a tomogram. This may lead to misinterpretation of the results. In Figure 7.15 three possible errors and their typical tomograms are presented.

Mainly during investigation on civil structures first and third error are quite common and can completely distort the data. Second error-velocity anisotropy is less expected. This quality check is made on tomograms.

4. Choice of the most capable mesh (suitable element size) – dependence on inversion software

The size of the elements depends on the measuring set-up (e.g. distance of transducer and geometry of the cross section). A helpful hint to receive stable information is 10 rays should pass one element at least in different angles. Other tip can be that the size of each element should be not smaller than the distance between transmitters (for SIRT algorithm in GeoTom and Reflex). In Conjugate Gradient (CG) algorithm in WinTomo grid size should be chosen as small as possible, but too small grid size can cause program to terminate. In practical experience half distance between transmitter and receiver antennas should be sufficient.

5. Check of the stability of the tomographic calculation (residuals/artefacts)

Residual travel time is defined as the measured travel time minus estimated travel time for a homogenous medium with a constant velocity. The first step is to check the behaviour of the RMS residuals for each iteration (Figure 7.16). They should decrease. In mathematics, root mean square (abbreviated RMS), also known as the quadratic mean, is a statistical measure of the magnitude of a varying quantity. The next step is to visualise the residuals of each T-R combination of the last iteration.

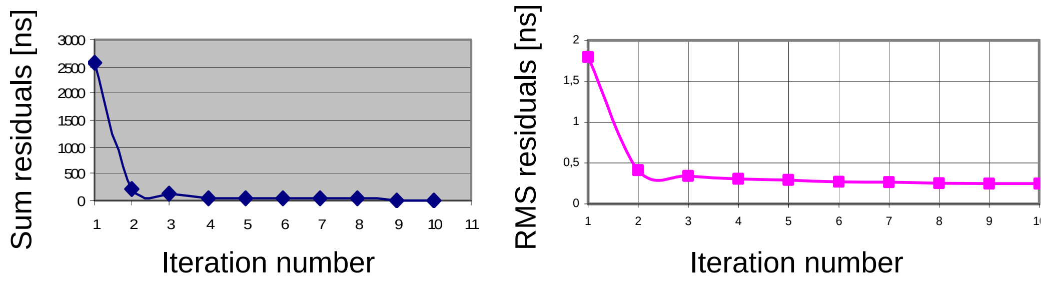

Figure 7.16 - An example of sum and RMS of residuals of travel times.

In those two examples 10 iterations were performed. However after 4th iteration process could be stopped.

6. Second tomographic calculation using data subsets

The operator can exclude some information from data sets, which can contain some additional errors, for example to exclude some travel times with strong dependence on transmitter-receiver angles; or to exclude some travel times with travel time differences between two measurements (the same travel paths). Only filtered data can be taken into the final inversion.

7. Final Tomographic calculation

Inversion based on a chosen most reliable mesh size and data set. After the final inversion process tomograms should be ready for the interpretation.

7.4.5 Data interpretation

In case of a velocity tomography a typical tomogram shows a velocity distribution inside tested structure. In case of electromagnetic waves, areas with higher propagation velocities can represent materials with lower dielectric constant and areas with lower propagation velocities can represent materials with higher dielectric constant. In general, areas with velocity above 0.2 m/ns can represent air voids and areas with a velocity around zero can represent steel or presence of high amounts of water or salt inside structure.

In attenuation (slowness) tomography operator can distinguish between materials with a high attenuation (e.g. water, sea water, high chloride content, or Ferro-magnetic materials), or materials with a low attenuation (air voids, dry timber).

1. Concrete structures

In general velocity distribution inside concrete structures can tell operator a lot about quality of tested material. In case of estimation of humidity or salt content, the following velocity values can be taken into consideration:

V = 0.06 - 0. 08 m/ns – wet concrete

V = 0.09 - 0.13 m/ns – dry concrete

Higher velocities could mean also presence of poorly compacted concrete with a presence of air voids. Lower velocities operator can interpret as areas with very well compacted concrete. In practical terms, different compaction qualities of concrete can be distinguished.

2. Masonry structures

In case of masonry structures a list of possible materials is much longer and thus interpretation is much more complex. Masonry walls or bridges can contain large number of materials with different properties, and thus interpretation must be preceded by an extensive desk study about possible materials used.

Chapter 8 - Conclusions

8.1 Summary and general conclusions

The present research work addressed the inspection of concrete bridges using Ground Penetrating Radar (GPR). GPR technique was applied and improved for the verification of structural geometry (location of rebars and tendon ducts) and structural geometry (location of areas with very poorly compacted concrete). The task was divided in three parts:

The first one, described in chapters 2 and 3, aimed to show the current state of the art of NDT for the inspection of concrete bridges in general, and of Ground Penetrating Radar, in particular. It was concluded that GPR can be successfully applied for the inspection of many civil structures, but it is necessary more validation work using 2D, 3D and tomography techniques for the verification of structural geometry and integrity of concrete bridges.

The second part consisted of the experiments using radar technique in reflection and transmission mode on laboratory specimens and on real bridges. Chapter 4 included calibration measurements using radar in reflection and transmission mode in the laboratory conditions, for the verification of structural geometry and integrity. Reflection measurements were performed on a large concrete specimen. The use of GPR with 3D reconstruction showed good potential in geometrical evaluation of structural elements, as well as in the mapping of typical defects and inclusions frequently found in structures. In the case of prestressed concrete elements, the location of tendon ducts, including the curvature of a curved tendon duct, was correctly assessed. Nevertheless, not all targets could be resolved due to their unfavourable orientation with respect to the direction of the profiles. Because the profiles started and ended 0.10-0.15 m after and before the specimen end, some objects located very close to the edges of the specimen were also not detected. Moreover, the poor contrast between materials resulted in poor reflectivity and thus weak detection, particularly in the case of a lightweight concrete specimen placed inside a concrete mass. Finally, triangularly shaped inclusions did not reflect favourably for detection by the radar signals.

To complement this approach, transmission measurements were performed in BAM and UMinho laboratories. In case of BAM specimens, voids and metallic tendon duct inside both tested specimens were successfully detected using GSSI system with two 1.5 GHz antennas and using GeoTomCG software. The antennas proved their usefulness and very good penetration. However, the results were far from being perfect. Although the voids and metallic tendon ducts were detected, significant number of artefacts (misleading or wrong results) was present in the final tomograms. Detailed quality checks of input data strongly indicated, that significant time variations are present in the radar signal and the source of them is unknown. It led to the conclusion that additional tests are needed for checking of the time axis stability.

Thus, calibration tests of MALA Geoscience and GSSI antennas for the time axis stability were performed in the BAM and UMinho laboratories. The tests indicated that in the every radar equipment time drift effect is present. To control that, calibration procedures were proposed and applied in the BAM laboratories.

After the stage of experimental testing, validation measurements of the radar technique in transmission and in the reflection mode were proposed and applied on three big prestressed concrete bridges in the north of Portugal.

In the first two case studies bridge inspection using GPR system with high frequency antennas allowed to accurately detect the position of the tendon ducts, which is a fundamental element for the safety of bridges. The inspection concluded that the tendon ducts were, in some cases, shifted with respect to the original design location. This information is important for efficient structural assessment and strengthening design. First, the information allows to take into account the real contribution of existing structural elements in the numerical and analytical models for strengthening design. Secondly, by determining the true position of tendon ducts and most important steel bars, the strengthening with external prestressing can be better planned and damage of the existing elements can be avoided during rehabilitation works. It must be noted that with the results of this work, the engineers responsible for the strengthening design were able to change the previous design in order to avoid drilling in locations where this would cross through existing tendon ducts.

In the last case study, GPR was used for the early detection of material and construction defects. The early detection of defects can help to adopt corrective measures (if necessary) to prevent further damage and to understand early occurrence of deterioration. The inspection of the support columns in a recent highway concrete bridge, which seems to register the occurrence of high levels of corrosion, allowed to detect deficiently positioned steel bars. Some of those bars were located very close to the surface, favouring the early occurrence of corrosion, while other bars where positioned deeper towards the centre of the column, affecting the design stresses, which can cause cracking and deformation of those structural members. Additionally, the application of advanced GPR tomography allowed to characterize the quality of concrete, indicating the presence of execution defects. Radar tomography system has shown its usefulness and the data for the final inversion was almost free of not reliable signals, what made the interpretation of the tomograms much easier. Also combination between radar reflection profiling and radar tomography was successfully applied.

The last phase of proposed research included the creation of methodologies for radar in reflection and transmission mode, including the newest achievements in the technology itself, advanced testing and data processing procedures, and possible areas of applicability. The purpose of those guidelines was to clarify and present in a very systematic way that testing using radar technique is a very expensive and complex process and requires deep explanation of all aspects of radar investigation on concrete bridges to the bridge owners, design offices, or radar operators. Only carefully planned NDT inspection using radar technique with deep understanding of its advantages and limitations can make the inspection worth its price.

The research has successfully proven, that radar inspection in reflection and transmission mode are not separated techniques, but they should be applied together to solve specific problems during non destructive inspection of concrete bridges.

8.2 Suggestions for future work

The future work can include software and hardware improvements for radar systems. Development of more stable antennas for transmission measurements should be demanded by radar users. Combination between velocity tomography (information about material dielectric properties) and migration algorithms (precise location and shape of the target) could be an interesting subject for further research as well as the combination between acoustic and radar tomography. There is also a strong necessity of providing to the normal radar users simple and light commercial scanning systems, which could significantly improve the accuracy of radar acquisitions. Another field of further research can include the combination between dynamic methods and GPR. While the dynamic measurements could predict the general damage location, radar measurements could precisely localise it and quantify.

In the near future the GPR technology should be used widely in various practical applications for the civil engineering industry and to become an integral part of a structural assessment process. That is because the quality control and diagnosis by non destructive inspection using GPR can increase the structural safety and reduce the associated costs for future repair and replacement as indicated in the chapter 5. Thus, there are significant future implications for the success of GPR techniques for the civil engineering industry, such as:

1. Performance evaluation and updating of the assumptions made in the models used for the assessment of structural safety in existing structures for the design of new structures.

2. Validation of geometry surveys used for assessment or retrofit actions of existing structures and quality control of new structures.

3. Damage detection of the structure or infrastructure caused by inadequate or faulty workmanship, or any external action.

Among those applications, the one, which, in the author's opinion has a big future, is the model updating considering the information obtained from the non destructive test (like radar), regarding the geometry and integrity. Updating can include: numerical modelling of the structure, modelling of the resistance of structural elements, modelling of load (structure self weight or other permanent loads). Depending on the precision of the test and on the number of measurements performed, the obtained geometrical results can be considered as deterministic quantities (e.g. to adjust the dimensions of the bridge elements in the models) or as probabilistic quantities (e.g. to use in the probability based assessment).

References and Bibliography

Abrams, D.P., Epperson, G.S. (1989), Nondestructive evaluation of masonry buildings, Res. Rep. no. 89-26-03, Advanced Construction Technology Center, Univ. Illinois at Urbana-Champaign, 208 pp.

AASHTO (2000), Manual for Condition Evaluation of Bridges, ISBN Number: 1-56051-136-2

Abraham, O., Cote, P. (2002), Thickness frequency profile for the detection of voids in tendon duct, *ACI Structural Journal* 99 (3), 239-247

Annan, A.P., Davis, J.L., Gendzwill, D. (1988), Radar Sounding in Potash Mines: Saskatchewan, Canada. Geophysics, vol. 53, p. 1556–1564.

Annan, A.P. (2003), GPR for infrastructure imaging. Proc. NDT-CE, Berlin

Annan, A.P., Chua, L.T. (1992), Ground Penetrating Radar Performance Predictions: The Geological Survey of Canada, Paper 90-4, pp. 5–13.

Annan, A.P. (2002), GPR-History, Trends, and future developments, *Subsurface Sensing Technologies and Applications* vol.3, (4)

Becht, A., Tronicke, J., Appel, E., Dietrich, P. (2004), ‘Inversion strategy in crosshole radar tomography using information of data subsets’, Geophysics, vol. 69, (1), 222-230.

Berra, M., Binda, L., Anti, A., Fatticcioni, A. (1992), Utilisation of sonic tests to evaluate damaged and repaired masonries, Proc. Conf. Nondestructive Eval. of Civil Struc. and Mat., Boulder, Colorado, p. 329-338.

Berryman, J.G. (1991), Lecture notes on nonlinear inversion and Tomography, University of California, Lawrence Livermore National Laboratory, USA.

Bergmeister, K., Aktan, A.E., Bucher, Chr., Dorfmann, L., Fehling, E., Frey, R.P., Geier, R., Huth, O., Inaudi, D., Maier, J.E., Santa, U., Schwesinger, P., Slowik, V., Wenzel, H. (2003), Monitoring and safety evaluation of existing concrete structures, State of the art report, FIB.

Binda, L., Saisi, A., Tiraboschi, C., Valle, S., Colla, C., Forde, M. (2003), 'Application of sonic and radar tests on the piers and walls of the Cathedral of Noto', Construction and Building Materials, vol. 17 (8), 613-627.

Bungey, J.H., Millard, S.G. (1996), Testing of concrete in structures, Chapman&Hall

Buyukozturk, O. (1998), Imaging of concrete structures, *NDT&E International*, vol 31 (4), 233-243

Buyle-Bodin, F., Ammouche, A., Garciaz, J.L. (2003), Contribution of coupling non-destructive methods for the diagnosis of concrete structures. Proc. NDT-CE, Berlin

Birken, R., Versteeg, R. (2000), Use of Four-Dimensional Ground Penetrating Radar and Advanced Visualization Methods to determine the subsurface fluid migration, *Journal of Applied Geophysics*, vol 43 (2-4), 215-226,

Brauchler, R., Liedl, R., Appel, E. (2003), A travel time based hydraulic tomographic approach, *Water Resources Research*, vol. 39 (12)

Brown, K., St Leger, J. (2003), Use of the MEGASCAN^{TM} imaging process in inspection systems for post-tensioned bridges and other major structures, NDT-CE 2003, BAM, Germany

Cartz, L. (1995), Nondestructive Testing: Radiography, Ultrasonics, Liquid Penetrant, Magnetic Particle, Eddy Current, ASM International, Materials Park, Ohio,

Capineri, L., Grande, P., Temple, J.A.G. (1998), Advanced Image-processing technique for real time interpretation of Ground Penetrating Radar Images, *International journal of imaging systems and technology*, vol 9 (1), 51-59

Chen, H.L.R., Halabe, U.B., Sami, Z., Bhandarkar, V. (1994), Impulse radar reflection waveforms of simulated reinforced concrete bridge decks, *Materials Evaluation*, vol. 52 (12), 1382-1388

Colla, C. (2001), Two-dimensional impact-echo for NDT testing of masonry bridges, Proc. 3rd Int. Arch Bridge Conf., p. 207-211

Colla, C., Das, P.C., McCann, D., Forde, M.C. (1997), Sonic, electromagnetic and impulse radar investigation of stone masonry bridges, *NDT&E International* 30 (4), 249-254

Colla, C., Schneider, G., Woestmann, J., Wiggenhauser, H. (1999), Automated impact-echo: 2D and 3D imaging of concrete elements, BAM, Report 66-Cd DGZfp, 307-318

Colla, C., Lausch, R. (2003), Influence of source frequency on impact-echo data quality for testing concrete structures, *NDT&E Internationa*l, vol.36 (4), 203–213

Colla, C., Burnside, C. D., Clark, M. R., Broughton, K. J., Forde, M. C. (1998), Comparison of laboratory and simulated data for radar image interpretation, *NDT&E International*, Vol. 31(6), 439–444

Clark, M.R., Crabb, G. (2003), “Detection of water movement below a concrete road using ground penetrating radar.” Proc., Structural Faults and Repair, 10th International Conference and Exhibition, London, UK, 15p.

Crawford, G.I. (1997), Guide to Nondestructive Testing of Concrete, FHWA-SA-97-105, 60pp.

Cruz, P.J.S., Wisniewski, D.F. (2004), Ave River Bridge - A Major Precast Prestressed U-Girder Bridge in Portugal, *PCI Journal*, 2004, July-August issue, 72-85.

Cruz, P.J.S., Topczewski, L., Fernandes, F., Trela, Ch., Lourenço, P.B, "Application of radar techniques to the verification of design plans and the detection of defects in concrete bridges", Journal of Structure and Infrastructure Engineering (submitted for publication)

Cruz, P.J.S., Topczewski, L., Fernandes, F.M., Lourenço, P.B. (2006) “Utilização do Radar de Prospecção Geotécnica na localização das baínhas de pré-esforço nas pontes da Barra e de Lanheses”, JPEE 2006 - 4as Jornadas Portuguesas de Engenharia de Estruturas, Lisboa, LNEC, 13 a 16 de Dezembro de 2006.

Davey, N. (1961), “A History of Building Materials”. Phoenix House, London

Daniels, D.J. (2004), “Ground Penetrating Radar – 2nd Edition.” Radar, sonar, navigation and avionics series 15, IEE, London, UK, ISBN 0-86341-360-9, 726p.

Davis, J.L., Annan, A.P. (1986), Borehole Radar Sounding in CR-6, CR-7 and CR-8 at Chalk River, Ontario. Technical Record TR-401, Atomic Energy of Canada Ltd.

Davis, J., Huang, Y., Millard, S.G:, Bungey, J.H. (2003), Determination of dielectric properties of insitu concrete at radar frequencies, NDT-CE 2003, BAM, Germany

Derobert, X., Aubagnac, C., Abraham, O. (2002), Comparison of NDT techniques on a post-tensioned beam before its autopsy, *NDT&E International* 35 (8), 541-548

Derobert, X., Klysz, G., Balayssac, J.P., Lataste, J.F. (2003), Cover concrete evaluation by electromagnetic and electric techniques. Case study: Empalot Bridge (Toulouse, France), Structural Faults and Repair Congress Proceedings, London, United Kingdom, 11p.

Doerksen, K. (2002), Improved optical positioning for GPR based structure mapping, Proceedings 9th Int. Conf. on Ground Penetrating Radar GPR2002, April 29 - May 2, Santa Barbara, California.

Doolittle, J.A., Asmussen, L.E. (1992), Ten years of applications of ground penetrating radar by United States Department of Agriculture, Proceedings of the Fourth International Conference on Ground Penetrating Radar, Geological Survey of Finland, Special Paper 16, p. 139–147.

Dolphin, L.T., Beatty, W.B., Tanzi, J.D. (1978), Radar Probing of Victorio Peak, New Mexico, *Geophysics*, vol. 43 (7), 1441–1448.

Duke, J.C. (2004), “Thermal Methods: An Introduction with Emphasis on Transportation Applications”, Proc., Introduction to Non-destructive Evaluation Technologies for Bridges Conference, Transportation Research Board, 20p.

DMJM Harris (2003), Tests and assessment of NDT methods for post-tensioning systems in segmental balanced cantilever concrete bridges, FDOT

El Said, M.A.H. (1956), Geophysical prospection of underground water in the desert by means of electromagnetic interference fringes: Pro. I.R.E., vol. 44, p. 24–30 and 940.

Fernandes, F.M. (2006), Evaluation of two novel NDT techniques: microdrilling of clay bricks and ground penetrating radar in masonry. PhD thesis, University of Minho, Available from www.civil.uminho.pt/masonry.

Forde, M.C. (2004), "Ground Penetrating Radar." Proc., Introduction to Non-destructive Evaluation Technologies for Bridges Conference, Transportation Research Board, 20p.

Golis, M. (1991), An Introduction to Nondestructive Testing. American Society of Nondestructive Testing, Columbus, OH,

Giannopolous, A., Macintyre, P., Rodgers, S., Forde, M., Koppenjan S. K., Hua L. (2002), GPR detection of voids in post-tensioned concrete bridge beams, 9th International conference on ground penetrating radar

Groenenboom, J., van der Kruk, J., Zeeman, J.H. (2001), 3D GPR data acquisition and the influence of positioning errors on image quality, 63rd Conference and Technical Exhibition, Amsterdam, 11-15 June 2001, 4 pp.

Greandjean, G., Gourry, J.C., Bitri, A. (2000), Evaluation of GPR techniques for civil-engineering applications: study on test site, *Journal of Applied Geophysics*, vol.45 (3), 141-156

Guy, E., Daniels, J., Radzevicius, S. (1999), Demonstration of Using Crossed Dipole GPR Antennae for Site Characterisation, *Geophysical Research Letters*, vol.26, 3421-3424

IAEA (2002), Guidebook on non-destructive testing of concrete structures, IAEA, Vienna, ISSN 1018-5518

Hugenschmidt, J. (2002), "Concrete bridge inspection with a mobile GPR system." *Construction and Building Materials*, 16 (3), 147-154.

Hugenschmidt, J., De Witte, H. (1998), "GPR inspection of a mountain motorway in Switzerland." *Journal of Applied Geophysics*, 40, 95-105.

Kak, A.C., Slaney, M. (1988), 'Principles of Computerized Tomographic Imaging', Institute for Electrical and Electronic Engineers, IEEE Press.

Kingsley, G.R., Noland, J.L., Atkinson, R.H. (1987), Nondestructive evaluation of masonry structures using and ultrasonic pulse velocity technique, Proc. 4th North American Masonry Conf.

Krause, M., Mielentz, F., Milman, B., Muller, W., Schmitz, V. (2000), Ultrasonic imaging of concrete members using an array system, *INSIGHT* vol. 42 (7), 447-450

Krause, M., Barmann, M., Frielinghaus, R., Kretzschmar, F.,Kroggel, O., Langenberg, K. J., Maierhofer, C., Muller, W., Neisecke, J., Schickert, M. Schmitz, V., Wiggenhauser, H., Wollbold, F. (1997), Comparison of pulse-echo methods for testing concrete, *NDT&E International*, vol. 30 (4), 195 204

Kohl, Ch., Krause, M., Maierhofer, Ch., Wöstmann, J., Wiggenhauser, H., Mayer, K. (2003), 3D-visualisation of NDT data using a data fusion technique, *Insight* 45 (12), 800-808

Laurens, S., Balayssac, J.P., Rhazi, G.J., Klysz, G. Arliguie (2003), Non destructive evaluation of concrete moisture by GPR technique: experimental study and direct modeling, Proc. NDT-CE, Berlin Sept. 2003,

Laksameethanasan, D. (2004), 3D Modelling and Imaging based on Transmission Diffraction Tomography and Algebraic Reconstruction Techniques as applied in NDT – Master Thesis, Univ. of Kassel, Germany, Germany.

Lualdi, M., Zanzi, L., Binda, L. (2003), "Acquisition and processing requirements for high quality 3D reconstructions from GPR investigations." Proc., International Symposium Non-DestructiveTesting in Civil Engineering (NDT-CE), Berlin, Germany, 13p., CD-ROM.

Lualdi, M., Zanzi, L. (2003), 'A new system to perform 3D GPR surveys for utility mapping', Proceedings 3rd International Conference on Applied Geophysics, December 8-12, Orlando (FL), USA.

Malhorta, V.M., Carino, N.J. (eds.) (1991), CRC Handbook on nondestrutive testing of concrete, CRC Press

Maierhofer, Ch., Brink, A., Rollig, M., Wiggenhauser, H. (2003), Detection of shallow voids in concrete structures with impulse thermography and radar, *NDT&E International* 36 (4), 257–263.

Maierhofer, Ch., Kind, T. (2002), Application of impulse radar for non-destructive investigation of concrete structures, Proceedings of SPIE -- Volume 4758 Ninth International Conference on Ground Penetrating Radar, Steven Koppenjan, Hua Lee, Editors, April 2002, pp. 382-387

Maierhofer, Ch., Brink, A., Rollig, M., Wiggenhauser, H. (2002), Transient thermography for structural investigation of concrete and composites in the near surface region, *Infrared Physics & Technology* 43 (3-5), 271–278

McCann, D.M., Forde, M.C. (2001), Review of NDT methods in the assessment of concrete and masonry structures, *NDT&E International* 34 (2), 71–84.

Martin, J., Broughton, K.J. Giannopolous, A. Hardy, M.S.A. Forde, M.C. (2001), Ultrasonic tomography of grouted duct post-tensioned reinforced concrete bridge beams, *NDT&E International* 34 (2), 107–113

Mast, J.E., Johansson, E.M. (1994), Three-dimensional ground penetrating radar imaging using multi- frequency diffraction tomography Advanced Microwave and Millimeter-Wave Detectors. Proceedings, San Diego, California (United States), 25-26 Jul. 1994. pp. 196-204. Edited by S.S. Udpa and H.C. Ham. SPIE Vol. 2275

Marklein, R., Mayer, K., Hannemann, R., Krylow, T., Balasubramanian, Langenberg K. J, Schmitz, V. (2002), Linear and Nonlinear inversion algorithms applied in Non Destructive Evaluation, *Inverse problems* 18, 1733-1759.

Meju, M.A. (2001), Geophysical Data Analysis: Understanding Inverse Problem Theory and Practice

McGuire, S.A., Peabody, C.A. (1995), Working Safely in Gamma Radiography, US Government Printing Office, Washington D.C,

Millard, S.G., Davis, J., Huang, Y., Bungey, J.H., Koppenjan Steven, K., Hua L. (2002), A wide band system for measuring dielectric properties of concrete, 9th International Conference on GPR, pp. 416 – 421

Mitchell, T.M. (2004), Radioactive/Nuclear Methods, In CRC Handbook on Nondestructive Testing of Concrete, Second Edition, edited by V.M. Malhotra and N.J. Carino, (CRC Press, Florida).

Motz, M., Krüger, M., Grosse, C.U., Haller, P., Beutel, R. (2003), Impact-echo: New developments regarding hard- and software. Proc. NDT-CE, Berlin

Neal, A. (2004), "Ground-penetrating radar and its use in sedimentology: principles, problems and progress." *Earth-Science Reviews*, 66, 261-330.

Olhoeft, G.R. (1975), The electrical properties of permafrost, Ph.D. Thesis, University of Toronto., 172 pages.

Olhoeft, G.R. (1987), Electrical properties from 10^{-3} to 10^{+9} Hz—physics and chemistry: Proceedings of the 2nd International Symposium on the Physics and Chemistry of Porous Media, American Institute of Physics Conference Proceedings, v. 154, p. 281–298.

Olson, L.D. (2004), "Stress Waves NDE Methods for Condition Assessment of the Superstructure and Substructure of Concrete Bridges.", Olson Engineering, Inc., FHWA, TRB NDE Workshop,

Orrey, J.L., Sirles, P.C., and Archambeau, C.B. (2000), 3-D imaging of subsurface features using GPR array beam imaging, EEGS – Annual Meeting, USA

Pinelli, G., De Pasquale, G., Manacorda, G., Papeschi, P., A dedicated radar system for preliminary no/dig investigation, IDS S.p.A. Pisa, Italy

Padaratz, I.J., Forde, M.C. (1995), "A theoretical Evaluation of Impulse Radar Wave Propagation" *Nondestructive Testing and Evaluation* 12, 9-32.

Reynolds, J.M. (2002), "An introduction to applied and environmental geophysics." John Wiley & Sons, Chichester, ISBN 0-471-95555-8.

Redman, J.D., Kunert, Gilson, E.W., M., Pilon, J.A., Annan, A.P. (1996), Borehole radar for environmental applications: selected case studies: Proceedings of the Sixth International Conference on Ground Penetrating Radar (GPR '96), September 30–October 3,1996, Sendai, Japan.

Rhazi, J., Dous, O., Ballivy, G. (2003), Nondestructive health evaluation of concrete bridge decks by GPR and half-potential techniques. Proc. NDT-CE, Berlin Sept. 2003,

Roberts, R., Cist. D, Koopenjan, S. K., Hua, L. (2002), Enhanced target imaging in 3-D using GPR data from orthogonal profile lines, 9th International Conference on GPR, pp. 256 - 261

Rhim, H.C., Buyukozturk, O., Blejer, D.J. (1995), Radar imaging of concrete slabs with and without a rebar, *Materials Evaluation*, vol. 53, (2), 295-299

Reppert, P.M., Roffman, R.A., Dale Morgan, F. (2002), The effects of antenna orientation on GPR data quality, Proceedings of the Symposium on the Application of Geophysics to Environmental & Engineering Problems SAGEEP 2002, February 10-14, Las Vegas.

Ryall, M.J. (2001), "Bridge Management", Butterworth-Heinemann, Oxford,

Sansalone, M.J., Street, W.B. (1997), Impact-echo, non-destructive evaluation of concrete and masonry. Bullbrier Press, Ithaca, N.Y.

Shaari, A., Millard, S.G., Bungey, J.H. (2003), "GPR antenna medium coupling effects: experimental and 2D FTDT modelling results." Proc., International Symposium Non-Destructive Testing in Civil Engineering (NDT-CE), Berlin, Germany, 8p., CD-ROM.

Shaw, P., Bergström, J. (1998), In-Situ Testing of Reinforced Concrete Structures Using Stress Waves and High Frequency Ground Penetrating Radar, 7th European Conference on Non-Destructive Testing

Shevaldykin, V.G., Kozlov, V.N., Samokrutov, A.A. (2003), Inspection of Concrete by Ultrasonic Pulse-Echo Tomograph with Dry Contact, MSIA Spectrum, Russia

Shihab, S., Al-Nuaimy, W., Huang, Y., Eriksen, A. (2003), A Comparison of Segmentation Techniques for Target Extraction in Ground Penetrating Radar Data, 2nd International Workshop on Advanced GPR, Delft.

Shihab, S., Al-Nuaimy, W., Huang, Y., Eriksen, A., Koppenjan S. K., Hua, L. (2002), Neural network target identifier based on a statistical features of GPR signals, 9th International Conference on GPR, pp. 135-138

Shaw, M.R., Millard, S.G., Molyneaux, T.C.K., Taylor, M.J., Bungey, J.H. (2005), Location of Steel Reinforcement in Concrete using Ground Penetrating Radar and Neural Networks, 10th International Conference on Structural Faults and Repair, pp. 203-212

Shaw, P., Xu, A. (1997), High energy radiography and radar applications to concrete inspection, The 4th International Conference on NDT, NDT-CE'97

Scott, M., Rezaizadeh, A., Delahazab, A., Santos, C.G., Moore, M., Graybeal, B., Washer, G. (2003), A comparison of nondestructive evaluation methods for bridge deck assessment, *NDT&E International*, vol. 36 (4), 245–255.

Scales, J., Smith, M., Treitel, S. (2001), Introductory Geophysical Inverse Theory, Center for wave phenomena, Department of Geophysics, Colorado School of Mines, USA.

Tronicke, J., Knoll, M.D. (2005), Vertical radar profiling: influence of survey geometry on first-arrival traveltimes and amplitudes. *Journal of Applied Geophysics* 57, 179-191.

Tronicke, J., Dietrich, P., Appel, E. (2002), Quality improvement of crosshole georadar tomography: pre- and post-inversion data analysis strategies. European *Journal of Environmental and Engineering Geophysics* 7, 59-73.

Tronicke, J., Tweeton, D. R., Dietrich, P., Appel, E. (2001), Improved crosshole radar tomography by using direct and reflected arrival times. *Journal of Applied Geophysics* 47, 97-105.

Taffe, A., Borchardt, K., Wiggenhauser, H. (2003), Specimen for the improvement of NDT methods, Design and construction of a large concrete slab for NDT methods at BAM, Non-Destructive Testing in Civil Engineering (NDT-CE), DGZfP & BAM, September 16-19, 2003, on CD, Berlin.

Taffe, A., Maierhofer, Ch. (2003), Guidelines for NDT methods in civil engineering, Proc. NDT-CE, Berlin Sept. 2003,

Topczewski, L., Fernandes, F., Cruz, P.J.S., Lourenço, P.B. and Ramos, L. (2006a), Radar investigation on civil structures using 3D data reconstruction and transmission tomography. Structural Faults and Repair conference, Edinburgh, United Kingdom, CD-ROM.

Topczewski, L., Fernandes, F., Cruz, P.J.S., Lourenço, P.B, "Practical implications of GPR investigation using 3D data reconstruction and transmission tomography" Journal of Building Appriasal (invited paper), (accepted for publication, in press)

Topczewski, L., Fernandes, F., Cruz, P.J.S., Lourenço, P.B. (2006b), "Verification of construction plans of concrete bridges and detection of possible deficiencies using Ground Penetrating Radar", 3rd International Conference of Association for Bridge Maintenance and Safety and Management(IABMAS), July 16-19, Porto, Portugal

Topczewski, L., Cruz, P.J.S., Fernandes, F., (2005), Deliverable 3.8 "Radar Tomography" WP3-27-T-050210-F-3_8_Radar_Tomography, Sustainable Bridges European Project, Work Package 3,

Ulriksen, C.P.F. (1982), Application of impulse radar to civil engineering: Unpublished Ph.D. Thesis, Dept. of Engr. Geol., U. of Technology, Lund, Sweden, p. 175.

Warhus, J.P., Mast, J.E., Johansson, E.M., Nelson, S.D. (1998), Improved ground-penetrating radar, bridge decks, Lawrence Livermore National Lab., California (United States), DE94004863/GAR, 8pp.

Waite, A.H., Schmidt, S.J. (1961), Gross errors in height indication from pulsed radar altimeters operating over thick ice or snow, IRE International Convention Record, Part 5, p. 38–54.

Watts, R.D., England, A.W. (1976), Radio-echo sounding of temperate glaciers: Ice properties and sounder design criteria: *Journal of Glaciology*, vol. 21, (85), 39–48.

Young S. Cho. (2003), Non Destructive Testing of High Strength Concrete using Spectral Analysis of Surface Waves, *NDT&E International* 36, 229-335

Zanzi, L. (2001), Notes on Ground Penetrating Radar, DIS, Polimi, Italy

Valle, S., Zanzi, L., Rocca, F. (1999), 'Radar tomography for NDT: comparison of techniques', *Journal of Applied Geophysics*, vol. 41 (2-3), 259-269

Valle, S., Zanzi, L., Lenzi, G. (2000), '2D and 3D focusing of ground penetrating radar data for NDT', 8th International Conference on Ground Penetrating Radar, Gold Coast, Queensland, Australia, 23-26 May, pp. 157-162.

USER MANUALS AND OTHER RESOURCES

RAMAC GROUNDVISION – SOFTWARE MANUAL, VER. 1.3

RAMAC/GPR – OPERATING MANUAL, VER. 3.0

Luigi Zanzi, Notes on Ground Penetrating Radar, Dip. di Ingeneria Strutturale, Politecnico di Milano, February 2003

Webpages as of 5th March 2007

1. http://www.g-p-r.com
2. www.malgags.com
3. www.geophysical.com
4. www.ids-spa.it
5. www.ndt-ed.org
6. www.ndt.net
7. www.ndt.com
8. www.georadar.com/howitwrk.htm
9. ukta.tripod.com/NDTMethods.html
10. www.asnt.org
11. www.bam.de
12. www.sustainablebridges.net
13. www.leica-geosystems.com
14. www.logitech.com
15. www.impact-echo.com
16. http://ciks.cbt.nist.gov/~carino/ieprin.html
17. http://www.colorado.edu/physics/
18. http://www.isvr.soton.ac.uk/
19. http://www.physicsclassroom.com
20. http://www.intuitor.com/resonance/abcRes.html

Appendix A – Basic terminology

As it was mentioned in the introduction, a person who is performing NDT investigation must have a basic knowledge about waves and their properties. In this appendix it will be mentioned the basic terms and definitions about acoustic and electromagnetic waves. Below definitions of main physical terms are provided together with definition of decibel.

Period

The period of a wave is the unit of time for a wave to cycle through one oscillation. (see Figure A)

Frequency

The frequency of a wave is an expression of the number of oscillations per second. For engineering applications, this is expressed as cycles/second or hertz.

Wavelength

The wavelength is the unit of space required for one cycle of a wave. The wavelength is a function of the frequency of the wave and its propagation velocity according to:

$$\lambda = \frac{v}{f} \qquad \text{(I)}$$

where v is a propagation velocity, f is the frequency

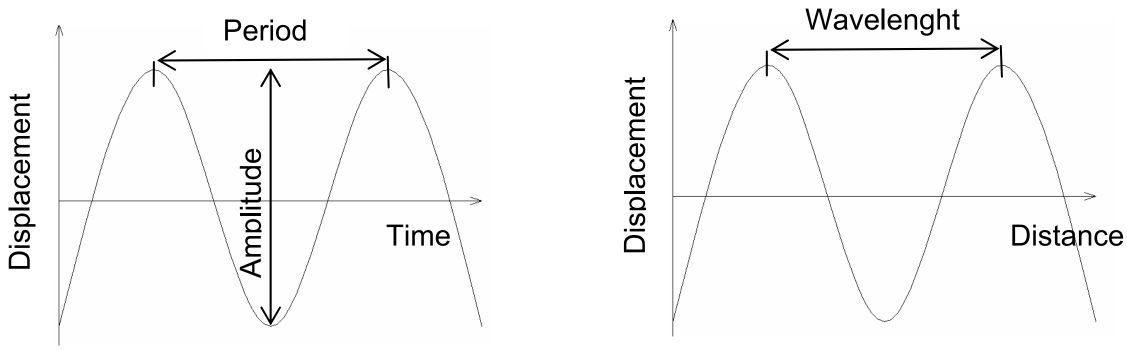

Figure A - Basic wave properties

Amplitude

The amplitude of the wave is the magnitude of the disturbance caused by a wave (See Figure A).

Attenuation

Attenuation of a wave is the loss in amplitude resulting from energy being transferred from the wave to the medium in which the wave propagates (see also chapter 3). Generally speaking, the higher frequency waves attenuate faster in a given medium than lower frequency waves. This is true of both mechanical waves and electromagnetic waves.

Superposition of waves (Interference)

Waves can be combined together such that, at a given location and time, they may cause either constructive effects, in which the amplitude is strengthened, or destructive effects in which the amplitude is reduced. A remarkable property of waves is that they can pass through one another without being disturbed. While they are passing through, the resulting acoustic pressure is always just the sum of the acoustic pressures of each individual wave at that moment and location.

Reflection and Refraction

If a wave crosses a boundary between two media 1 and 2 in which the wave speeds are v_1 and v_2 respectively, then the ratio v_1/v_2 obeys Snell's law of refraction:

$$\frac{v_1}{v_2} = \frac{\sin\alpha_1}{\sin\alpha_2} = \frac{\lambda_1}{\lambda_2} \qquad \text{(II)}$$

where α_1 and α_2 are the angles made by the waves and the normal to the boundary in media 1 and 2 respectively. The symbols λ_1 and λ_2 correspond to the wavelength in the media 1 and 2 respectively. Refraction effect can be seen in Figure B Part of the wave is also partially or totally reflected, when it encounters a boundary of two different media. It is called a law of reflection (see Figure C).

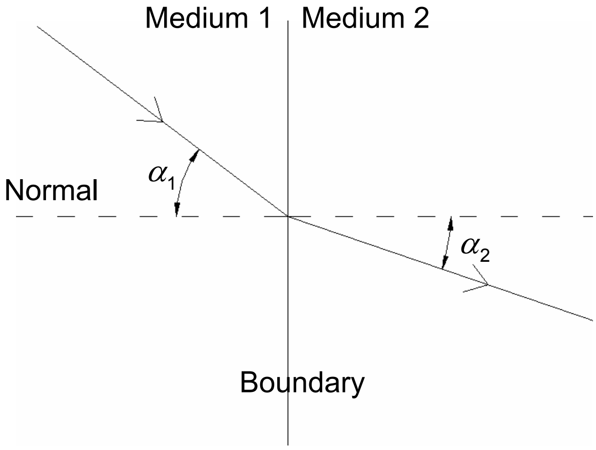

Figure B - Refraction effect at the interfaces

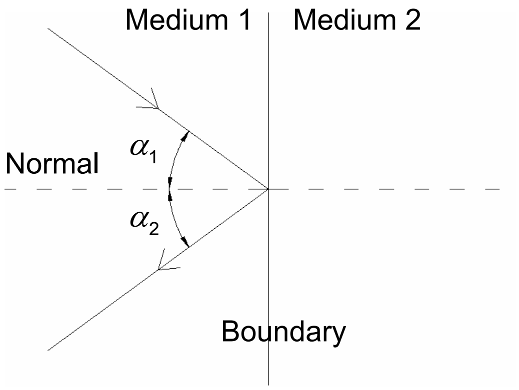

Figure C - Reflection effect at the interfaces

Diffraction

The spreading of waves when they pass through an opening, or around an obstacle into regions where we would not expect them, is called diffraction (see Figure D). Diffraction occurs if a wave encounters an object and if the wavelength is of the same size (or greater than) the object size.

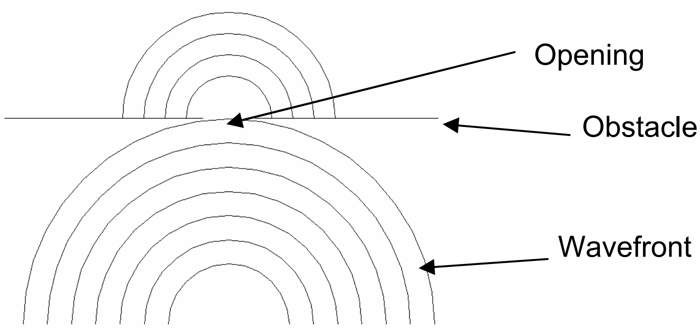

Figure D - Diffraction.

Polarization

Is the property of electromagnetic waves, such as light, that describes the direction of their transverse electric field. More generally, the polarization of a transverse wave describes the direction of oscillation in the plane perpendicular to the direction of travel. Longitudinal waves such as sound waves do not exhibit polarization, because for these waves the direction of oscillation is along the direction of travel.

Mode conversion

When sound travels in a solid material, one form of wave energy can be transformed into another form. For example, when a longitudinal wave hits an interface at an angle, some of the energy can cause particle movement in the transverse direction to start a shear (transverse) wave. Mode conversion, occurs when a wave encounters an interface between materials of different acoustic impedance and the incident angle is not normal to the interface